WASHINGTON UNIVERSITY

SEVER INSTITUTE OF TECHNOLOGY

Fourth-Order Partition Dynamics for a Two-Dimensional Model of the Cochlea

by

Stephen T. Neely

Prepared under the direction of Professor J. R. Cox

A dissertation presented to the Sever Institute of
Washington University in partial fulfilment
of the requirements for the degree of

DOCTOR OF SCIENCE

August, 1981

Saint Louis, Missouri

WASHINGTON UNIVERSITY
SEVER INSTITUTE OF TECHNOLOGY

ABSTRACT

Fourth-Order Partition Dynamics for a

Two-Dimensional Model of the Cochlea

by Stephen T. Neely

ADVISOR: Professor J. R. Cox

August, 1981

Saint Louis, Missouri

A commonly used model of the cochlea has been enhanced by including more complex cochlear partition dynamics and by including a model of the middle ear. A two-dimensional, linear, mathematical model of the cochlea is solved numerically in both frequency-domain and time-domain by using a finite-difference spatial-approximation of the model equations. At each point along the cochlear partition the model allows two mechanical degrees-of-freedom, which results in fourth-order equations of motion for the partition at each point. The fourth-order partition dynamics make possible the representation of a resonant tectorial membrane as a mechanical "second-filter" coupled to the resonant basilar membrane. Model parameters chosen according to this resonant tectorial membrane hypothesis are shown to produce model solutions for hair-cell shearing which resemble certain neural response

versus place data [D. O. Kim, J. H. Siegel, and C. E. Molnar (1979), Scandanavian Audiology, Suppl. 9, pp. 63-81.]. The fourth-order partition dynamics also make possible the inclusion of a negative damping element which sharpens basilar membrane tuning without causing dynamic instability. The inclusion of negative damping provides a means of obtaining "active" model results which resemble certain direct measurements of cochlear partition motion [W. S. Rhode (1971), J. Acous. Soc. Am., Vol. 49, pp. 1218-1231.]. The finite-difference method of solving the cochlear model equations allows simultaneous solution of middle-ear and cochlear mechanics and, therefore, is a useful tool for investigating bi-directional interactions (including nonlinear interactions) among various mechanical stages of the peripheral auditory system. Some experimental measurements of ear-canal sound pressure have shown an apparent delayed-reflection of acoustic power which has been attributed to an "evoked cochlear mechanical response." [D. T. Kemp (1978), J. Acoust. Soc. Am., Vol. 66, pp. 1386-1391.] The present cochlear model did not produce this type of reflection for any of the linear, stable parameter sets used in this research. The model results included in this dissertation demonstrate that the formulation and solution of the model for the biomechanics of the ear as described here, provide useful means for exploring and implementing interesting hypotheses about cochlear-partition mechanisms.

TABLE OF CONTENTS

TABLE OF CONTENTS
(continued)

LIST OF TABLES

LIST OF FIGURES

LIST OF FIGURES

(continued)

LIST OF FIGURES

(continued)

LIST OF FIGURES

(continued)

LIST OF FIGURES

(continued)

Fourth-Order Partition Dynamics for a Two-Dimensional Model of the Cochlea

1. INTRODUCTION

The cochlea is the principal sensory organ of the mammalian auditory system. It is a spiralling, fluid-filled tunnel which is embedded in the temporal bone. A flexible cochlear partition spans the diameter of this tunnel throughout most of its length. In the human cochlea this partition is about 35 millimeters long. The mechanical structure of the cochlea is such that the component frequencies of an acoustical signal are distributed along the cochlear partition. Sensory hair cells within the cochlear partition detect extremely small motions of the partition and convey information about this motion to the auditory nerve. The middle ear provides input to the cochlea and has relatively constant response over a wide range of frequencies; whereas, the single nerve fibers exiting from the cochlea respond over a very narrow range of frequencies. The cochlea is one of the most intricate mechanical system in the body and has been the subject of intensive research for many years (e.g. 1, 2)*.

* The numbers in parentheses in the text indicate references in the Bibliography.

Mathematical models of the cochlea have been important tools in understanding the function of the cochlea because the signal processing which takes place within the cochlea is complex and direct observations of the cochlear partition are difficult. Experimental observations of cochlear mechanics are difficult because: (a) the behavior of the cochlea is dependent on its physiological state which is highly vulnerable to a variety of disturbances, (b) motions within the cochlea are normally very small [probably less than one angstrom at the threshold of hearing (3)], and (c) access to the cochlea is blocked by the surrounding bone structures (e.g. 4, 5, 6). Experimental and modeling research in cochlear mechanics is discussed further in chapter 2.

In the past few years, a two-dimensional model of the cochlea has been widely used to demonstrate the mechanical frequency analyzing capabilities of the cochlea. This model is a fluid-filled rectangle, which is divided into two symmetric halves by an elastic partition. The geometrical and mechanical simplifications associated with this two-dimensional model are discussed in chapter 3.

The primary focus of this dissertation is on the elastic partition of such a two-dimensional model and its interaction with the cochlear fluid and the middle ear. The cochlear partition of the model is intended to represent the organ of Corti including the basilar membrane and the tectorial membrane. In models of the cochlea the partition is usually assumed to have no direct longitudinal coupling and each point of the partition is represented by a simple mechanical system with one degree-of-freedom (1-DOF). The behavior of

a 1-DOF system can be described, in general, by a second-order equation of motion. The cochlear partition model considered in this dissertation retains the assumption of no direct longitudinal coupling, but allows at each point of the partition a simple mechanical system with two degrees-of-freedom (2-DOF). In the 2-DOF system, the first degree-of-freedom is assigned to represent the basilar membrane in the traditional manner of the 1-DOF system; the second degree-of-freedom is not directly influenced by fluid pressure, but is mechanically coupled to the first and has an influence on the frequency response of the cochlear partition. The mathematical description of a 2-DOF system leads, in general, to fourth-order equations of motion (7). This enhancement of cochlear partition representation has provided a means of obtaining useful extensions to the range of solutions that are possible with the two-dimensional model. Model results are presented in this dissertation for two different cochlear partition models.

First, the 2-DOF partition is used to investigate the idea that mechanical excitation to the sensory hair cells is more sharply tuned than the motion of the basilar membrane. The apparent discrepancy between the frequency responses of the motion of a point on the basilar membrane and the rate of discharge of a single nerve fiber (8, 9) has led to the consideration of the tectorial membrane as a separately resonant, but coupled, structure leading to a second mechanical degree-of-freedom (10, 11, 2, 12, 13). Model results based on a resonant tectorial membrane hypothesis are presented in chapter 4 and compared with neural response data.

Second, the 2-DOF partition is used to investigate the idea that the sensory hair cells are capable of converting metabolic energy into mechanical energy. The apparent inability of previous cochlear models to reproduce, with a single set of model parameters, the amplitude and phase of experimental measurements of basilar membrane motion (14, 15), together with current speculation concerning possible "active" behavior of the cochlear partition (16, 17, 18, 19) has led us to consideration of the outer hair cells as a controlled source of mechanical energy influencing the cochlear partition. This type of energy source can be simulated in a linear cochlear model by including "negative damping" elements. The effects of negative damping in the cochlear partition on the frequency selectivity of the cochlea has recently been demonstrated for frequency-domain solutions of a two-dimensional cochlear model with a 1-DOF partition (19). When negative damping is incorporated in a 2-DOF partition model it is possible to achieve similar effects on frequency selectivity for time-domain solutions of a two-dimensional cochlear model. Model results based on this type of cochlear partition model are presented in chapter 5 and compared with direct measurements of basilar membrane displacement.

The model results in this dissertation are all based on the assumption of linear partition mechanics. Experimental research has established a definite nonlinear behavior of cochlear mechanics, which is probably due to nonlinear partition mechanics (4, 17, 3, 20). Although the time-domain model solution method described in chapter 3 of this dissertation allows for the incorporation of nonlinear

mechanical elements in the 2-DOF partition model (with or without negative damping), consideration of nonlinear 2-DOF partition mechanics is not a part of this dissertation. The subject of passive, nonlinear, 1-DOF partition mechanics in a two-dimensional model has recently been addressed by Matthews (21).

The major objective of this dissertation is to present a methodology for dealing with fourth-order partition dynamics in a cochlear model (which includes a middle ear model) in order to provide an improved tool for studying the biomechanics of the ear. This dissertation attempts to: (a) demonstrate a numerical procedure for implementing the 2-DOF partition (in both frequency and time domains) in the cochlear model, while maintaining bi-directional interaction with the middle ear and ear-canal sound pressure; (b) discuss the problems associated with choosing mechanical partition parameters from the greatly enlarged parameter space associated with the 2-DOF partition model; (c) illustrate the advantages of the 2-DOF partition model in providing a more detailed representation of cochlear morphology and better agreement between model solutions and experimental data.

2. BACKGROUND

The primary use of the mathematical model presented in this dissertation is to provide a description of cochlear partition motion in the mammalian cochlea. It is widely believed that the cochleas of all mammals function in a similar manner, since the cochleas of human, cat, guinea pig, and so on, are similar in anatomy and neural response. In order to understand human hearing, it is therefore useful to study other mammalian cochleas (13). The purpose of this chapter is to provide a proper context for the remainder of the dissertation. A brief description of the anatomy and physiology of the ear is followed by a review of relevant cochlear mechanical research. [The work of Viergever (15) was helpful in preparing the review of research.]

2.1 ANATOMY AND PHYSIOLOGY OF THE EAR

The anatomy of the ear is usually divided into three parts: the outer ear, the middle ear, and the inner ear. A sectional diagram of the human ear is shown in Figure 2.1. The outer ear consists of the pinna and the external auditory meatus or ear canal. The pinna is the exposed flap of skin on the side of the head and the ear canal is a short curved tube which leads inward from the pinna to the eardrum. The outer ear provides a protective interface to the environment and aids in the localization of sound sources. The middle ear apparatus lies in an air-filled cavity (tympanic cavity) just beyond the eardrum in the mastoid portion of the temporal bone. Acoustic vibrations of the eardrum are transmitted through the middle ear by means of three

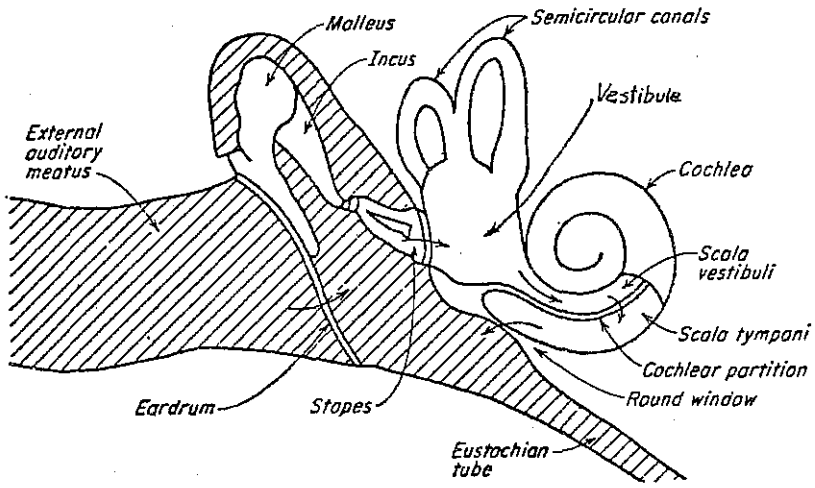

Figure 2.1. Sectional diagram of the ear. The arrows indicate the paths of sound. [Figure from von Békésy (1), after Helmholtz (22).]

small bones: the malleus, the incus, and the stapes. A passageway from the middle ear to the pharynx, called the auditory tube or eustachian tube, allows air pressure to be equalized across the eardrum. The middle ear provides mechanical impedance matching between the air vibration of the outer ear and the fluid vibration of the inner ear. The inner ear consists of the cochlea, the vestibule, and three semi-circular canals; these structures are communicating spaces within the petrous temporal bone. The semi-circular canals are oriented in three, orthogonal, spatial planes and serve the sense of spatial orientation. The cochlea is the primary receptor organ for hearing; it receives the acoustic signals delivered by the stapes and distributes sound information to the individual auditory nerve fibers (23).

The cochlea is a tapered tube coiled spirally and gets its name from its resemblance to the shell of a snail. The cochlear chamber is divided into three ducts by a thin bony shelf called the spiral lamina, by a stiff, gelatinous basilar membrane, and by a more compliant Reissner's membrane. Figure 2.2 shows a schematic cross-section of the cochlea and identifies the three cochlear ducts. The upper duct is called the scala vestibuli because it is continuous with the vestibule at its basal end. The lower duct is called the scala tympani because it is closer to the tympanic cavity. The scala tympani and scala vestibuli are filled with a liquid called perilymph and communicate with each other at the apical end of the cochlea through an opening called the helicotrema. The central duct, the scala media, is filled with a different liquid called endolymph, which

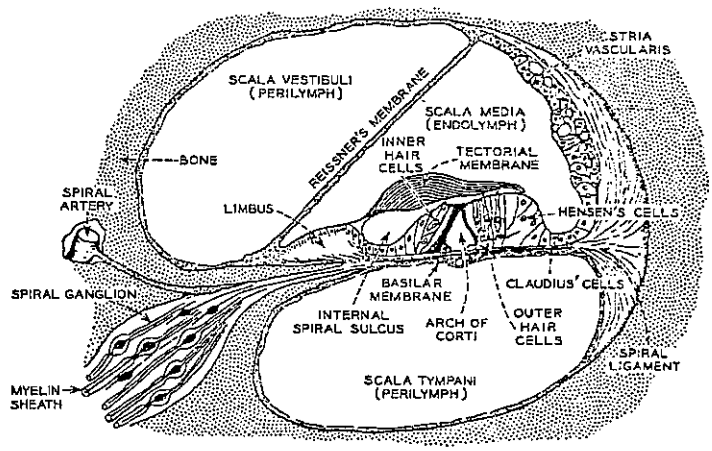

Figure 2.2. Schematic cross-section of the cochlear ducts. [Figure from Flanagan (24), adapted from Davis (25).]

provides nutrients to the sensory hair cells and has a different ionic composition than perilymph. Reissner's membrane provides a chemical barrier between scala media and scala vestibuli, but is probably not important mechanically (15).

In the outer wall of the vestibule, near the basal end of the scala vestibuli, is an opening to the middle ear called the oval window. The oval window is covered by the footplate of the stapes and an annular ligament. A corresponding opening in the bony outer wall of the scala tympani called the round window, is covered simply by a thin membrane.

The basilar membrane and spiral lamina extend from the vestibule to the helicotrema. The basilar membrane is mechanically tuned; it is stiff near the base and becomes progressively more compliant toward the apex. In human, the basilar membrane is about 35 mm long and tapers from a width of about 0.08 mm at the base to about 0.5 mm at the helicotrema; the helicotrema has an area of about 0.15 mm^2 (26).

The process of hearing begins with an acoustic signal in the vicinity of the ear which propagates through the air as a wave of alternating compression and rarefaction. The variation of air pressure in the ear canal causes the eardrum to vibrate. These vibrations are conveyed through the malleus and incus to the stapes. The motion of the footplate of the stapes produces a volume displacement of the cochlear fluid. Very slow vibrations of the stapes result in to-and-fro movement of the cochlear fluid through the helicotrema and higher frequency vibrations are transmitted through the yielding cochlear partition. In either case, the relative

incompressibility of the cochlear fluid forces a volume displacement of the round window which is equal to that initiated by the oval window. (1)

Within the cochlear partition and lying on the basilar membrane is the organ of Corti containing the final receptor cells, the hair cells. These hair cells are innervated by nerve fibers which originate in the spiral ganglion, which is located adjacent to the cochlea toward the axis of the cochlear spiral. The motion of the cochlear partition stimulates the hair cells by means of stereocilia, or tufts of hair, which protrude from the top of each hair cell (see Figure 2.3). The shearing motion between the basilar membrane and tectorial membrane will bend the (stereo-) cilia, create a corresponding intracellular potential change, and cause the release of synaptic vesicles in the vicinity of the afferent nerve fiber synapses (29).

2.2 REVIEW OF EXPERIMENTAL RESEARCH

Much of what we know today about the functioning of the ear is due to the experimental observations of von Békésy (1). His studies of animals, human cadavers and models began in 1928 and earned him a Nobel prize in 1961. von Békésy used light microscopy with stroboscopic illumination to measure the displacement of the cochlear partition in response to sinusoidal stimuli. Figure 2.4 shows a sample of von Békésy's results from a human cadaver cochlea. It should be noted that von Békésy was able to measure cochlear partition motion in two different ways; he could observe a fixed position as a function of frequency or fixed frequency as a function of place. The

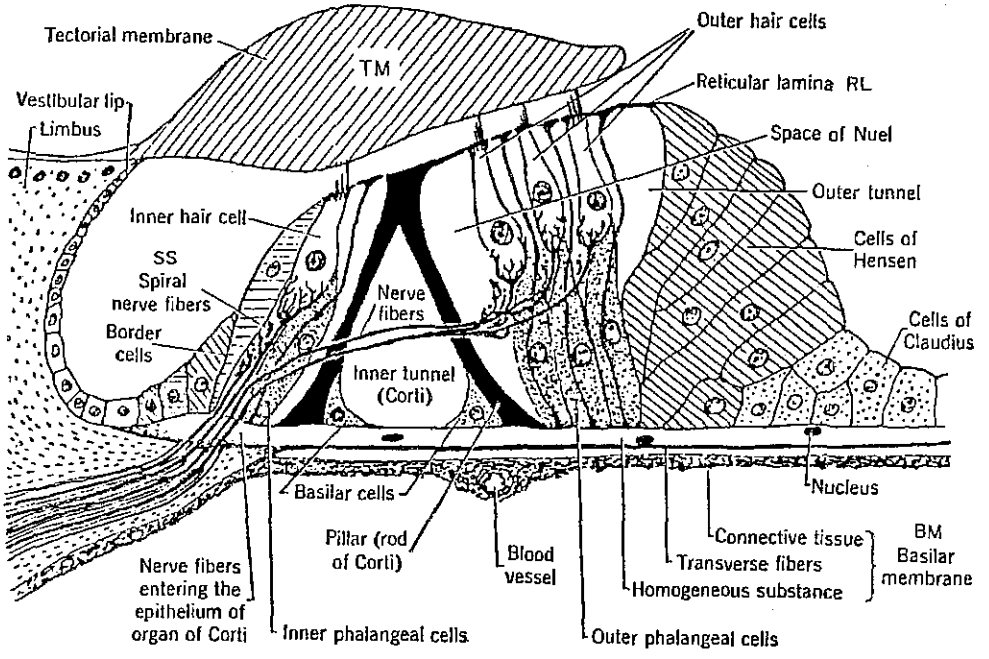

Figure 2.3. Cross-section of the organ of Corti. [Figure from Allen (27), adapted from Rasmussen (28).]

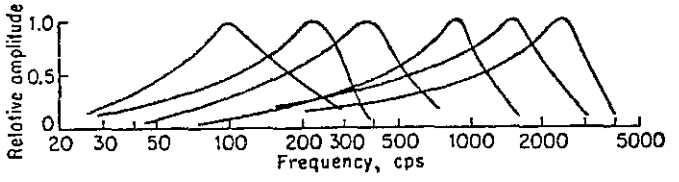

(a)

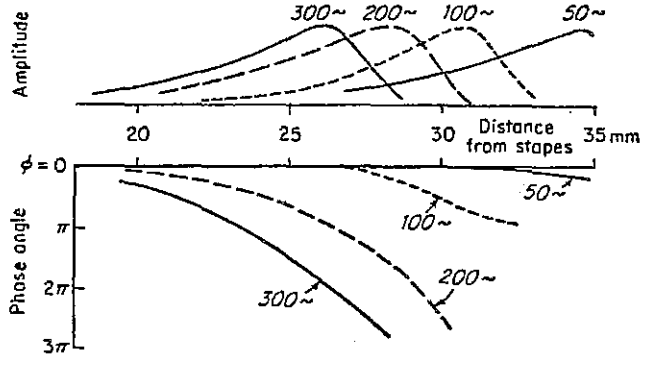

(b)

Figure 2.4. Vibration of the cochlear partition in human. Results of von Békésy's observations of basilar membrane displacement using stroboscopic illumination. (a) Relative amplitude of the displacement versus frequency at six positions. (b) Relative amplitude and phase of the displacement at four frequencies. [Figures from von Békésy (1).]

appearance of traveling waves in the motion of the cochlear partition in response to sinusoidal stimulation was a characteristic feature of von Békésy's observations. These waves travel from the base to the apex with increasing amplitude. At a certain point the amplitude of the wave reaches a maximum and the wave is rapidly attenuated beyond that point. The location of the maximum (called the characteristic place) varies with frequency; high frequency waves travel only a short distance along the partition and low frequency waves travel further toward the helicotrema.

The application of the Mössbauer technique to the measurement of cochlear partition motion was a great improvement over visual observations. In the Mössbauer technique a tiny gamma-emitter is placed on the basilar membrane (or other moving structure) and a stationary absorber with a scintillation counter is placed in its vicinity. The velocity of the emitter relative to the absorber causes a Doppler shift in the frequency of the gamma rays. The high sensitivity of the absorber to frequency shifts permits measurement of velocities as small as 0.1 mm/sec (30). The Mössbauer technique has been used for in vivo measurements of basilar membrane motion by Johnstone and Boyle in guinea pig (31), by Rhode in squirrel monkey (3), and by Helfenstein in cat (32).

An example of Rhode's Mössbauer measurements are shown in Figure 2.5. The amplitude and phase of the basilar membrane displacement are shown relative to malleus displacement for a fixed place on the basilar membrane as a function of frequency. Rhode's data typically show amplitude curves which have a sharper peak and larger phase lags

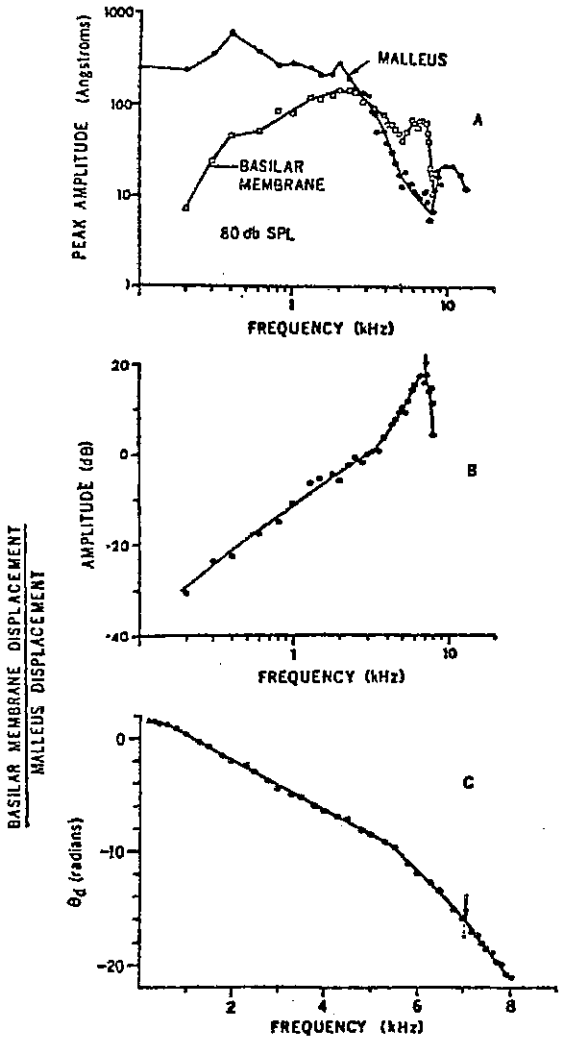

Figure 2.5. Mössbauer measurements of basilar membrane displacement in squirrel monkey. Rhode's experimental results using the Mössbauer technique in a living squirrel monkey. (a) Amplitude of malleus displacement and basilar membrane displacement versus frequency at a stimulus intensity of 80 dB SPL. (b) and (c) Amplitude and phase of the ratio of basilar membrane displacement to malleus displacement as a function of frequency. [Figure from Rhode (3), animal 70-15.]

than observed by other experimenters. Another important aspect of Rhode's data is the nonlinearity observed in basilar membrane motion at frequencies near the peak with respect to changes in stimulus intensity (see Figure 2.6). Both the sharp amplitude peak and nonlinearity were physiologically vulnerable; these features were not observed in postmortem animals (33). Figure 2.7 compares basilar membrane response in a squirrel monkey before and after death; the peak of the magnitude of the postmortem response is substantially less than that of the antemortem response.

Wilson and Johnstone used a capacitive probe technique to measure basilar membrane motion in guinea pig (34, 35). The capacitive probe is a thin metal rod which is connected to a source of radio frequency current. The perilymph is drained from the scala tympani and the probe is placed very near to the basilar membrane. The changing separation between the basilar membrane and the tip of the probe causes a corresponding variation in the capacitance of the probe and modulates the amplitude of the radio frequency signal. Wilson and Johnstone's data show less prominent amplitude peaks (see Figure 2.8) than those observed by Rhode and the motion of the basilar membrane was linear from 40 to 110 dB SPL. (The notation SPL indicates sound pressure level relative to the level of a 1 kHz tone which is just audible. The reference level has been standardized internationally to 20 μPa rms = 2×10^{-7} N/m^2 rms.)

Le Page and Johnstone (20) used an improved capacitive probe technique to measure basilar membrane motion. Their data show the same type of nonlinearity in the guinea pig as Rhode had observed in

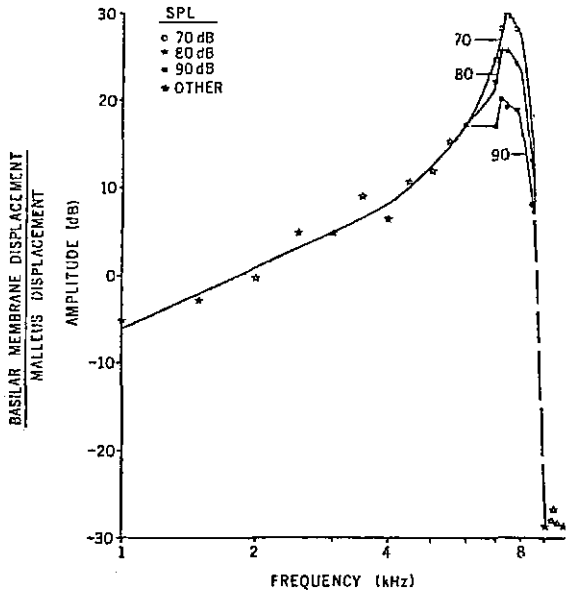

Figure 2.6. Basilar membrane displacement in squirrel monkey at three stimulus intensities. Amplitude of the ratio of basilar membrane displacement to malleus displacement at 70, 80, and 90 dB SPL. [Figure from Rhode (3), animal 69-473.]

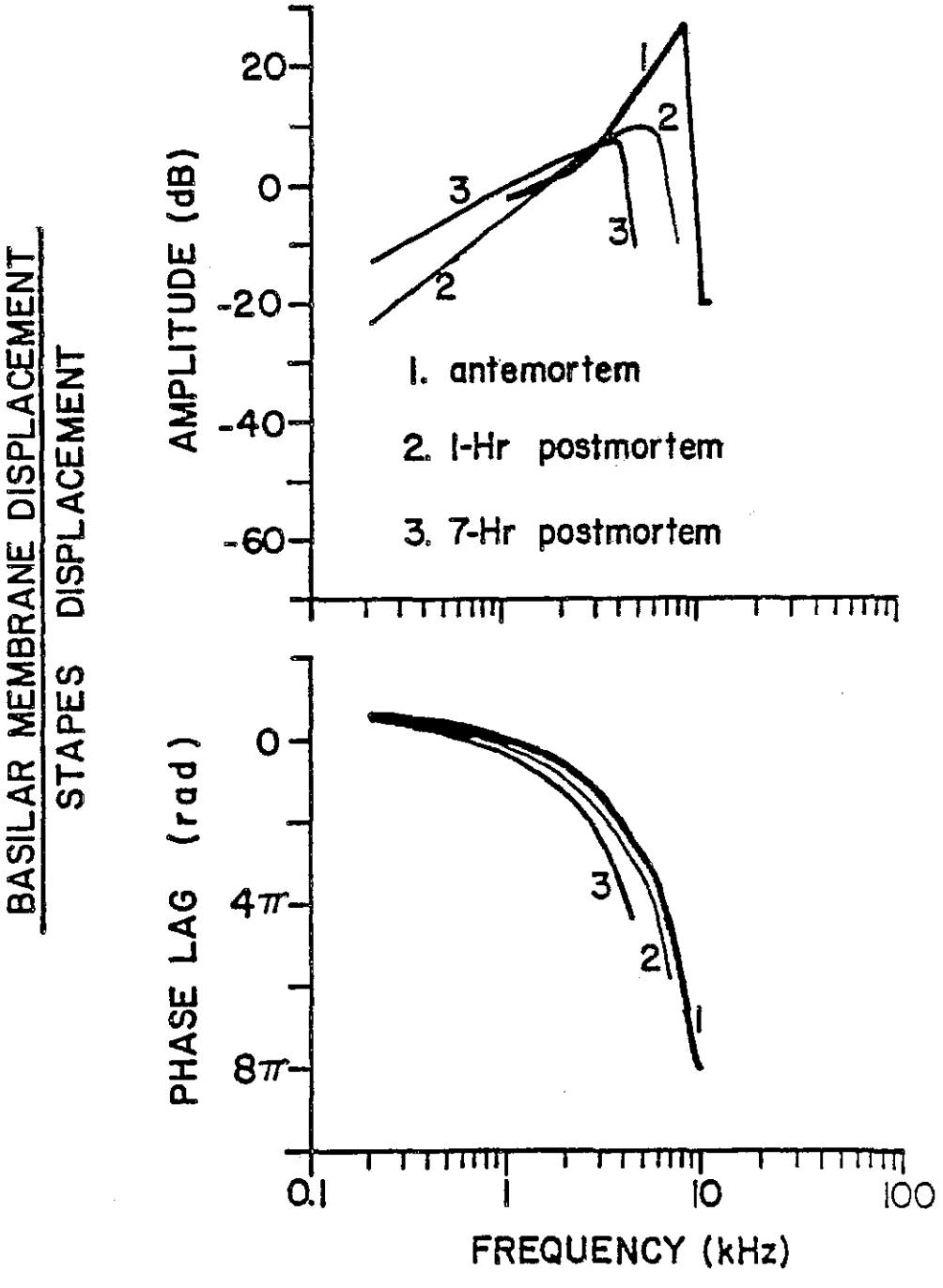

Figure 2.7. Basilar membrane displacement in squirrel monkey before and after death. Curves are based on data from living squirrel monkey, one hour postmortem, and seven hours postmortem. [Figure from Kim et al. (19), adapted from Rhode (33), animal 72-314.]

(a)

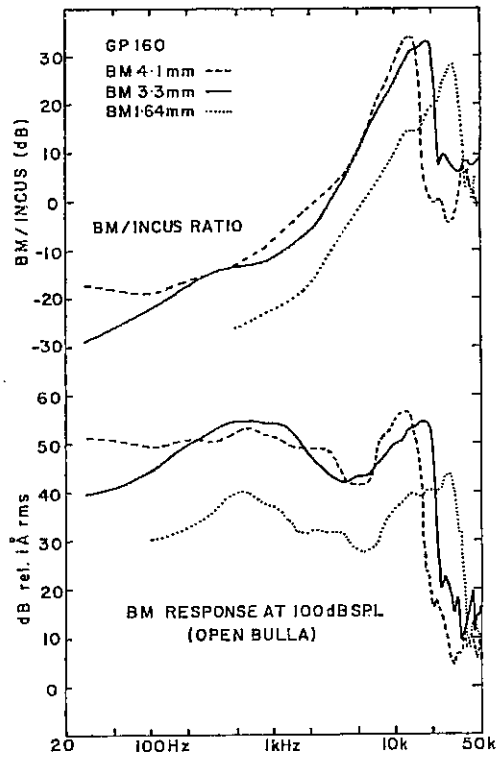

(b)

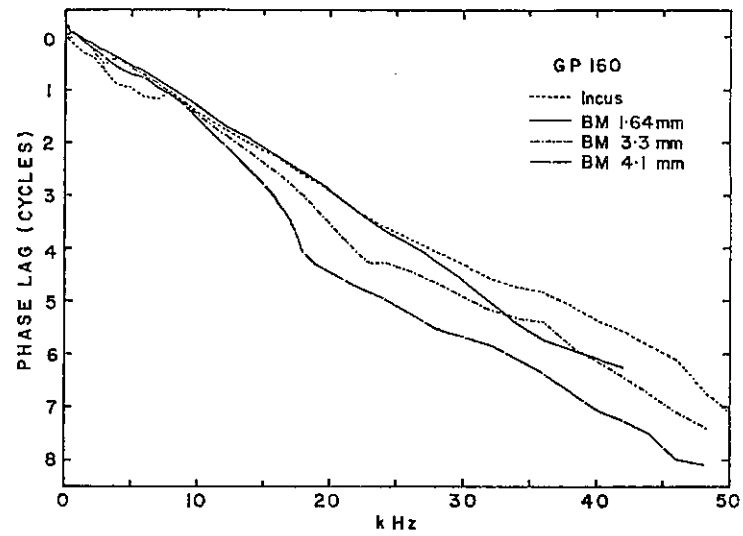

Figure 2.8. Capacitive probe measurements of basilar membrane motion in guinea pig. (a) Amplitude of the ratio of basilar membrane displacement to incus displacement and amplitude of basilar membrane RMS displacement re 1 angstrom, both as a function of frequency. (b) Phase of basilar membrane displacement and incus displacement relative to the stimulus. [Figures from Wilson and Johnstone, (35).]

the squirrel monkey. Again, the nonlinearity was contingent on the physiological integrity of the cochlea.

Kohllöffel (36, 37, 38) used an optical technique to measure basilar membrane motion based on detecting the "fuzziness" of laser illumination. Due to its coherence, the laser light reflected from various parts of the basilar membrane interferes on the retina and gives the membrane a speckled appearance. If the membrane vibrates with sufficient amplitude the individual specks lose their sharpness and become fuzzy. Kohllöffel's in vivo measurements in guinea pig generally agree with those of Wilson and Johnstone. In postmortem observations, Kohllöffel observed a basal shift of the characteristic place and a flatter amplitude peak as compared to the living animal (37), consistent with Rhode's observations in the squirrel monkey (33).

There are several other experimentally observable physiological responses which can provide objective, but indirect, information about cochlear partition motion. A micro-electrode can be inserted into one of the sensory hair cells to monitor the intracellular potential changes due to cochlear partition motion (39). There are electrical, stimulus-frequency signals present in the fluid of the cochlear ducts called cochlear microphonics (40). A miniature pressure probe can be used to measure the pressure difference across the basilar membrane at a fixed position as a function of frequency (41). Measurement of the discharge rates of single auditory nerve fibers provides an indication of the motion of the cochlear partition at the place that the fiber synapses with a hair cell (e.g. 42). The sound pressure in the ear

canal contains both spontaneous and evoked acoustic emissions which apparently have their origin in the motion of the cochlear partition.

Russel and Sellick (39) observed intracellular potentials of inner hair cells in guinea pig and found that isoamplitude curves for the DC response component of the receptor potential were "indistinguishable from threshold tuning curves for auditory nerve fibers". Their experimental observations led them to conclude that this sharp tuning is due to "mechanical properties of the cochlear partition".

The threshold tuning curve is one of the best known measures of single nerve fiber responses. Figure 2.9 shows a collection of cat neural tuning curves from Kiang and Moxon (42). These curves show the stimulus intensity necessary to produce a criterion increase in the nerve spike discharge rate over the spontaneous rate. The data for each curve is obtained from a single nerve fiber as a function of frequency. [Pfeiffer and Molnar (43), Littlefield (44), and Allen (13) have obtained similar tuning curves together with corresponding phase information.]

Another useful measure of single nerve fiber responses was reported by Kim, Siegel and Molnar (4) and is shown in Figure 2.10. These curves show the amplitude and phase of the stimulus-frequency component of the single nerve fiber response relative to the spontaneous rate of the nerve fiber. The data for each curve is obtained from many individual nerve fibers in one cat for a fixed stimulus frequency; the horizontal axis indicates the characteristic frequency of the nerve fibers. An independent determination of a

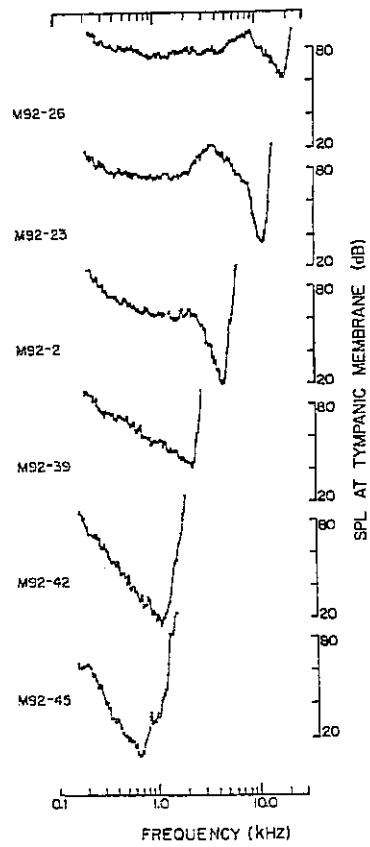

Figure 2.9. Single nerve fiber tuning curves in cat. These tuning curves indicate the "threshold" of neural response as a function of frequency for six auditory nerve fibers, each with a different characteristic frequency. [Figure from Kiang and Moxon (42).]

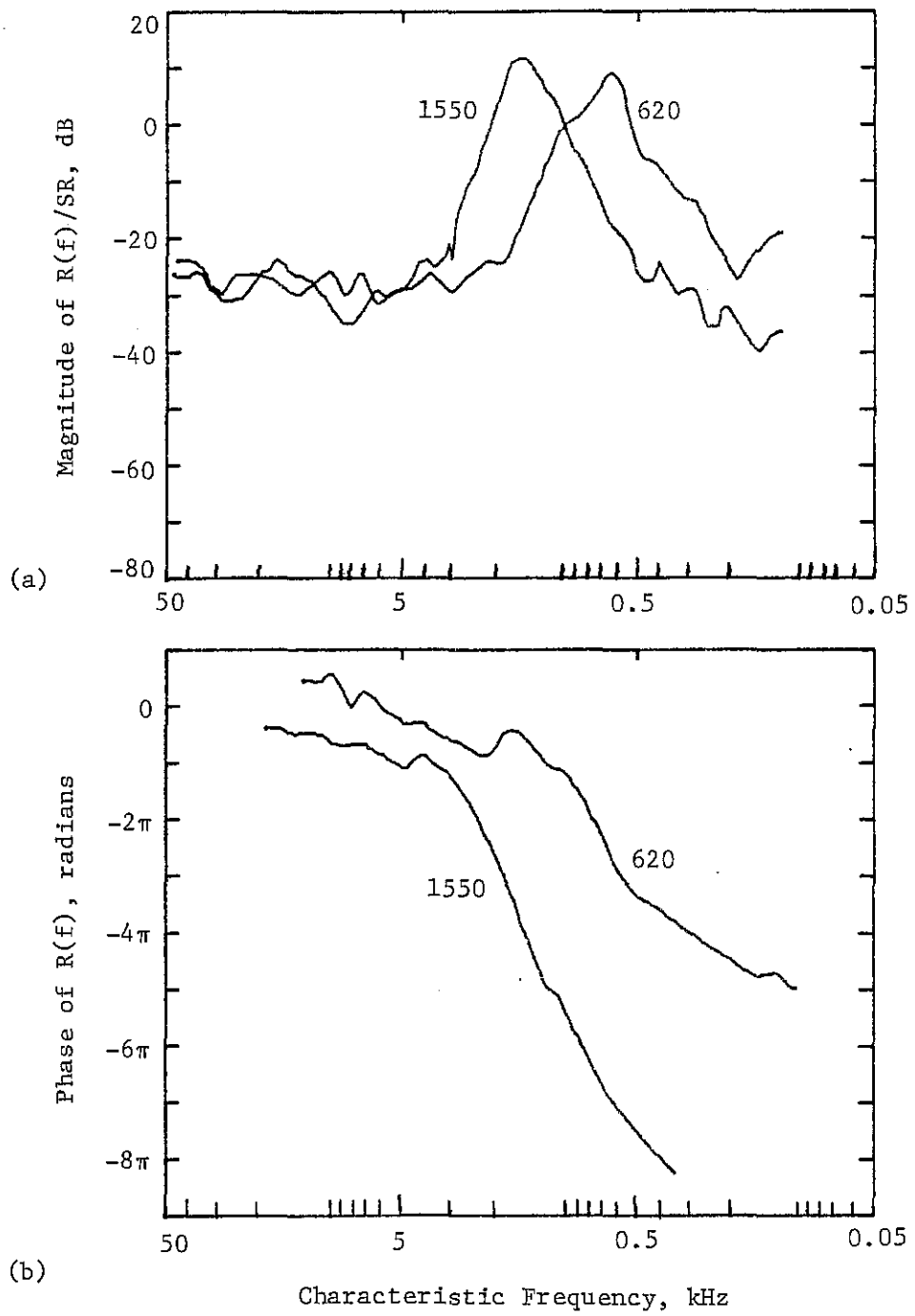

Figure 2.10. Single-tone neural responses in cat as a function of characteristic frequency of the nerve fiber. The curves are based on data indicating the response of many cochlear nerve fibers in one cat. The numerals indicate the stimulus frequency in Hz. The 620 Hz curve represents data obtained with stimulus intensities of both 15 dB SPL and 45 dB SPL combined. The 1550 Hz curve represents data obtained with a stimulus intensity of 20 dB SPL. [Figure redrawn from Kim et al. (4).]

cochlear frequency-to-place map (45) was used to associate the characteristic frequency with position along the cochlear partition. Thus, the data shown in Figure 2.10 can be considered to represent a measure of neural response as a function of place on the cochlear partition.

Evans and Wilson (9) measured basilar membrane and neural tuning curves "concurrently" in a guinea pig. They found sharp neural tuning before and after measuring broad basilar membrane tuning, indicating a significant discrepancy between these two tuning curves. This observation supports the existence of some sort of "second-filter" in the cochlear partition which provides additional sharpening prior to excitation of the nerve fiber. The concept of a "second-filter" will be discussed further in section 2.3.

The "evoked cochlear mechanical response" (ECMR) observed by Kemp in the ear canal provides indirect evidence of the mechanical frequency analyzing properties of the cochlea (17). For a wideband click stimulus the ECMR appears to be a delayed reflection of the stimulus, with low frequencies being delayed more than high frequencies. Figure 2.11 shows a tuning curve obtained by determining the amplitude of a continuous masking tone necessary to suppress a given frequency component of the transient ECMR. The sharpness of the ECMR-derived tuning curve is comparable to psychophysical or single nerve fiber data.

Spontaneous acoustic emissions from the cochlea are believed to be present in a significant percentage of normal human ears (47, 48). Zurek (48) obtained objective iso-suppression tuning curves on a

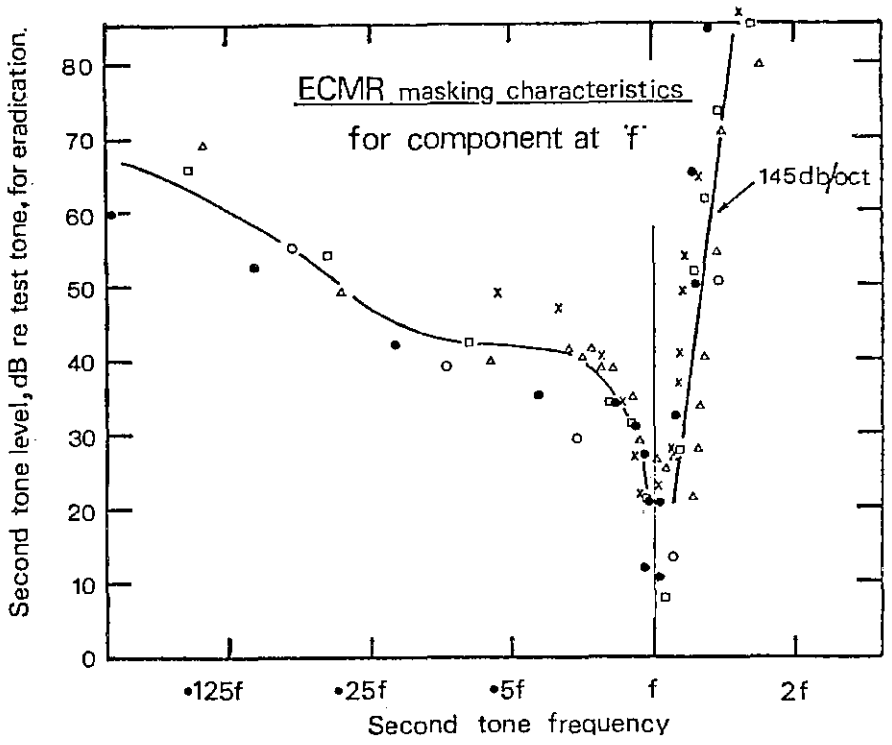

Figure 2.11. ECMR-derived tuning curve from a human subject. The level of a continuous masking tone of variable frequency was adjusted in level so as to just suppress a fixed frequency component of the transient ECMR. Data from 3 ears at 5 different ECMR frequencies between 1270 and 2210 Hz are shown. The selectivity demonstrated matches psychophysically derived tuning curves. [Figure and caption from Kemp (46).]

spontaneously emitted tone and found that contours of constant suppression exhibit frequency selectivity "like that commonly associated with cochlear frequency analysis". Similar spontaneous emissions are not normally present in chinchilla, but can be induced by noise exposure (49).

2.3 REVIEW OF MODELING RESEARCH

Research in cochlear mechanics has made use of both physical and mathematical models of the cochlea. Physical models include hydromechanical scale models (1, 50, 51) and electrical analogs of the cochlea (52). Mathematical models of the cochlea (such as the one utilized in this dissertation) are based on physical principles and have provided analytical insights and numerical simulations.

Around 1950, one-dimensional mathematical models of the cochlea were helpful in establishing the traveling-wave character of basilar membrane motion. The single, spatial dimension of the one-dimensional models corresponds with the length of the cochlear partition from base to apex. Usually, the type of model solutions being sought were steady-state responses of the cochlea to sinusoidal excitation. If the mechanics of the cochlea are assumed to be linear, then the mathematical model can be reformulated in such a way that the time-dependence is replaced by a frequency-dependence. This often leads to simplification of the mathematical problem, especially when the solutions of interest contain only a single frequency. The one-dimensional models of Zwislocki (53), Peterson and Bogert (54), Fletcher, (55), and Zweig et al. (56) assume that, for a given frequency, the wavelength of basilar membrane motion is long compared

to the height of the cochlear ducts. The long-wave models are able to reproduce the experimental observation of a traveling wave which reaches a maximum amplitude at a characteristic place; unfortunately, experimental data indicates that the long-wave assumption is not valid in the vicinity of the characteristic place. In order to find model solutions which were valid in this important region, Ranke (57), developed a short-wave, one-dimensional model which assumed that the cochlear ducts were much taller than a wavelength of basilar membrane motion. Inspite of the dilemma of choosing between short-wave and long-wave theories, the one-dimensional models still provide useful insight into cochlear mechanics.

Two-dimensional models can reproduce both long-wave and short-wave behavior, but are more difficult to deal with mathematically. Ranke (57) was probably the first to formulate a two-dimensional mathematical model of the cochlea. He emphasized that the velocity of the fluid perpendicular to the basilar membrane could not be neglected near the place of maximum amplitude. Complete solutions for two-dimensional models, however, required the development of improved numerical solution methods and the availability of modern digital computers.

In 1972 Lesser and Berkley described and obtained numerical solutions for a two-dimensional model of the cochlea (58). The two-dimensional model proposed by Lesser and Berkley is essentially the same as the one used in this dissertation. With the assumption that the cochlear fluids are incompressible and inviscid, the mathematical problem reduces to solving Laplace's equation in a

rectangle. Analytic solutions are not possible because of the type of boundary condition necessary to represent the cochlear partition. (See chapter 3 for a more complete description of the two-dimensional model.) Lesser and Berkley used a Fourier series approach to obtain numerical, frequency-domain solutions for the model; however, their results were limited and highly sensitive to computational errors (59).

In 1973 Lien (60) described a three-dimensional model of the cochlea which retained fluid viscosity. He used a Green's function approach to obtain an integral equation formulation of the mathematical problem. However, before obtaining numerical solutions, Lien was forced to make analytical approximations which essentially reduced the mathematical representation to that of a one-dimensional model.

Allen (59) used a Green's function approach to obtain an integral equation formulation for the two-dimensional cochlear model of Lesser and Berkley. He was able to obtain frequency-domain solutions for the model by evaluating the integral equation numerically. Sondhi (61) derived an analytic expression for Allen's Green's function and showed how solutions to the integral equation could be approximated by a set of coupled, second-order differential equations.

Other, more direct numerical solution methods for the two-dimensional model have also been developed. The finite-difference method used by Neely (62, 63) retains a two-dimensional representation of fluid pressure and discretizes Laplace's equation directly. The analysis and computation required by the finite-difference method are

substantially less than required by Allen's integral equation method for comparable accuracy. Viergever (15) used a finite-element method to obtain numerical solutions for the two-dimensional model. The finite-element method is similar to the finite-difference method in that they both retain a two-dimensional pressure representation after the spatial dimensions have been discretized. Viergever (15) has compared model results obtained with the finite-difference and finite-element methods.

Steele and Taber (64) used a WKB-approximation to obtain numerical solutions for a two-dimensional, frequency-domain model. Their approach involves the solution of a transcendental equation at many discrete points along the cochlear partition to determine the "local wavelength" of the solution at each point. With this information, one can identify the long-wave region, the short-wave region, the region of exponential decay (no waves), and the transitions between these regions. The WKB method has the restriction that the "local wavelength" of the cochlear traveling-wave must be slowly varying with distance from the stapes. [See Viergever (15) for a discussion of the validity of the WKB method.]

Some limited cochlear model results have been reported for three-dimensional cochlear models. Steele and Taber (65, 66, 67) have adapted their WKB solution method to obtain approximate solutions to a three-dimensional model. de Boer (68) has used an alternative approach to obtain numerical results for a three-dimensional, frequency-domain model. His solution method requires that the basilar membrane impedance have some mathematically tractable form.

Time-domain solutions of one-dimensional cochlear models have been used in studies of cochlear nonlinearities by Kim et al. (69), Hall (70), and others. Time-domain solutions of the two-dimensional model are also of interest. Allen and Sondhi (14) have developed a time-domain solution method for Allen's integral equation and used it to obtain transient solutions of the two-dimensional model in response to impulsive stimuli. Matthews (21) used a similar time-domain solution method to investigate steady-state responses of the two-dimensional model with non-linear damping in the cochlear partition. These time-domain solution methods represent time in discrete steps and require that a spatial boundary-value problem be solved at each step in time.

2.4 THEORIES OF COCHLEAR MECHANICS

Experimental observations and mathematical models of the cochlea have evolved together and complement each other in providing insight into the mechanical signal processing capabilities of the cochlea. The two-dimensional representation of cochlear fluid-mechanics of the type proposed by Lesser and Berkley (58) appears to be adequate for our current level of understanding of cochlear mechanics (15). At this time, the most controversial cochlear mechanical issues are related to the "micromechanics" of the cochlear partition.

In recent years, there has been much argument about the linearity of cochlear partition mechanics. It now appears that there is convincing evidence that (at least in some mammals) the cochlea responds to sounds of normal intensity in a nonlinear manner and that this nonlinearity is present and observable in the motion of the

cochlear partition (4, 17, 3, 20). Recently, Matthews has provided modeling support for the presence of partition nonlinearities with a two-dimensional cochlear model.

Another question of long-standing controversy is whether basilar membrane motion is as sharply tuned as single nerve-fiber responses. Direct measurements of basilar membrane motion have typically shown tuning which is much broader than the tuning of nerve fiber discharge rate. A traditional view has been that a broadly-tuned response of the basilar membrane drives a sharply-tuned "second-filter" leading to sharp neural tuning (8). A large number of models have been put forth in an attempt to explain the discrepancy between basilar membrane and neural frequency selectivity; some of these models propose that the increased selectivity is achieved mechanically by some sort of mechanical "second-filter" (71, 72, 73, 10, 12). On the other hand, experimental observations of the nonlinearity and physiological vulnerability of cochlear response (6, 4, 5) suggest that the invasive procedure and high intensity stimulus required by any direct observation of cochlear partition motion, could significantly degrade the signal processing performance of the cochlea. Consequently, the "normal" state of the cochlea might be capable of much sharper basilar membrane tuning than any direct experimental measurements would ever indicate.

Evans and Wilson have argued that the experimental evidence points toward a second-filter being interposed between basilar membrane motion and neural excitation (8, 9). Zwislocki and Kletsky (11, 2, 10) have described several means by which hair cell shearing

might be more sharply tuned than basilar membrane motion. The sharpening mechanisms postulated by Zwislocki and Kletsky require that the tectorial membrane have some special property, such as longitudinal stiffness or loose attachment to the spiral limbus. Allen (27) observed that much of the discrepancy between model solutions for partition displacement and experimental neural response data could be resolved by invoking a second-filter which has a "spectral zero" in its transfer function, about an octave below the characteristic frequency. He showed how a combined tuning of both the tectorial membrane and the basilar membrane could provide a physiological basis for this type of second-filter (12).

From anatomical and physical considerations one might expect that the viscous damping of the cochlear partition is too large to be compatible with the degree of resonance required for sharp tuning of the basilar membrane. In 1948, Gold (16) suggested that the biochemical energy available within the cochlear partition might be utilized mechanically to counteract the viscous damping. This idea led to consideration of the presence of some "active" mechanism in the cochlear partition, capable of producing mechanical energy at the expense of metabolic energy.

There has been a renewed interest in active cochlear mechanisms in the past two years because of the evoked cochlear mechanical responses observed by Kemp in ear canal sound pressure (17). Kemp's interpretation of the evoked cochlear mechanical responses which he observed (commonly called cochlear echoes) is that they are the result of reflection of individual frequency components at their

characteristic places on the cochlear partition. Kemp suggests that there is likely to be an active mechanism within the cochlear partition which is capable of producing mechanical energy, such that "the stimulated release of mechanical energy by the transduction mechanism onto the basilar membrane may serve to locally modify wave propagation parameters." An abrupt change in wave propagation parameters with respect to distance along the cochlear partition would, presumably, cause the traveling wave to be reflected. The ECMR-hypothesis is that: "Acoustic excitation of the healthy ear evokes an active mechanical response within the cochlea which results in re-emission of sound from the ear" (18). Another possible consequence of this active mechanism, according to Kemp (17), is that "useful wave amplification by stimulated mechanical energy release might occur, perhaps contributing to the enhancement of cochlear mechanical tuning." [See Kim et al. (19).] Present knowledge of the physiology of the cochlear partition is still insufficient to make any conclusions about the physical basis of this active mechanism; Kemp (17) speculates that one of the functions of the outer hair cells may be the generation of this mechanical energy.

2.5 TRADITIONAL 1-DOF PARTITION

In previous models of the cochlea, the cochlear partition is usually assumed to behave as a simple mechanical resonator (with mass, spring and damper) at each point along its length and, furthermore, is assumed to have no direct coupling between adjacent points (54, 58, 60, 59, 62, 15). This type of cochlear partition has one mechanical

degree-of-freedom (1-DOF) at each position, which is associated with vertical displacement of the basilar membrane. It is generally accepted that displacement of the basilar membrane (BM) causes a sliding motion between the tectorial membrane (TM) and the reticular lamina (RL) (74) (see Figure 2.3). The cochlear partition representation described in this section has only 1-DOF at each position and includes a shearing displacement of RL relative to TM; this 1-DOF model will be referred to in the remainder of the dissertation as the traditional 1-DOF partition since it represents generally accepted and previously used concepts.

Rhode and Geisler (74) studied the displacement between opposing points on TM and RL for an assumed model of the cochlear partition (see Figure 2.12). They made specific assumptions about the way in which BM deflection might cause a sliding motion between TM and RL:

> It is assumed that vertical displacement of the basilar membrane results in rotation of the organ of Corti about a pivot near the foot of the inner pillars and also causes the rotation of the tectorial membrane about the edge of the limbus. Because there are two different axes of rotation, sliding motion occurs between the tectorial membrane and the organ of Corti. Therefore, when the basilar membrane is deflected, a point on the underside of the tectorial membrane will move relative to an opposing point on the reticular lamina. Explicitly, we assume that the tectorial membrane is rigid and always touches the reticular lamina. Further, we assume that the complex consisting of the pillars and the reticular lamina is rigid and is rigidly attached to the basilar membrane.

Rhode and Geisler found an exact relationship between "opposing point displacement" and "vertical displacement of the basilar membrane" based on the above assumptions. Numerical results based on the morphology of a cat cochlea showed that the exact relationship was in good agreement with a linear relationship. Their numerical results

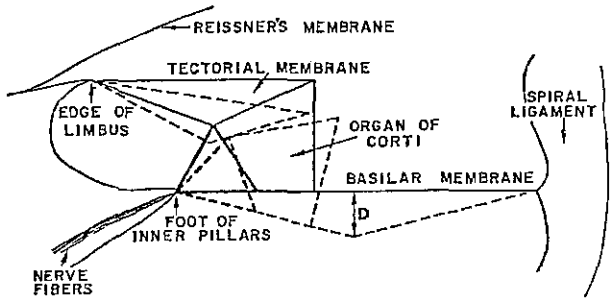

Figure 2.12. Schematic diagram of deflection of the cochlear partition. Diagram shows the deflections of the organ of Corti and the tectorial membrane caused by a deflection of the basilar membrane according to a model proposed by Rhode and Geisler. [Figure from Rhode and Geisler (74).]

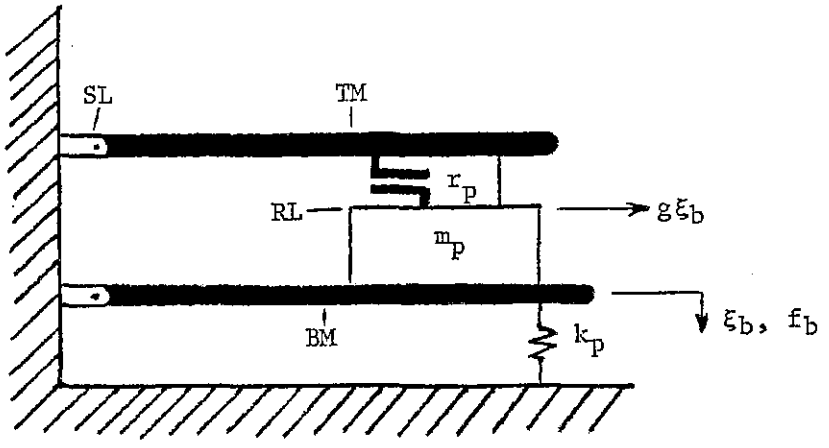

Figure 2.13. Schematic diagram of a simple mechanical system with 1-DOF representing the cochlear partition. Two levers represent the basilar membrane (BM) and tectorial membrane (TM). Lateral displacement of the reticular lamina (RL) is proportional to vertical displacement of BM ξ_b, where g is the shear lever gain. Separation between RL and TM is assumed to be constant. TM is rigid and is hinged at the spiral limbus (SL). The force f_b, mass m_p, damping r_p, and stiffness k_p are described in the text.

led them to suggest that the particular assumptions made about the motions of the structures were not critical.

Figure 2.13 shows a schematic diagram of a simple mechanical model which represents the traditional 1-DOF cochlear partition. A physical interpretation of this model requires essentially the same assumptions made by Rhode and Geisler regarding motions of the structures. The basilar membrane (BM) and tectorial membrane (TM) are shown as rigid levers. The lateral displacement of the reticular lamina (RL) is assumed to be proportional to vertical displacements of BM (since the motions of interest are extremely small compared to the width of the basilar membrane). The shear lever gain g is determined from the morphology of the cochlear partition cross-section (74). The separation between RL and TM is assumed to be constant. (Some constraint of this sort is required in order to restrict the model to only 1-DOF.) The fluid pressure difference across BM creates a force (per unit length) f_b which is applied to the BM lever at the same place where BM displacement ξ_b is measured. Riding on the BM lever is a lumped mass (per unit length) m_p which represents the total mass of a cochlear partition cross-section. Vertical motion of the BM lever causes a shearing motion between TM and RL. This motion is opposed by the bending stiffness of the partition k_p and the viscous damping r_p due to fluid in the sub-tectorial space.

The various assumptions outlined above are used to derive a mathematical description for this model of the cochlear partition. The equation of motion for the traditional 1-DOF cochlear partition model is:

$$f_b = m_p \ddot{\xi}_b + g^2 r_p \dot{\xi}_b + k_p \xi_b \ . \qquad (2.1)$$

The 2-DOF cochlear partition models presented in this dissertation will be introduced as extensions to the traditional 1-DOF cochlear partition model.

3. TWO-DIMENSIONAL COCHLEAR MODEL

The modeling procedure used to obtain the model results presented in this dissertation required the application of assumptions and algorithms which were chosen according to various modeling objectives. This chapter describes the two-dimensional cochlear model at various stages in the modeling procedure. The identification of mathematical modeling stages (as shown in Figure 3.1) is useful in illustrating the relationship between frequency-domain results and time-domain results and in dealing with questions such as the uniqueness or stability of model solutions.

3.1 CONCEPTUAL MODEL

A conceptual model is an idealized approximation to a physical system which retains features and behaviors of the physical system that are of interest to the model designer. Conceptual models are useful for subjective analysis of the physical system, or as a precursor to a mathematical model.

Some simplifying assumptions must be made in order to arrive at a conceptual model of the cochlea which, in a subsequent stage, will be mathematically tractable. The set of assumptions used to derive the two-dimensional cochlear model are presented in this section. The choice of assumptions represents a compromise between resemblance to reality and mathematical feasibility. The primary modeling objective is to provide increased understanding of the behavior of the cochlea through "physical intuition" and model simulation. In designing a cochlear model, the major emphasis is on simulating realistic motion

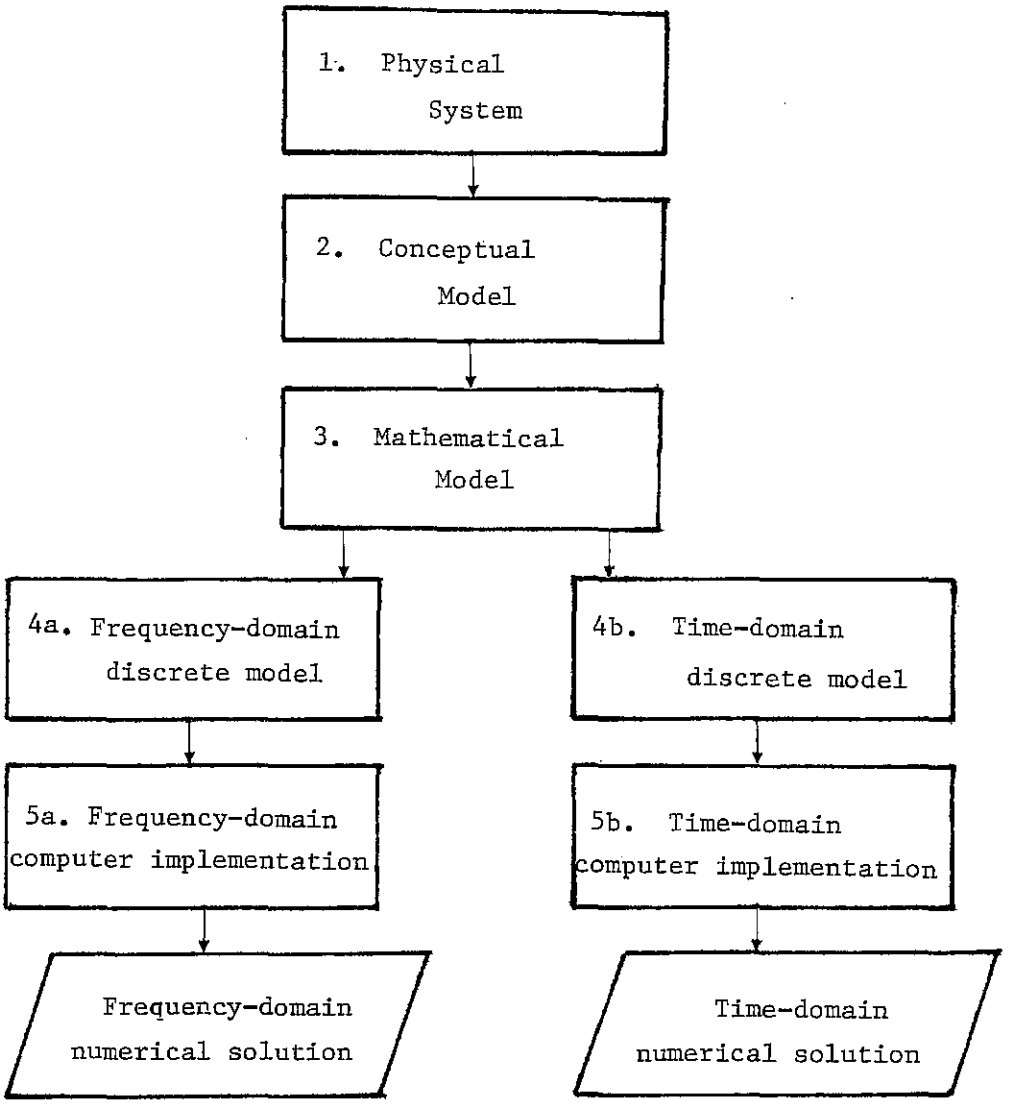

Figure 3.1. Block diagram of the stages of the modeling procedure.

of the cochlear partition. The conceptual model discussed in this section closely follows the previous work of Lesser and Berkley (58), Lien (60), Allen (59), Matthews (21), and Viergever (15).

The conceptual model of the cochlea is assumed to have the following physical properties:

a. The cochlear chamber is assumed to be an isolated cavity with rigid boundaries, except for the oval window and round window.

b. The spiral coiling of the cochlea is ignored.

c. The presence of Reissner's membrane is neglected; The cochlear chamber has two scalae which are separated by the cochlear partition.

d. The cross-sectional areas of the cochlear scalae are equal and constant along the length of the cochlea.

e. The oval and round windows coincide with the basal ends of the cochlear scalae, have the same cross-sectional area as the cochlear scalae, and move as pistons.

f. All motion within the cochlea is small compared to the dimensions of the cochlear scalae; the geometry of the cochlear scalae does not change with time.

g. The fluid is incompressible.

h. The fluid behaves linearly.

i. The fluid is inviscid.

j. The fluid flow is two-dimensional.

k. The cochlear partition has motion only perpendicular to its resting plane, has an "effective" width which is constant along its length, and has no mechanical coupling between adjacent longitudinal sections, except through the fluid.

l. The cochlear partition moves linearly in response to fluid pressure differences across its upper and lower surfaces.

m. Each point on the cochlear partition behaves as a simple mechanical system with two degrees-of-freedom.

Each of these assumptions is discussed briefly in the following paragraphs.

a. The actual cochlea is not completely isolated from surrounding structures; at the basal end of the cochlea there are several fluid "leaks" which enable the cochlear fluids, both perilymph and endolymph, to mix with the fluids of nearby spaces. In the model, the vestibule, the endolymphatic duct, and the perilymphatic duct are ignored. The extent to which the cochlear fluids flow out of the actual cochlea can be judged experimentally by observing the relative displacement of the round window in response to displacements of the stapes. von Békésy found volume displacements at the oval and round windows in a human temporal bone to be approximately equal (1); this result suggests that the flow of cochlear fluid into other spaces is negligible. The presence of the vestibule and the vestibular organ may have an effect on cochlear mechanics, but the effect should be limited to high frequencies and influence only the response near the basal end of the cochlear partition. (15)

b. The functional significance of the spiral coiling of the cochlea (found only in mammals) is not known. Primitive animal species have a hearing organ in the form of a straight or slightly bent tube, e.g. birds and a very primitive mammal, the platypus (1). The assumption that the spiral coiling has negligible influence on the mechanics of hearing is supported by the work of Viergever (15) who has formulated a mathematical model for a spiral-shaped cochlea; his approximate analysis leads him to the conclusion that basilar membrane motion is only slightly affected by the spiral.

c. Reissner's membrane is very thin and much more flexible than the basilar membrane, according to the experimental measurements of von Békésy (1). The main function of Reissner's membrane is probably that of an ionic barrier between the perilymph in scala vestibuli and the endolymph in scala media (15). The cochlear partition in the model is intended to represent the organ of Corti including the basilar membrane and the tectorial membrane.

d. Experimental measurements of the cross-sectional areas of the cochlear scalae in human show that scala vestibuli and scala tympani have approximately equal cross-sectional areas and that the areas are approximately constant along the length of the cochlea, except at the basal end (see Figure 3.2) (26). The scala media has a significantly smaller cross-sectional area which is also approximately constant along its length. The assumption that the cochlear scalae have constant cross-sectional areas allows the two-dimensional model to take the form of a simple rectangle. The assumption that the two scalae are of equal size makes the model geometrically symmetric about

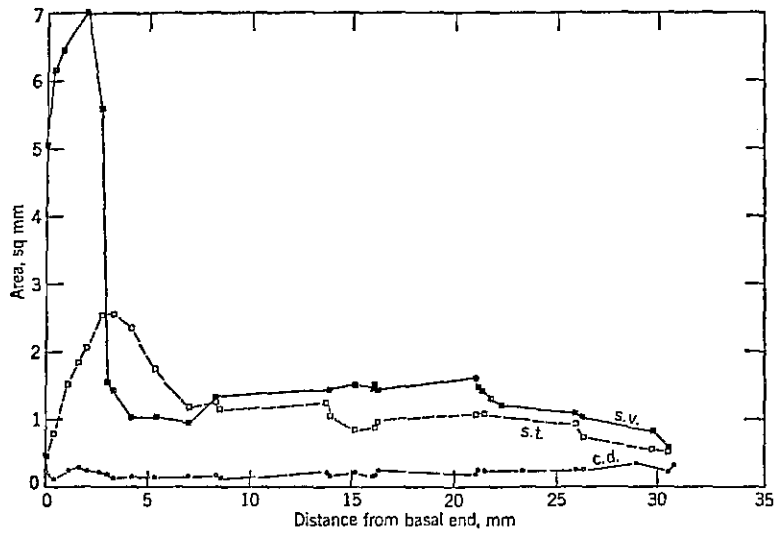

Figure 3.2. Cross-sectional areas of the three cochlear scalae. The cross-sectional area is shown for scala vestibuli (s.v.), scala tympani (s.t.), and scala media (c.d.) as a function of distance from the basal end for a human cochlea. [Figure from Wever (26).]

the cochlear partition; this symmetry makes it possible to obtain a complete solution of the mathematical model in a single cochlear scala. Small deviations from exact scala symmetry would have only a small effect on motion of the cochlear partition. In the two-dimensional model, the solutions for basilar membrane displacement are not particularly sensitive to small changes in scala height; halving the scala height has an effect similar to halving the stiffness of the cochlear partition (62).

e. The oval and round windows are represented in the model by the basal ends of the cochlear scalae. Results with models of the cochlea indicate that fluid flow is approximately one-dimensional at the basal end for all but the highest audible frequencies (21). In the two-dimensional model, the (one-dimensional) fluid flow through the basal plane will be the same as if it were driven by a pair of pistons at the ends of the cochlear scalae (see Figure 3.3); the mode of stimulus excitation in the model is similar to the dominate mode of fluid motion at the basal end.

f. The geometry of the conceptual model should be time-invariant for mathematical tractability. On the other hand, motion of the basal and partition boundaries is an essential part of the cochlear model. To meet these conflicting requirements we must assume that the moving boundaries are never displaced from their resting positions by any significant amount. The reasonableness of this assumption is supported by experimental evidence. Rhode measured basilar membrane displacements in squirrel monkey of about 10^{-5} mm for stimuli which were more intense than the animal would normally

encounter (3). It has been estimated that basilar membrane displacements are as small as 10^{-9} mm at the threshold of hearing (3). These displacements are significantly smaller than the diameter of the cochlear scalae, which is about 1 mm. The small amplitude of fluid motion also contributes to the assumption of fluid linearity.

g. The cochlear fluids are assumed to be incompressible for all frequencies of interest. The effect of fluid compressibility has been estimated by other investigators (26, 60, 15) and found to be negligible for all but the highest audible frequencies. The formulation of a mathematical model with compressible fluid does not significantly complicate frequency-domain solutions, but it seems to be unwarranted when one considers the level of accuracy of the present cochlear model.

h. The fluid mechanics of the cochlea are assumed to be linear because the motions of interest are extremely small. The Navier-Stokes equation for an incompressible, Newtonian fluid has a linear convection term and a nonlinear (quadratic) convection term. Viergever (15) has estimated the magnitudes of these convection terms and concludes that the nonlinear term is negligible compared to the linear term, even at very high sound pressures (100 dB SPL).

i. Estimates of the viscous effects of the cochlear fluids have shown that the viscous effects are much less than the inertial effects, so that the fluid may be regarded as inviscid, except near the boundaries (15). Lien (60) included fluid viscosity of the boundary layer in his mathematical formulation and concluded that it was not negligible for frequencies below 10 kHz. Viergever (15)

applied a boundary-layer viscous correction to the solution of an inviscid model; the viscous correction was only significant at the lowest audible frequencies (around 100 Hz). A major reason for ignoring these viscous effects in the present research is the added difficulties that they pose mathematically.

j. The assumption of two-dimensional fluid flow in the cochlea requires that fluid pressure does not vary in the third-dimension. The two-dimensional model of the cochlea represents a currently popular compromise between physical realism and mathematical feasibility. One-dimensional models and three-dimensional models of the cochlea are also being used by some investigators. Estimates of the wavelength of basilar membrane motion based on experimental data indicate that cochlear fluid motion should not be considered to be one-dimensional. The finite-difference method used in this dissertation has also been applied to a box-shaped three-dimensional model; preliminary results indicate that the effect of the third dimension on basilar membrane motion can be largely accounted for by scaling cochlear model parameters in a two-dimensional cochlear model. On the other hand, some investigators (66, 68) feel that full consideration of the three-dimensional fluid motion is important in a cochlear model.

k. The assumption that there is no longitudinal coupling within the cochlear partition is made primarily for mathematical convenience but is supported by physiological, anatomical and modeling studies. von Békésy's experimental observations indicate that the basilar membrane is not under tension, so there should be no significant

stretching forces in either the transverse or longitudinal dimension (1). Iurato observed transverse fibers in his studies of basilar membrane anatomy (75) which should make the basilar membrane much stiffer transversely than it is longitudinally. The experimental measurements of Völdrich (76) indicate that the basilar membrane of a "fresh" cochlea (15 minutes post-mortem) behaves as a set of transverse fibers without longitudinal stiffness, but at 24 hours post-mortem the basilar membrane stiffness appears to be isotropic. [Some mathematical model formulations have included longitudinal stiffness in the basilar membrane (73, 77, 78, 14).]

l. The mechanics of a living cochlea has been shown experimentally to have observable nonlinear characteristics (even at low sound levels) which have been attributed to nonlinear elements in the cochlear partition (4, 17). These nonlinear characteristics are not observed when the animal is dead or the cochlea has been damaged. The linearity assumption is made here for convenience, with the hope that progress can be made in understanding mechanical sharpening mechanisms in the cochlea. It is the intent of this research that the linear representation of the cochlea should serve as a basis for the inclusion of mechanical nonlinearities in some future research project.

m. Allowing the cochlear partition-point mechanics to have two degrees-of-freedom in a comprehensive two-dimensional model of the cochlea is one of the innovations of this research. Traditionally, only one degree of freedom is allowed, under the assumption that the organ of Corti motion is tightly coupled to basilar membrane motion.

Allen (79) has considered a cochlear partition model with two degrees-of freedom, but the second degree-of-freedom in Allen's model had no influence on the first degree-of-freedom. Zwislocki and Kletsky (2, 80, 81) have presented frequency-domain solutions for a one-dimensional model which included two degrees-of freedom in the cochlear partition. Steele and Taber (65, 67) have obtained solutions for a cochlear model which allowed four modes of deflection (4-DOF) in the cochlear partition; their frequency-domain results indicate that the additional deflection modes have much less effect on cochlear frequency selectivity than the sharpening mechanisms presented in this dissertation. The 2-DOF partition models presented in this dissertation have a large effect on the range of possible cochlear model solutions.

The terms "cochlear partition" and "basilar membrane" are both used in this dissertation to refer to the fluid boundary between the two cochlear scalae. The modeling concept of the cochlear partition is that it consists of the basilar membrane, which separates the two fluid-scalae, and a second mechanical structure, which is mechanically coupled to the basilar membrane, but does not directly interact with the fluid-scalae. Further restrictions on allowable partition properties will be discussed in chapters 4 and 5.

In summary, our conceptual model of the cochlea is a rectangular region which is filled with an inviscid, incompressible fluid and divided into two, geometrically-symmetric compartments by a thin, elastic partition. The conceptual model is illustrated in Figure 3.3.

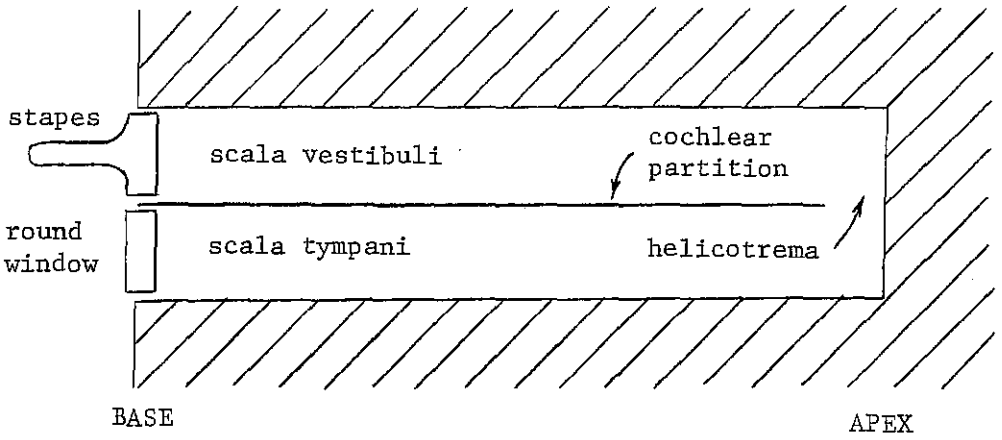

Figure 3.3. Pictorial representation of the conceptual model of the cochlea.

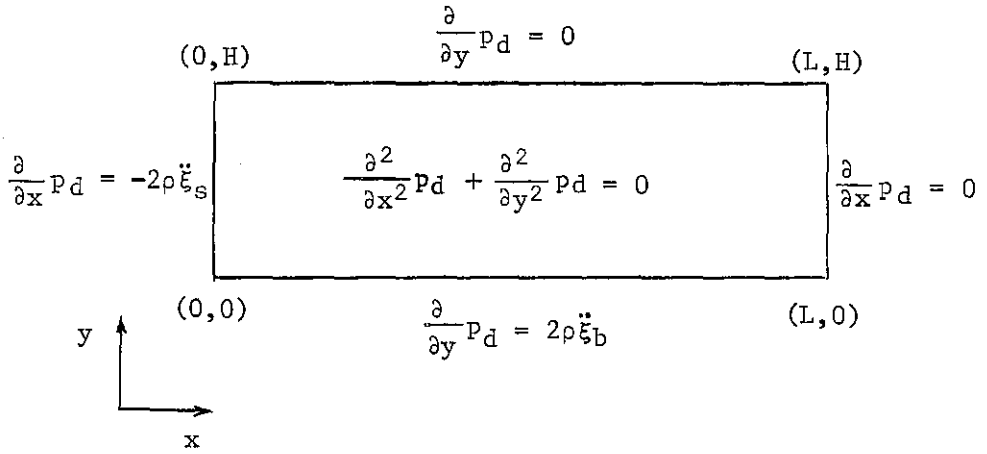

Figure 3.4. Pictorial representation of the mathematical model of the cochlea.

3.2 MATHEMATICAL MODEL

The two-dimensional mathematical model of the cochlea presented in this section has evolved through the work of many investigators (57, 54, 58, 60, 82, 83, 84, 85, 59). The geometrical and mechanical assumptions introduced in the preceding section are utilized in this section to formulate the mathematical model. In order to define physical quantities, an x-y coordinate system will be associated with the two-dimensional model. The total length of the rectangle L in the x dimension is equal to the length of the basilar membrane ($L-L_h$) plus the length of the helicotrema L_h. The height of the rectangle H in the y dimension is equal to the cross-sectional area of the cochlear scalae divided by the "effective" width of the partition w_p. The consideration of partition width in a two-dimensional model is necessary, if one is to reproduce both "short-wave" and "long-wave" behavior of a corresponding three-dimensional model. [For further discussion of this point see de Boer (68).] Assumption e requires that the cross-sectional area of the cochlear scalae be equal to the area of the footplate of the stapes A_s, so that the height of the two-dimensional model will be

$$H = A_s / w_p. \tag{3.1}$$

The additional assumptions d and k insure that the height of the cochlear scalae in the two-dimensional model are equal and constant along the length of the cochlea.

The mathematical model of the cochlea will be expressed in terms of fluid pressure, stapes acceleration, and basilar membrane acceleration. The incorporation of the middle ear and acoustic

stimulus-delivery system into the mathematical model will not be considered in detail, but is a straightforward extension of the methods presented in this section.

Since the basilar membrane in our model responds only to the difference in fluid pressure between its upper and lower surfaces, it is convenient to consider the component of fluid pressure which is anti-symmetric across the partition axis (x axis). Let $p_d(x,y,t)$ be a real-valued function which describes the pressure difference between the scala vestibuli and scala tympani,

$$p_d(x,y,t) = p_{sv}(x,y,t) - p_{st}(x,-y,t), \tag{3.2}$$

where $p_{sv}(x,y,t)$ is the total (observable) pressure in the scala vestibuli and $p_{st}(x,y,t)$ is the total pressure in the scala tympani. It should be noted that p_d is anti-symmetric in y about the x axis and is twice the anti-symmetric component of the total pressure in either scala. The symmetric component of total fluid pressure will have no effect on basilar membrane motion and no spatial variation (due to assumptions a, g, and e) so that it need not be included in the cochlear model. Therefore, it will be sufficient for our purposes to solve for $p_d(x,y,t)$ in a single cochlear scala.

The basic set of equations for the mathematical model establishes a boundary value problem for p_d in an L by H rectangle (86). The pressure difference function p_d is required by assumptions g, h, i, and j to satisfy Laplace's equation in this two-dimensional fluid space,

$$\frac{\partial^2}{\partial x^2} p_d(x,y,t) + \frac{\partial^2}{\partial y^2} p_d(x,y,t) = 0 , \tag{3.3}$$

for $0 \leqslant x \leqslant L$ and $0 \leqslant y \leqslant H$. The upper-wall boundary at $y = H$, is rigid by assumption a and will have no motion relative to our coordinate system. The upper-wall boundary condition is

$$\frac{\partial}{\partial y} p_d(x,H,t) = 0 , \tag{3.4}$$

for $0 \leqslant x \leqslant L$. The cochlear-partition boundary, however, will move in response to fluid pressure. The cochlear-partition boundary condition is

$$\frac{\partial}{\partial y} p_d(x,0,t) = 2\rho \ddot{\xi}_b(x,t) , \tag{3.5}$$

for $0 \leqslant x \leqslant L$. where $\ddot{\xi}_b(x,t)$ is the basilar-membrane acceleration in the y dimension (defined to be positive for downward acceleration, i. e. into scala tympani) and ρ is the volume density of the fluid. The basal-end boundary represents the stapes and round window and is assumed to have motion in the x dimension; the displacements of stapes and round window from their resting positions will always be of equal magnitude but in opposite directions, due to assumptions a and h. The basal boundary condition is

$$\frac{\partial}{\partial x} p_d(0,y,t) = -2\rho \ddot{\xi}_s(t) , \tag{3.6}$$

for $0 \leqslant y \leqslant H$. where $\ddot{\xi}_s(t)$ is the acceleration of the stapes in the x dimension (constant in the y dimension and defined to be positive for inward acceleration). The apical end is rigid and has no motion. The apical end boundary condition is

$$\frac{\partial}{\partial x} p_d(L,y,t) = 0 , \tag{3.7}$$

for $0 \leqslant y \leqslant H$. Some investigators have used a "zero pressure" boundary condition at the apical end to model the helicotrema connection

between the two scala (59, 62). In the present formulation, the helicotrema will be represented as a small, apical portion of the cochlear partition boundary. This basic set of equations for the mathematical model is summarized in Figure 3.4.

In order to obtain a solution for p_d, additional constraints are required at the stapes and cochlear-partition boundaries. At the stapes, we can specify $\ddot{\xi}_s(t)$ explicitly as the source of excitation. Alternatively, we can incorporate the middle ear and acoustic stimulus-delivery system into our mathematical model and specify the electrical voltage to an acoustic transducer as the source of excitation. Both methods are used in this dissertation. Mathematical models for the middle ear and acoustic stimulus-delivery system were adapted from Matthews (21) for use in this research and are described in Appendix 9.2.

The additional constraint at the cochlear partition boundary (at y=0) will be implemented by introducing two additional variables, $\xi_1(x,t)$ and $\xi_2(x,t)$, and three additional equations

$$\ddot{\xi}_b(x,t) = -\ddot{\xi}_1(x,t) \tag{3.8}$$

$$M_1\ddot{\xi}_1 + (R_1 + R_3)\dot{\xi}_1 + (K_1 + K_3)\xi_1 - R_3\dot{\xi}_2 - K_3\xi_2 = -p_d \tag{3.9}$$

$$M_2\ddot{\xi}_2 + (R_2 + R_3)\dot{\xi}_2 + (K_2 + K_3)\xi_2 - R_3\dot{\xi}_1 - K_3\xi_1 = 0\,, \tag{3.10}$$

for $0 \ll x \ll (L-L_h)$, where $M_1(x)$, $R_1(x)$, $K_1(x)$, $M_2(x)$, $R_2(x)$, $K_2(x)$, $M_3(x)$, and $R_3(x)$ are time-invariant, mechanical parameter functions of x.

To simplify the selection of cochlear partition parameters, the x variation of these micromechanical parameter functions will be

constrained to be exponential. This exponential variation has been used often by previous investigators (54, 58, 59, 62, 15) and is justified by the logarithmic nature of the cochlear frequency-to-place map (see section 4.2). The micromechanical properties of the cochlear partition can be expressed in terms of 16 parameters which are the exponents and multipliers of the exponential functions:

$$K_1(x) = K_{1o} \exp(K_{1e}x) \tag{3.11}$$

$$K_2(x) = K_{2o} \exp(K_{2e}x) \tag{3.12}$$

$$K_3(x) = K_{3o} \exp(K_{3e}x) \tag{3.13}$$

$$R_1(x) = R_{1o} \exp(R_{1e}x) \tag{3.14}$$

$$R_2(x) = R_{2o} \exp(R_{2e}x) \tag{3.15}$$

$$R_3(x) = R_{3o} \exp(R_{3e}x) \tag{3.16}$$

$$M_1(x) = M_{1o} \exp(M_{1e}x) \tag{3.17}$$

$$M_2(x) = M_{2o} \exp(M_{2e}x). \tag{3.18}$$

The interpretation and selection of partition parameters will be discussed in chapters 4 and 5. Equations (3.9) and (3.10) are general equations of motion for a simple, linear, time-invariant mechanical system with two degrees of freedom, except that the forcing function is applied only to the first degree of freedom; Figure 3.5 shows a schematic diagram of this type of mechanical system. Equations (3.8)-(3.10) will represent the cochlear-partition boundary except at the helicotrema.

A small interval at the apical end of the cochlear partition of length L_h is reserved to represent the helicotrema. The helicotrema is modeled as an extension of the basilar membrane with no mass, no stiffness, and a small amount of damping R_h. The helicotrema boundary

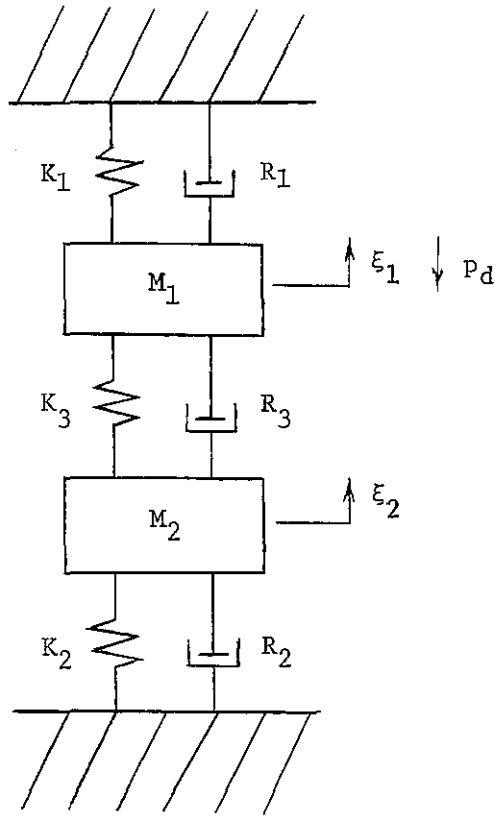

Figure 3.5. Schematic diagram of a simple mechanical system with two degrees-of-freedom.

condition is an extension of equation (3.9)

$$R_h \dot{\xi}_1 = -p_d \ , \tag{3.19}$$

for $(L-L_h)<x\leqslant L$.

The mathematical model of the cochlea used in this dissertation is described by equations (3.1)-(3.19). The model variables are listed in Table 3.1 and the model parameters are listed in Table 3.2. Frequency-domain and time-domain versions of the mathematical model are introduced in the next two sections.

3.3 FREQUENCY-DOMAIN MODEL

One type of model solution that will be required is the steady-state response of the cochlear model to sinusoidal excitation of the stapes boundary. The linearity of the problem allows for the time variable t to be eliminated from the model equations by the introduction of harmonic time functions (15). Each real-valued, time-dependent function in the model equations (3.3)-(3.10) can be replaced by a complex-valued function with $\exp(i\omega t)$ time-dependence, where $\omega = 2\pi f$ is the radian frequency of the sinusoidal excitation. Consider the following replacements in the model equations:

$$p_d(x,y,t) \Leftarrow p_d(x,y;i\omega)\exp(i\omega t) \tag{3.20}$$

$$\ddot{\xi}_b(x,t) \Leftarrow A_b(x;i\omega)\exp(i\omega t) \tag{3.21}$$

$$\ddot{\xi}_s(t) \Leftarrow A_o(i\omega)\exp(i\omega t) \ . \tag{3.22}$$

The method of harmonic analysis is a standard technique for dealing with vibrating systems (7, 87, 88). The phase "reference" of the

Table 3.1 Mathematical model variables

Independent variables:

x - distance from stapes along cochlear partition, cm.

y - distance from cochlear partition along stapes, cm.

t - time, sec.

Dependent variables:

$p_d(x,y,t)$ - fluid pressure difference, dyn/cm^2.

$\xi_s(t)$ - inward displacement of the stapes, cm.

(Sometimes a parameter.)

$\xi_b(x,t)$ - downward displacement of basilar membrane, cm.

$\xi_1(x,t)$ - first micromechanical degree-of-freedom, cm.

$\xi_2(x,t)$ - second micromechanical degree-of-freedom, cm.

Table 3.2 Mathematical model parameters

Macromechanical parameters:

L - length of the cochlea in x dimension, cm.

H - height of the cochlea in y dimension, cm.

ρ - fluid density, gm/cm^3.

A_s - area of the stapes footplate, cm^2.

w_p - effective width of the partition, cm.

Micromechanical parameters (all with exponential dependence on x):

$M_1(x)$ - mass associated with first DOF, gm/cm^2.

$R_1(x)$ - damping associated with first DOF, $dyn\text{-}sec/cm^3$.

$K_1(x)$ - stiffness associated with first DOF, dyn/cm^3.

$M_2(x)$ - mass associated with second DOF, gm/cm^2.

$R_2(x)$ - damping associated with second DOF, $dyn\text{-}sec/cm^3$.

$K_2(x)$ - stiffness associated with second DOF, dyn/cm^3.

$R_3(x)$ - damping associated with coupling 2 DOF's, $dyn\text{-}sec/cm^3$.

$K_3(x)$ - stiffness associated with coupling 2 DOF's, dyn/cm^3.

Helicotrema parameters:

L_h - length of helicotrema, cm.

R_h - damping at helicotrema, $dyn\text{-}sec/cm^3$.

complex-valued functions in equations (3.20)-(3.22) is determined by the positive senses of the corresponding real-valued functions.

The cochlear-partition constraints expressed by equations (3.8)-(3.10) can be represented in the frequency-domain formulation by the introduction of a complex-valued basilar-membrane admittance function $Y_b(x;i\omega)$, defined as the ratio of basilar-membrane velocity to fluid pressure. The convenience of the admittance function is that it allows basilar-membrane acceleration A_b to be expressed in terms of the pressure difference

$$A_b(x;i\omega) = i\omega Y_b(x;i\omega)\, P_d(x,0,i\omega) . \tag{3.23}$$

The admittance represents the assumed mechanical properties of the cochlear partition as seen from the fluid. It can be computed from the micromechanical and helicotrema parameters in Table 3.2 according to the constraints of equations (3.8)-3.10)

$$Y_b(x;i\omega) = \begin{cases} \dfrac{Z_2 + Z_3}{(Z_1 + Z_3)(Z_2 + Z_3) - Z_3^2} , & 0 \leq x \leq (L - L_h) \\ R_h , & (L - L_h) < x \leq L \end{cases} \tag{3.24}$$

$$Z_1(x;i\omega) = K_1(x)/i\omega + R_1(x) + i\omega M_1(x) \tag{3.25}$$

$$Z_2(x;i\omega) = K_2(x)/i\omega + R_2(x) + i\omega M_2(x) \tag{3.26}$$

$$Z_3(x;i\omega) = K_3(x)/i\omega + R_3(x) . \tag{3.27}$$

Numerical solution of the frequency-domain model by the finite-difference method requires the spatial dimensions to be represented by a finite number of discrete points; N points will be chosen to represent the x dimension and M points will be chosen to represent the y dimension. The spatially-discrete versions of

admittance and pressure difference are defined as follows:

$$Y(J) = Y_b [(J-1)\cdot\Delta x; i\omega] \tag{3.28}$$

$$P(I,J) = P_d [(J-1)\cdot\Delta x, (I-1)\cdot\Delta y; i\omega] , \tag{3.29}$$

for $I=1,2, \ldots ,M$ and $J=1,2, \ldots ,N$, where

$$\Delta x = L / (N-1) \tag{3.30}$$

$$\Delta y = H / (M-1), \tag{3.31}$$

The frequency-domain variables and parameters are described in Table 3.3.

The discrete frequency-domain model equations are (86)

$$\left[2P(J,I) - P(J+1,I) - P(J-1,I)\right] / (\Delta x)^2 + \left[2P(J,I) - P(J,I+1) - P(J,I-1)\right] /(\Delta y)^2 = 0 \tag{3.32}$$

$$P(J,M+1) - P(J,M-1) = 0 \tag{3.33}$$

$$P(J,2) - P(J,0) = -4\rho \left[i\omega Y(J)\, P(J,1)\right] \Delta y \tag{3.34}$$

$$P(2,1) - P(0,I) = -4\rho A_o \Delta x \tag{3.35}$$

$$P(N+1,I) - P(N-1,I) = 0 , \tag{3.36}$$

for $I=1,2, \ldots ,M$ and $J=1,2, \ldots ,N$. When the discrete equations are written in matrix form, the matrix has a block-tridiagonal structure. For the model results in this dissertation the matrix equation was solved by Gaussian block-elimination (89) as described by Neely (63).

The computer implementation of the frequency-domain model consisted of programming the numerical solution method in Fortran and executing the Fortran programs on a Texas Instruments 980-B minicomputer. The Fortran programs used for the frequency-domain model are described in Appendix 9.3.

Table 3.3 Frequency-domain model variables and parameters.

Frequency-domain model dependent variables:

$P_d(x,y)$ - complex-valued pressure-difference, dyn/cm^2.

$P(J,I)$ - complex-valued pressure-difference at position $x=(J-1)\cdot\Delta x$ and $y=(I-1)\cdot\Delta y$, dyn/cm^2.

$A_b(x)$ - complex-valued basilar-membrane acceleration, cm/sec^2.

Frequency-domain model parameters:

f - stimulus frequency, hertz.

M - number of discrete points representing the y dimension.

N - number of discrete points representing the x dimension.

$Y_b(x)$ - basilar-membrane admittance, $cm^3/dyn\text{-}sec$.

$Y(J)$ - basilar-membrane admittance at $x=(J-1)\cdot\Delta x$, $cm^3/dyn\text{-}sec$.

A_o - complex-valued stapes acceleration , cm/sec^2.

(Sometimes a dependent variable.)

3.4 TIME-DOMAIN MODEL

The model equations in section 3.2 are already formulated in the time domain. In this section we can proceed directly to variables which are discrete both in time t and in the spatial dimensions x and y:

$$p(J,I,K) = p_d [\, (J-1)\cdot\Delta x, (I-1)\cdot\Delta y, K\Delta t \,] \tag{3.37}$$

$$a_s(K) = \ddot{\xi}_s(K\Delta t) \tag{3.38}$$

$$v_s(K) = \dot{\xi}_s(K\Delta t) \tag{3.39}$$

$$d_s(K) = \xi_s(K\Delta t) \tag{3.40}$$

$$a_1(J,K) = \ddot{\xi}_1 [\, (J-1)\cdot\Delta x, K\Delta t \,] \tag{3.41}$$

$$v_1(J,K) = \dot{\xi}_1 [\, (J-1)\cdot\Delta x, K\Delta t \,] \tag{3.42}$$

$$d_1(J,K) = \xi_1 [\, (J-1)\cdot\Delta x, K\Delta t \,] \tag{3.43}$$

$$a_2(J,K) = \ddot{\xi}_2 [\, (J-1)\cdot\Delta x, K\Delta t \,] \tag{3.44}$$

$$v_2(J,K) = \dot{\xi}_2 [\, (J-1)\cdot\Delta x, K\Delta t \,] \tag{3.45}$$

$$d_2(J,K) = \xi_2 [\, (J-1)\cdot\Delta x, K\Delta t \,] , \tag{3.46}$$

for $I=1,2, \ldots ,M$, $J=1,2, \ldots ,N$, $K=0,1,2, \ldots ,N_t$, and where, as before,

$$\Delta x = L/(N-1) \tag{3.47}$$

$$\Delta y = H/(M-1) . \tag{3.48}$$

The quantity Δt will be specified as an independent parameter.

The x dependence of the mechanical parameters which describe the cochlear partition is discretized in an analogous manner. The middle-ear, acoustic coupler, and earphone variables are excluded from this discussion for simplicity; their inclusion is a straightforward extension of the methods presented in this section. The time-domain model parameters and variables are described in Table 3.4.

Quiescent initial conditions (zero velocity and zero displacement) are assumed at t=0:

$$v_s(0) = d_s(0) = 0 \tag{3.49}$$

$$v_1(J,0) = d_1(J,0) = 0 \tag{3.50}$$

$$v_2(J,0) = d_2(J,0) = 0. \tag{3.51}$$

for J=1,2, ... ,N. At each time-step, a spatial boundary-value problem must be solved. The model equations are, once again, discretized by the finite-difference method (86).

The first group of time-domain model equations are for pressure and acceleration at time-step K, assuming that the velocity and displacement for this time-step are already known

$$\left[2p(J,I,K) - p(J+1,I,K) - p(J-1,I,K)\right] / (\Delta x)^2$$

$$+\left[2p(J,I,K) - p(J,I+1,K) - p(J,I-1,K)\right] / (\Delta y)^2 = 0 \tag{3.52}$$

$$p(J,M+1,K) - p(J,M-1,K) = 0 \tag{3.53}$$

$$p(J,2,K) - p(J,0,K) = -4\rho\, a_1(J,K)\, \Delta y \tag{3.54}$$

$$p(2,I,K) - p(0,I,K) = -4\rho\, a_s(K)\, \Delta x \tag{3.55}$$

$$p(N+1,I,K) - p(N-1,I,K) = 0 \tag{3.56}$$

$$a_1(J,K) = \left[-P(J,1,K) + R_3 v_2(J,K) + K_3 d_2(J,K) - (R_1+R_3)\, v_1(J,K) - (K_1+K_3)\, d_1(J,K)\right] / M_1 \tag{3.57}$$

Table 3.4 Time-domain model variables and parameters.

Time-domain model dependent variables

(at time $t=K\cdot\Delta t$ and position $x=(J-1)\cdot\Delta x$ and $y=(I-1)\cdot\Delta y$):

$p(J,I,K)$ - pressure difference, dyn/cm^2.

$a_s(K)$ - acceleration of stapes, cm/sec^2.

$v_s(K)$ - velocity of stapes, cm/sec.

$d_s(K)$ - displacement of stapes, cm.

$a_1(J,K)$ - acceleration of first DOF, cm/sec^2.

$v_1(J,K)$ - velocity of first DOF, cm/sec.

$d_1(J,K)$ - displacement of first DOF, cm.

$a_2(J,K)$ - acceleration of second DOF, cm/sec^2.

$v_2(J,K)$ - velocity of second DOF, cm/sec.

$d_2(J,K)$ - displacement of second DOF, cm.

Time-domain model parameters:

Δt - time step, sec.

N_t - number of time steps to be computed.

M - number of discrete points representing the y dimension.

N - number of discrete points representing the x dimension.

$$a_2(J,K) = \left[R_3 v_1(J,K) + K_3 d_1(J,K) - (R_2+R_3)\, v_2(J,K) - (K_2+K_3)\, d_2(J,K)\right]/M_2 \quad , \qquad (3.58)$$

for I=1,2, ... ,M and J=1,2, ... ,N and it is understood that the micromechanical parameter functions are evaluated at $x=(J-1)\cdot\Delta x$. The present time-domain model implementation represents the helicotrema by an appropriate redefinition of the micromechanical parameters in the helicotrema region, consistent with equation (3.19). It should be noted that equations (3.52)-(3.57) are coupled and must be solved simultaneously.

The second group of time-domain model equations use the computed acceleration at time-step K to compute the velocity and displacement for the succeeding timestep K+1:

$$v_1(J,K+1) = v_1(J,K) + a_1(J,K)\,\Delta t \qquad (3.59)$$

$$v_2(J,K+1) = v_2(J,K) + a_2(J,K)\,\Delta t \qquad (3.60)$$

$$d_1(J,K+1) = d_1(J,K) + v_1(J,K+1)\,\Delta t \qquad (3.61)$$

$$d_2(J,K+1) = d_1(J,K) + v_2(J,K+1)\,\Delta t \qquad (3.62)$$

$$v_s(J,K+1) = -\left(\frac{\Delta x}{2H}\right) \sum_{J=1}^{N-1} \left[v_1(J,K+1) + v_1(J+1,K+1)\right] \qquad (3.63)$$

$$d_s(J,K+1) = -\left(\frac{\Delta x}{2H}\right) \sum_{J=1}^{N-1} \left[d_1(J,K+1) + d_1(J+1,K+1)\right], \qquad (3.64)$$

for J=1,2, ... ,M. Equation (3.55) assumes that stapes acceleration will be specified at each time-step. Alternatively, the specified quantity could be eardrum pressure or earphone voltage; in these cases equation (3.55) is modified to include the driving force of the malleus through the incudo-malleolar joint and the combined restoring forces of the cochlear windows. It should be noted that equations

(3.63) and (3.64) compute stapes velocity and stapes displacement based on spatial-integration of basilar-membrane velocity and displacement, instead of temporal-integration of stapes acceleration. This method forces fluid-volume to be conserved in the model as required by model assumptions a and g.

The discrete time-domain model equations are solved at each time-step by using the same Gaussian block-elimination procedure as for the frequency-domain model. This method is feasible because only a small part of the block-elimination procedure must be repeated at each time-step: The Gaussian procedure requires about $3NM^3$ multiply-and-add operations for matrix factorization and about $3NM^2$ operations for subsequent evaluations (89); in the time-domain model the matrix is time-invariant, so the matrix factorization is done only once for each set of parameters and only subsequent evaluations of the Gaussian procedure must be repeated each time step. The FORTRAN programs used to implement the time-domain model are described in Appendix 9.3.

4. RESONANT TECTORIAL MEMBRANE

In this chapter we will consider a model of the cochlear partition with two-degrees of freedom (2-DOF) under the assumption that the tectorial membrane and basilar membrane are both mechanically tuned structures. The presentation of the resonant tectorial membrane hypothesis in section 4.1 is similar to recent work by Allen (12). Section 4.2 describes the method used to select model parameters for this type of cochlear partition. Model results are presented in section 4.3 and compared with neural response data.

4.1 COCHLEAR PARTITION-POINT MODEL WITH RESONANT TM

Since our cochlear model is two-dimensional and has no direct longitudinal coupling in the partition, each partition-point in the model corresponds with a particular transverse cross-section of the actual cochlear partition. (A typical cochlear partition cross-section was shown in Figure 2.3.) The "micromechanical" model parameters introduced in section 3.2 will be related in this section to the cochlear partition cross-section, according to the hypothesis that the tectorial membrane acts as a mechanically tuned "second filter".

It is the shearing motion between tectorial membrane (TM) and reticular lamina (RL) that causes the cilia of the hair cells to deflect and, thereby, causes excitation of the auditory nerve fibers. In the 1-DOF partition-point model shown in Figure 2.13 the hair-cell shearing $\xi_h(x,t)$ is completely determined by the basilar membrane

displacement $\xi_b(x,t)$ and the geometry of the partition cross-section;

$$\xi_h(x,t) = g(x)\,\xi_b(x,t)\,, \tag{4.1}$$

where $g(x)$ is the shear-lever gain and is independent of time.

The notion of a second-filter being interposed between basilar membrane displacement and hair-cell shearing was discussed in section 2.4. The primary motivation for including a mechanical second-filter in the model is that it provides a means of obtaining solutions for hair-cell shearing which more closely match the experimental measurements of neural response. The resonant TM hypothesis provides a possible physical interpretation for a mechanical second-filter.

The resonant tectorial membrane hypothesis allows a "stretch" $\xi_t(x,t)$ in the portion of TM between spiral limbus and RL, as illustrated in Figure 4.1. The variable ξ_t represents lateral displacement of TM; it is assumed that vertical displacement of TM is the same as the vertical displacement of BM. The stiffness k_t associated with TM-stretch, together with the lumped mass m_t which moves when TM is stretched, provide TM with a natural resonance at some frequency. The TM-stretch gives the partition-point model a second degree-of-freedom.

The 2-DOF partition model with resonant tectorial membrane shown in Figure 4.1 has the property that it reduces to the traditional 1-DOF model in Figure 2.13 when the TM-stretch ξ_t is constrained to be zero. In this 2-DOF partition, the relation between ξ_h and ξ_b is (in general) no longer independent of time and, therefore, equation (4.1) no longer holds. However, the vertical separation between TM and RL is still assumed to be constant and the shear-lever gain can be

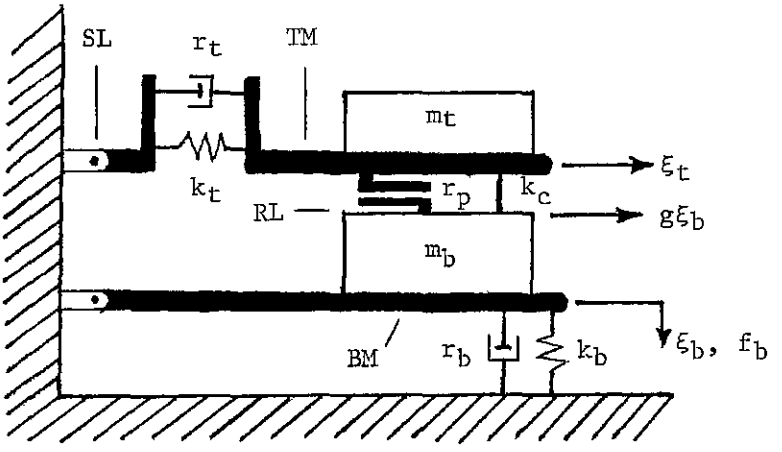

Figure 4.1. A 2-DOF partition model with resonant tectorial membrane. TM - tectorial membrane; BM - basilar membrane; SL - spiral limbus; RL - reticular lamina. Other symbols are described in Table 4.1. [Figure adapted from Allen (12).]

defined as before by considering ξ_t to be zero. The cilia bending stiffness k_c and the basilar membrane internal damping r_b are added to the model for generality and do not increase the order of the equations-of-motion for this system.

The equations of motion for the 2-DOF partition with resonant TM are

$$f_b = (m_b + m_t)\ddot{\xi}_b + r_b\dot{\xi}_b + k_b\xi_b + g[r_p(g\dot{\xi}_b + \dot{\xi}_t)] + k_c(g\xi_b + \xi_c) \quad (4.2)$$

$$0 = m_t\ddot{\xi}_t + r_t\dot{\xi}_t + k_t\xi_t + r_p(\dot{\xi}_t - g\dot{\xi}_b) + k_c(\xi_t - g\xi_b), \quad (4.3)$$

where f_b is the vertical force (per unit length) applied to the basilar membrane at the same place where basilar membrane displacement ξ_b is measured. Both f_b and ξ_b are defined to be positive downward. The tectorial membrane displacement ξ_t is defined to be positive away from the spiral limbus (SL). Equations (4.2) and (4.3) are the same as the general equations of motion given by equations (3.9) and (3.10) with the following change of variables

$$p_d = f_b / w_p \quad (4.4)$$

$$\xi_1 = -\xi_b \quad (4.5)$$

$$\xi_2 = -\xi_t / g \quad (4.6)$$

$$M_1 = (m_b + m_t) / w_p \quad (4.7)$$

$$M_2 = g m_t / w_p \quad (4.8)$$

$$K_1 = k_b / w_p \quad (4.9)$$

$$K_2 = g k_t / w_p \quad (4.10)$$

$$K_3 = g^2 k_c / w_p \quad (4.11)$$

$$R_1 = r_b / w_p \quad (4.12)$$

$$R_2 = g r_t / w_p \tag{4.13}$$

$$R_3 = g^2 r_p / w_p \ , \tag{4.14}$$

where, as before, w_p is the effective width of the cochlear partition associated with the two-dimensional model. The micromechanical parameters which characterize the resonant tectorial membrane partition model are described in Table 4.1.

4.2 MODEL PARAMETERS TO MATCH NEURAL RESPONSE DATA

In order to obtain solutions for the cochlear model we must first specify the model parameters. In this section we will choose model parameters according to the objective of matching the neural response data of Kim, Siegel, and Molnar (4) (see Figure 2.10). Since the neural data was obtained from cat, we will also base the model parameters on anatomical measurements of the cat cochlea (26, 74, 45).

First, we will consider the macromechanical parameters which are not dependent on the resonant tectorial membrane hypothesis (see Table 3.1). The length of the cochlear partition is the total length of the cochlea L minus the helicotrema length L_h. The partition length from Schuknecht (45) is $(L-L_h) = 2.2$ cm. The area of the stapes footplate from Guinan and Peake (90) is $A_s = 0.0126$ cm^2. The height of the cochlear scalae in the model is chosen to be approximately equal to the diameter of the actual cochlear scalae, $H = 0.1$ cm (26). Choosing values for both A_s and H constrains the effective width of the cochlear partition, $w_p = 0.126$ cm [see equation (3.1)]. [There is some discrepancy here since the actual width of BM in cat is about 0.02 cm (74).] The helicotrema parameters are chosen simply to

Table 4.1. Dependent variables and parameters for the cochlear partition model with resonant tectorial membrane. (See Figure 4.1).

Cochlear partition variables:

ξ_b - basilar membrane vertical-displacement, cm.

ξ_t - tectorial membrane stretch-displacement, cm.

ξ_h - hair cell shearing-displacement, cm.

f_b - vertical force applied to basilar membrane, dyn/cm.

Cochlear partition parameters:

k_b - basilar membrane bending stiffness, dyn cm^{-2}

r_b - basilar membrane internal damping, dyn sec cm^{-2}.

m_b - basilar membrane mass, gm/cm.

k_t - tectorial membrane stretch stiffness, dyn cm^{-2}.

r_t - tectorial membrane stretch damping, dyn sec cm^{-2}.

m_t - tectorial membrane mass, gm/cm.

k_c - hair-cell cilia bending stiffness, dyn cm^{-2}

r_p - sub-tectorial fluid space damping, dyn sec cm^{-2}.

g - radial shear lever gain with $\xi_t = 0$.

represent a small opening between the scalae at the apical end with a small amount of viscous damping, $L_h = 0.05$ cm and $R_h = 50$ dyn-sec/cm^3.

The "micromechanical" model parameters are those associated with the cochlear partition. In section 3.2 the micromechanical parameters were assumed to have exponential variation with distance from the stapes in order to put a reasonable limit on the parameter space from which the micromechanical parameters must be chosen. In the remainder of this section, we will define 12 constants which will characterize selected experimental data and use these 12 constants to place further constraints on the micromechanical parameter space.

A cochlear map gives a relationship between frequency of maximum response (CF) and place on the cochlear partition. The cochlear map of Schuknecht (45) (shown in Figure 4.2) will be used here because it was used by Kim, Siegel, and Molnar in presenting the neural response data. The cochlear map of Greenwood (91) (also shown in Figure 4.2) is quite similar to the one of Schuknecht. For the purpose of constraining partition parameters we will use an approximation to the cochlear map which has the functional form

$$f_p(x) = a_1 \exp(a_2 x), \tag{4.15}$$

where $f_p(x)$ is the frequency of maximum response at position x and the constants a_1 and a_2 are given in Table 4.2.

The neural data of Kim, Siegel, and Molnar are shown in Figure 2.10 as the amplitude and phase of a particular measure of neural response as a function of CF for a sinusoidal stimulus. (See section 2.2 for a description of the neural response measure.) We will

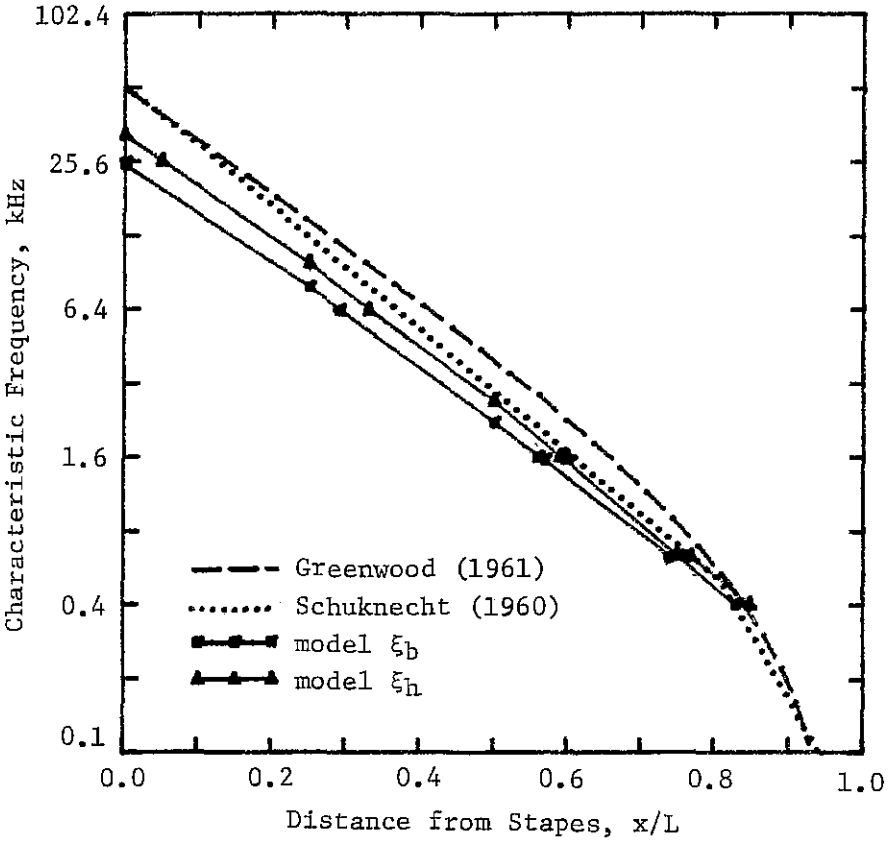

Figure 4.2. Cochlear frequency-to-place map for cat. Comparison of experimentally determined cochlear maps of Schuknecht (45) and Greenwood (91) with computed cochlear map from the frequency-domain model. (Model data from files A001, A002, A003, A004, A005, A006, and A007.)

Table 4.2. Values of a-constants based on experimental data from cat.

From the cochlear map of Schuknecht (45):

$a_1 = 5.0 \times 10^4$ Hz $\qquad a_2 = -2.55$ cm^{-1}

From the neural response phase of Kim, Siegel, and Molnar (4):

$a_3 = -1.3 \times 10^{-4}$ $\qquad a_4 = 1.6$ cm^{-1}

$a_5 = 2.31 \times 10^4$ Hz $\qquad a_6 = -2.78$ cm^{-1}

$a_7 = 0.17$ $\qquad a_8 = -0.5$ cm^{-1}

From the anatomical measurements of Rhode and Geisler (74):

$a_9 = 3.8 \times 10^{-4}$ $\qquad a_{10} = 0.8$ cm^{-1}

$a_{11} = 1.2$ $\qquad a_{12} = -0.5$ cm^{-1}

consider the neural phase data at the two frequencies (f=620 and 1550 Hz) to be represented by two functions of x, $\phi(x;620)$ and $\phi(x;1550)$, where x is related to CF by means of Schuknecht's cochlear map. Each phase function can be separated into four component parts, motivated by analysis of the cochlear model:

$\phi_0(f)$ - due to transmission delay and definition of the phase reference which is independent of x;

$\phi_1(x;f)$ - due to the traveling wave in cochlear fluid pressure;

$\phi_2(x;f)$ - due to the transfer admittance which relates fluid pressure to hair-cell shearing; and

$\epsilon(x;f)$ - due to random phase variations in the cochlea, experimental measurement errors, and error due to modeling approximations. The total measured phase is assumed to be the sum of these four parts:

$$\phi(x;f) = \phi_o(f) + \phi_1(x;f) + \phi_2(x;f) + \epsilon(x;f). \qquad (4.16)$$

Two of the phase components, ϕ_1 and ϕ_2, will be related to cochlear model parameters below. These two phase components are illustrated in Figure 4.3 for f=620 Hz. The component due to the traveling-wave ϕ_1 is characterized by exponential dependence on x. The component due to the resonant TM ϕ_2 has a prominent "phase jump" at the TM resonant frequency.

If we assume that basilar membrane stiffness (as represented by K_1) is slowly varying with x and dominates partition mechanics for most of the neural response data, then it is possible to derive an approximate relationship between K_1 and ϕ_1 based on a one-dimensional model (see Appendix 9.2)

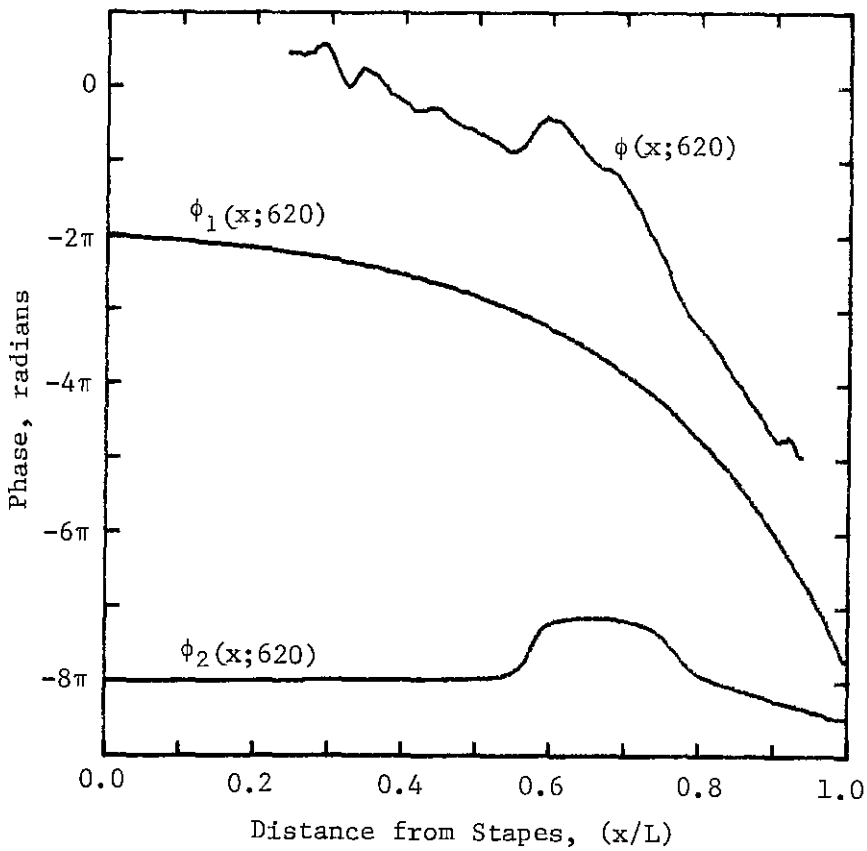

Figure 4.3. Separation of neural phase data into assumed components. The neural data $\phi(x;620)$ is the same as shown in Figure 2.10 from Kim, Siegel, and Molnar (4). The transformation from characteristic frequency to place was made according to Schuknecht's (45) cochlear map. The phase components ϕ_1 and ϕ_2 represent contributions from the pressure traveling-wave and from the resonant tectorial membrane, respectively.

$$K_1(x) = \left(\frac{8\pi^2 f^2}{H}\right)\left[\frac{d}{dx}\phi_1(x;f)\right]^{-2} . \tag{4.17}$$

In order to make use of this relationship, we will assume that ϕ_1 has the form

$$\phi_1(x;f) = 2\pi f\, a_3\,[\exp(a_4 x) - 1] . \tag{4.18}$$

We can also relate ϕ_2 to the model parameters. By design, ϕ_2 is the phase difference between fluid pressure and hair-cell shearing-displacement

$$\phi_2(x;f) = \arg[Y_h(x;f)] - \pi/2 , \tag{4.19}$$

where arg(•) indicates the phase of the complex argument. The fourth-order hair-cell transfer admittance Y_h relates fluid pressure to hair-cell shearing velocity

$$Y_h(x;f) = \left[\frac{g Z_2}{(Z_1+Z_3)(Z_2+Z_3) - Z_3^2}\right] , \tag{4.20}$$

where Z_1,Z_2, and Z_3 are defined in equations (3.25)-(3.27). We will use ϕ_2 to estimate the frequency f_z and damping ζ_z of the "spectral zero" of Y_h (i.e., the zero of Z_2). The two sets of neural response data and the constraint of exponential variation are sufficient to express f_z and ζ_z in the form

$$f_z(x) = a_5 \exp(a_6 x) \tag{4.21}$$

$$\zeta_z(x) = a_7 \exp(a_8 x) . \tag{4.22}$$

The phase components ϕ_0, ϕ_1, and ϕ_2 were chosen to minimize the error function ϵ by a subjective "best fit" criterion. In this way, the values of ϕ_0 were chosen to be: $\phi_0(620) = 0.1$ rad and $\phi_0(1550) = 0.2$ rad. The various contributions to ϕ_0 will be further analyzed in section 6.2.

The mass of BM was determined by using the anatomical measurements of Rhode and Geisler (74) to estimate the cross-sectional area of the portion of the cochlear partition which moves with the BM and multiplying this area by ρ, the volume density of the cochlear fluid. The TM mass was assumed to be half of the BM mass based on a rough comparison of the cross-sectional area of TM with the cross-sectional area used to determine TM mass.

$$m_b(x) = \rho\, a_9 \exp(a_{10}x) \tag{4.23}$$

$$m_t(x) = m_b(x) / 2 \ . \tag{4.24}$$

The radial shear-lever gain g was also estimated from the anatomical measurements of Rhode and Geisler (74).

$$g(x) = a_{11} \exp(a_{12}x) \ . \tag{4.25}$$

The mass parameters M_1 and M_2 can now be determined from known quantities by using equations (4.7), (4.8), (4.23), and (4.24).

Additional assumptions made at this point are based partly on subjective trial-and-error experience with the cochlear model. The other TM related parameters K_2 and R_2 are determined by assuming that the spectral zero frequency f_z is the same as the natural resonant frequency of TM with its attachment to the spiral limbus and uncoupled to RL; the following formulas are applicable (7)

$$K_2(x) = \left[2\pi f_z(x)\right]^2 M_2(x) \tag{4.26}$$

$$R_2(x) = 2\zeta_z(x) \left[2\pi f_z(x)\right] M_2(x) \ . \tag{4.27}$$

Furthermore, the peak frequency f_p is assumed to be the same as the natural resonant frequency of TM with attachments to both the spiral limbus and the reticular lamina and with ξ_b=0; this assumption is used to estimate K_3 which is related to the bending stiffness of the

cilia

$$K_3(x) = (2\pi)^2 \left[f_p^2(x) - f_z^2(x) \right] M_2(x) . \tag{4.28}$$

An additional approximation to equation (4.28) is required because K_3 is constrained to have exponential x variation. We will assume that f_z has the same exponential variation as f_p for the purpose of performing the subtraction in equation (4.27).

In summary, various approximations and assumptions have been used together with selected experimental data to determine the 12 a-constants listed in Table 4.2. These a-constants can be used to explicitly determine 12 of the 16 micromechanical parameters.

$$K_{1o} = 2\rho\, a_3^{-2}\, a_4^{-2}\, H^{-1} \tag{4.29}$$

$$K_{1e} = -2a_4 \tag{4.30}$$

$$M_{1o} = 1.5\rho\, w_p^{-1}\, a_9 \tag{4.31}$$

$$M_{1e} = a_{10} \tag{4.32}$$

$$K_{2o} = 2\pi^2\, w_p^{-1}\, a_5^2\, a_9\, a_{11} \tag{4.33}$$

$$K_{2e} = 2_6 + a_{10} + a_{12} \tag{4.34}$$

$$R_{2o} = 2\pi\rho\, w_p^{-1}\, a_5\, a_7\, a_9 \tag{4.35}$$

$$R_{2e} = a_6 + a_8 + a_{10} + a_{12} \tag{4.36}$$

$$M_{2o} = 0.5\rho\, w_p^{-1}\, a_9\, a_{11} \tag{4.37}$$

$$M_{2e} = a_{10} + a_{12} \tag{4.38}$$

$$K_{3o} = 2\pi^2\rho\, w_p^{-1}\, (a_1^2 - a_5^2)\, a_9\, a_{11} \tag{4.39}$$

$$K_{3e} = 2a_2 + a_{10} + a_{12} . \tag{4.40}$$

Four of the damping parameters were not constrained by the a-constants and were determined by a subjective "best-fit" criterion with comparison to the neural data.

The model parameters used to represent the cat cochlea with resonant tectorial membrane are listed in Table 4.3. This set of model parameters will be referred to as parameter set A (PSA) to distinguish it from other sets of parameters used in this dissertation.

4.3 MODEL RESULTS FOR PARAMETER SET A (PSA)

In this section we present a collection of model results obtained by using parameter set A (PSA) in the two-dimensional cochlear model (see Table 4.3). The model solutions included in this section are intended to characterize the resonant tectorial membrane hypothesis and to provide comparison with experimental data.

Model solutions with the 2-DOF partition include two types of cochlear partition displacement. The displacements of interest are the basilar membrane vertical displacement ξ_b and the hair-cell shearing-displacement ξ_h. These two displacements can be defined in terms of the generalized displacements ξ_1 and ξ_2:

$$\xi_b = -\xi_1 \tag{4.41}$$

$$\xi_h = g(\xi_2 - \xi_1). \tag{4.42}$$

A map of frequency-to place was determined for both ξ_b and ξ_h by finding the frequency of maximum displacement for a given place. The characteristic frequency of each partition-point in the model is slightly different for ξ_b and ξ_h. Figure 4.2 compares the computed cochlear maps (using the frequency-domain model) with the cochlear maps of Schuknecht (45) and Greenwood (91).

Table 4.3. Values for the cochlear model parameters (PSA).

Macromechanical parameters:

$L = 2.25$ cm

$H = 0.1$ cm

$\rho = 1.0$ gm cm^{-3}

$A_s = 0.0126$ cm^2

$w_p = 0.126$ cm

Micromechanical parameters:

$K_{1o} = 4.6 \times 10^8$ dyn cm^{-3},	$K_{1e} = -3.2$ cm^{-1}
$R_{1o} = 50$ dyn sec cm^{-3},	$R_{1e} = 0.5$ cm^{-1}
$M_{1o} = 4.5 \times 10^{-3}$ gm cm^{-2},	$M_{1e} = 0.8$ cm^{-1}
$K_{2o} = 3.8 \times 10^7$ dyn cm^{-3},	$K_{2e} = -5.26$ cm^{-1}
$R_{2o} = 90$ dyn sec cm^{-3},	$R_{2e} = -3.0$ cm^{-1}
$M_{2o} = 1.8 \times 10^{-3}$ gm cm^{-3},	$M_{2e} = 0.3$ cm^{-1}
$K_{3o} = 1.5 \times 10^8$ dyn cm^{-3},	$K_{3e} = -4.7$ cm^{-1}
$R_{3o} = 100$ dyn sec cm^{-3},	$R_{3e} = -2.0$ cm^{-1}

Helicotrema parameters:

$L_h = 0.05$ cm

$R_h = 50$ dyn sec cm^{-3}

Spatial discretization parameters:

$M = 4$

$N = 240$

Figures 4.4 and 4.5 show families of solutions of the frequency-domain model for basilar membrane displacement ξ_b and hair cell shearing ξ_b at four frequencies: 0.4, 1.6, 6.4, and 25.6 kHz. Stapes displacement ξ_s was used as the reference for both the magnitude and phase curves.

Model solutions at 620 and 1550 Hz are compared with neural response data in Figure 4.6. The neural data is the same as that shown in Figure 2.10 with two modifications: the characteristic frequency has been mapped to place according to Schuknecht's cochlear map (36) and the phase has been shifted vertically by 0.58π for the 620 Hz curve and by 0.42π for the 1550 Hz curve (see section 6.2).

Figures 4.7 and 4.8 show two-dimensional views of the upper cochlear scala based on solutions of the frequency-domain model at 1.6 kHz. For these two figures the value of the discretizing variable M was increased to 16 in order to provide better spatial resolution in the y dimension. The x and y dimensions have been scaled differently to provide a better view of the y dimension.

Figure 4.7 shows the fluid pressure $P_d(x,y)$ in the frequency-domain model at 1.6 kHz by means of (a) iso-magnitude contours and (b) iso-phase contours. The iso-phase contours in Figure 4.7(b) can be used to identify three, distinct regions along the cochlear partition. A "long-wave" region (from x/L=0.00 to x/L=0.64) is characterized by phase contours which are nearly vertical and extend all the way from y=0 to y=H. A "short-wave" region (from x/L=0.64 to x/L=0.72) is characterized by phase contours which converge on pressure "nodes" located between y=0 and y=H. Finally, a

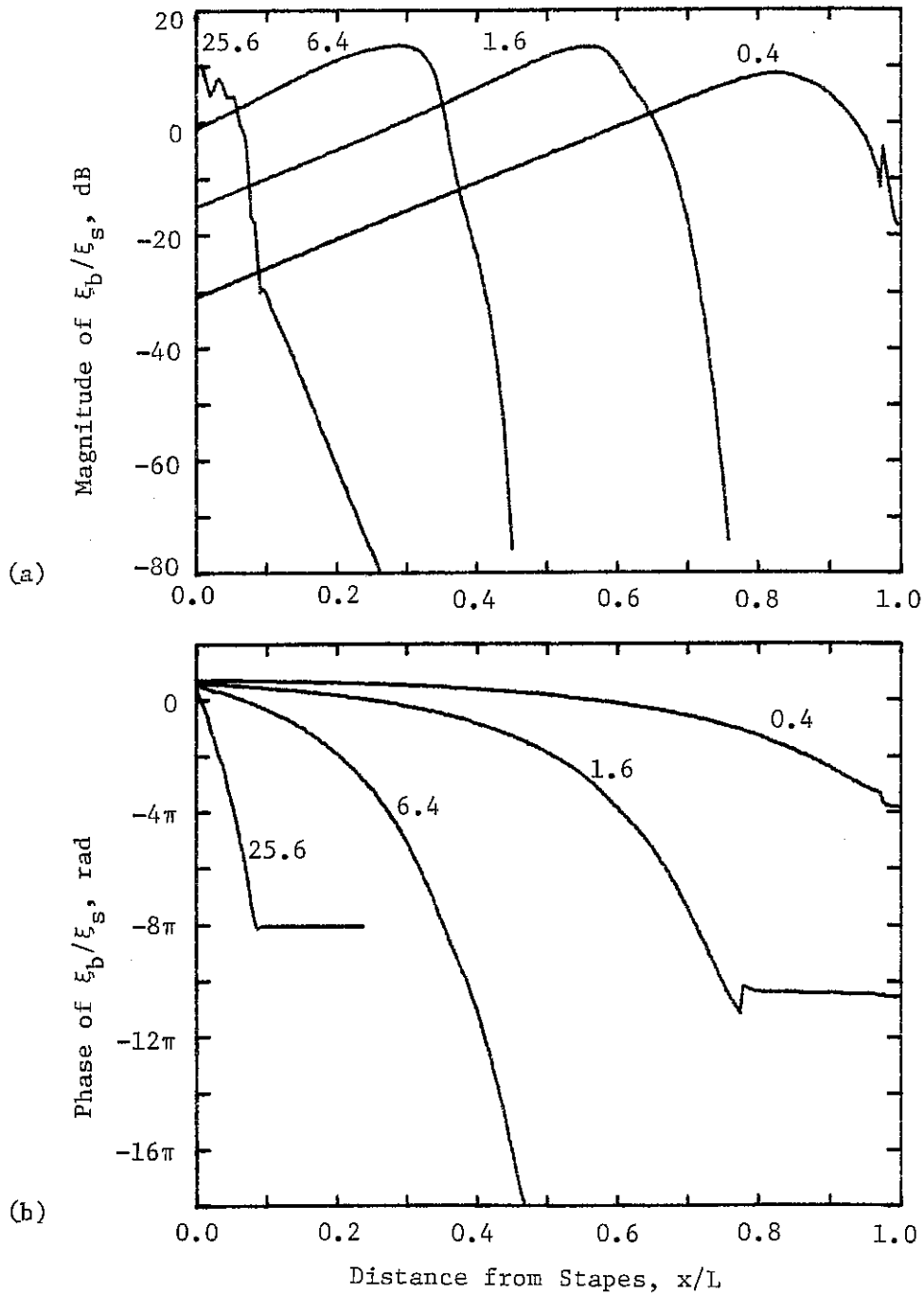

Figure 4.4. Basilar membrane displacement as a function of distance from the stapes (PSA). The curves show the ratio of basilar membrane displacement ξ_b to stapes displacement ξ_s from the frequency-domain model at four frequencies. (a) Magnitude. (b) Phase. The numerals denote frequency in kHz. (Model data from files A001, A002, A003, and A004.)

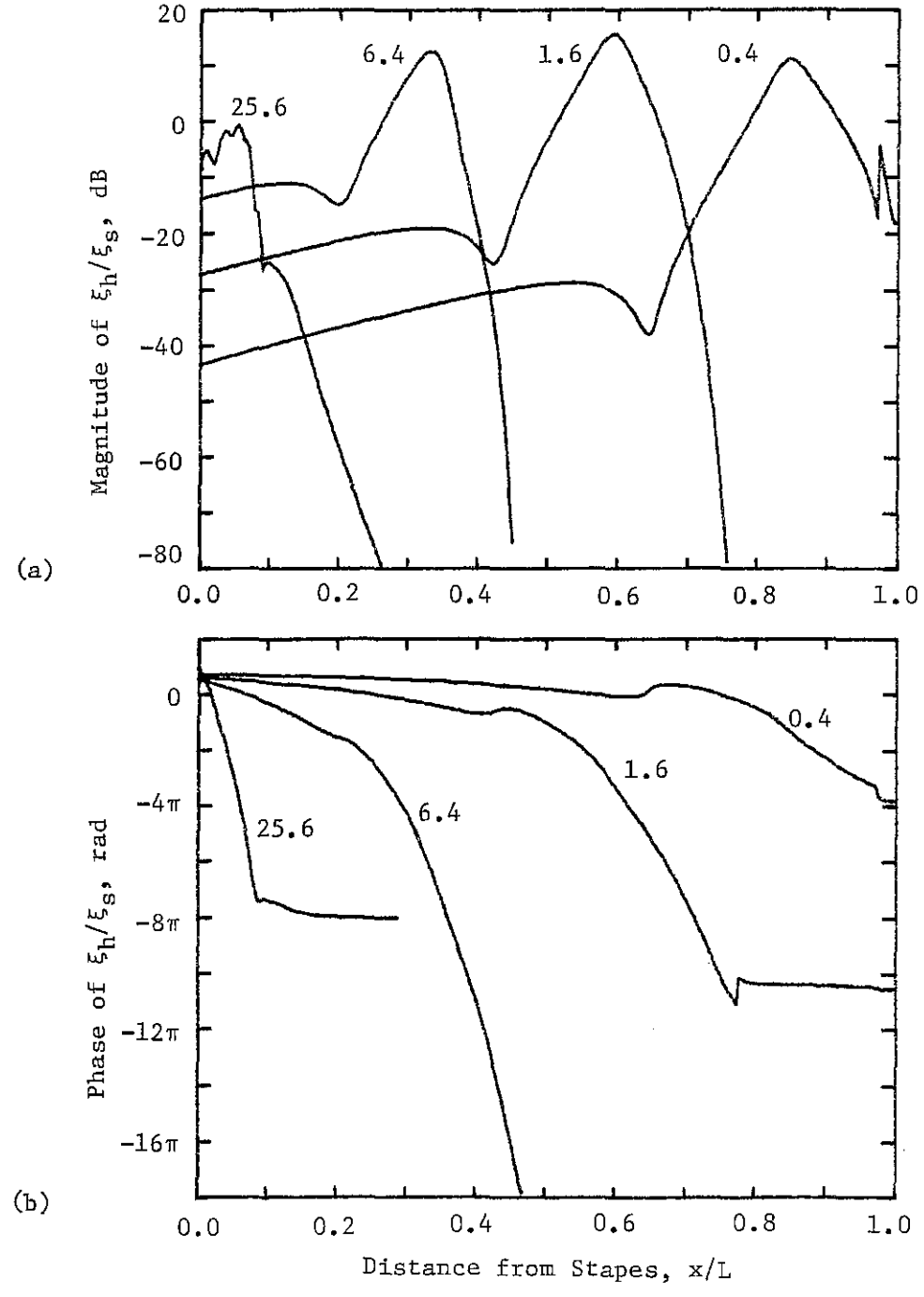

Figure 4.5. Hair cell shearing-displacement as a function of distance from the stapes (PSA). The curves show the ratio of basilar membrane displacement ξ_b to stapes displacement ξ_s from the frequency-domain model at four frequencies. (a) Magnitude. (b) Phase. The numerals denote the frequency in kHz. (Model data from files A001, A002, A003, and A004.)

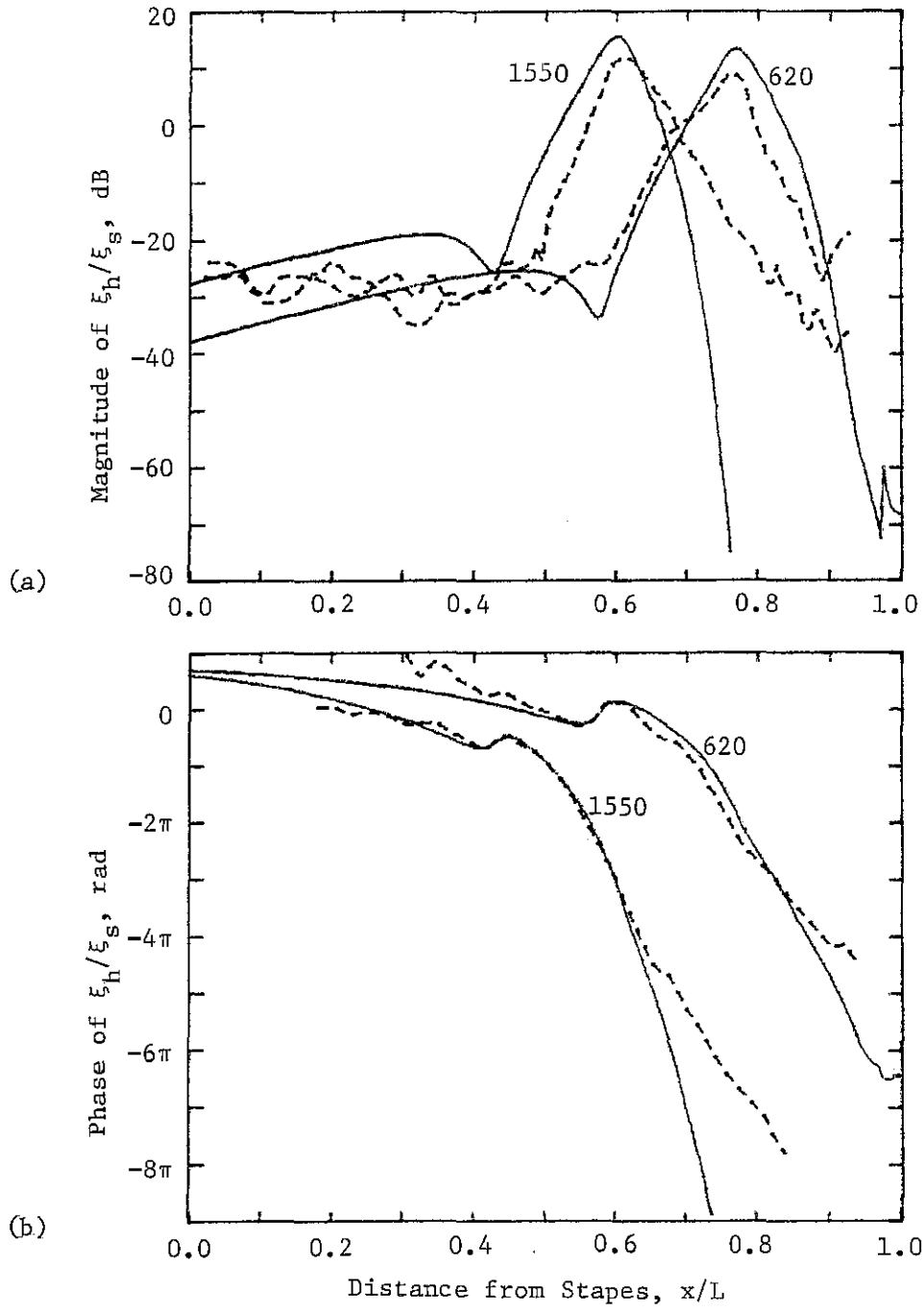

Figure 4.6. Comparison of model results for hair cell shearing-displacement with neural response data. The solid lines show the ratio of hair cell shearing-displacement ξ_h to stapes displacement ξ_s from the frequency-domain model at two frequencies. The dashed lines show the neural spatial-mapping data of Kim et al. (4) with a frequency-to-place transformation and a vertical shift of phase (see text). The numerals indicate frequency in Hz. (Model data from files A005 and A006).

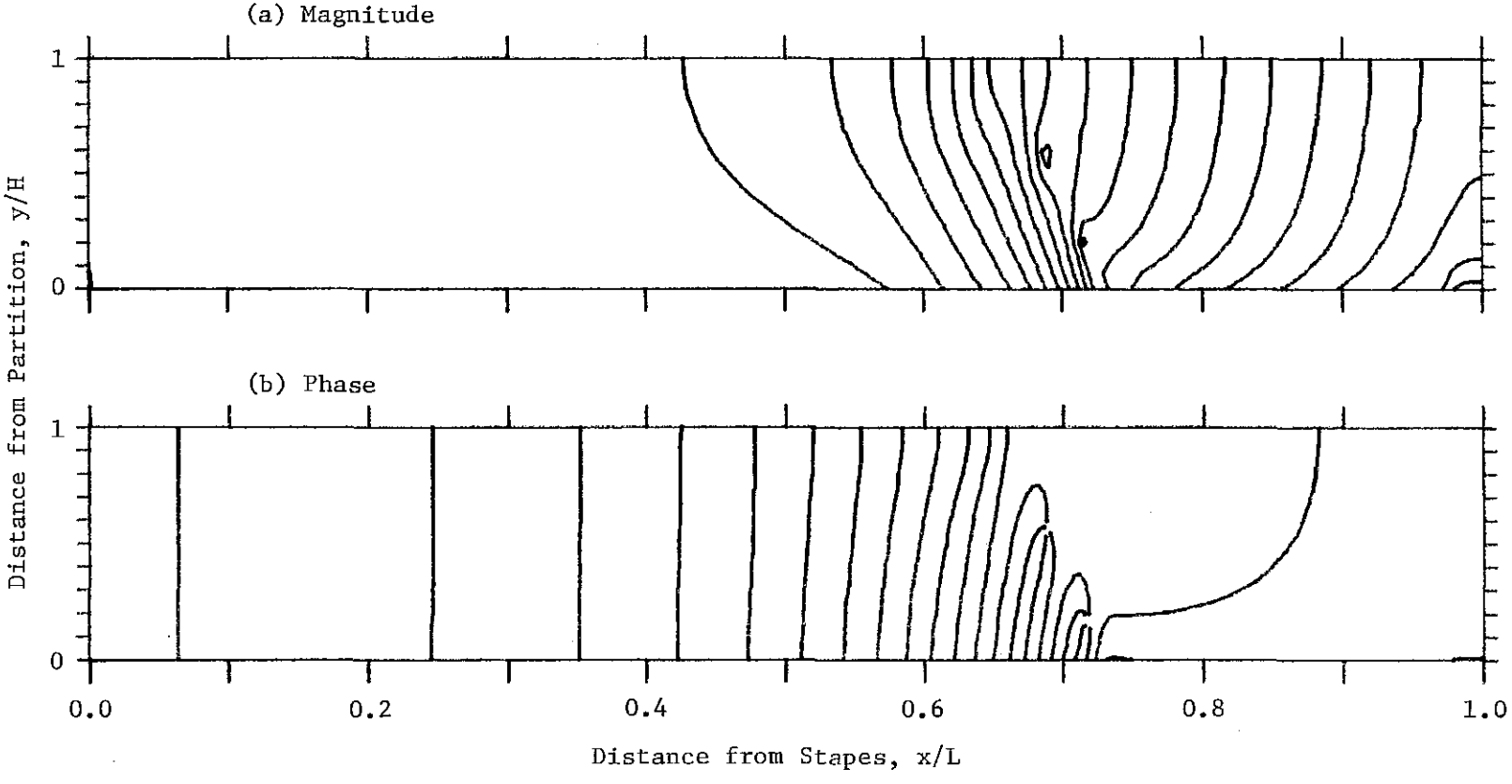

Figure 4.7. Iso-pressure contours in the two-dimensional, frequency-domain model (PSA). (a) Iso-magnitude contours with 10 dB separation between contours. (b) Iso-phase contours with a quarter cycle separation between contours. This figure represents a solution of the frequency-domain model at 1.6 kHz and with parameter set A, except with M=16. (Model data from file A007.)

"plateau" region (from x/L=0.72 to x/L=1.00) is characterized by widely spaced phase contours, indicating little phase variation in this region.

The pressure "nodes" of the short-wave region are often seen in solutions of the frequency-domain model. These nodes are characterized by a local minimum in the magnitude of the pressure and convergence of the phase contours at some point in the cochlear fluid. On a small circular path around one of these nodes the magnitude of the pressure is nearly constant and the phase changes by one full cycle. These pressure nodes are prominent features in the iso-magnitude and iso-phase contour plots, but are not obvious in plots of instantaneous pressure. The physical significance of the pressure nodes is not understood at this time.

In order to visualize the flow of energy through the two-dimensional fluid, we will define a time-average, energy-flux vector

$$\underline{E}(x,y;i\omega) = \tfrac{1}{2}\mathrm{Re}[\tfrac{1}{2}P_d(x,y;i\omega)\cdot V^*(x,y;i\omega)] \tag{4.43}$$

where

$$\underline{V}(x,y;i\omega) = \underline{\nabla}P_d(x,y;i\omega)/(2i\omega\rho). \tag{4.44}$$

The definition of $\underline{E}$ is after de Boer (92) and is analogous to the time-average, Poynting vector used in the study of electromagnetic fields (93). The component of energy-flux perpendicular to any surface equals the energy transported across that surface per unit area per unit time. The lines of energy-flux in Figure 4.8 indicate the flow of energy in the two-dimensional model. The flux lines are drawn in small, fixed-length segments oriented in the direction of the

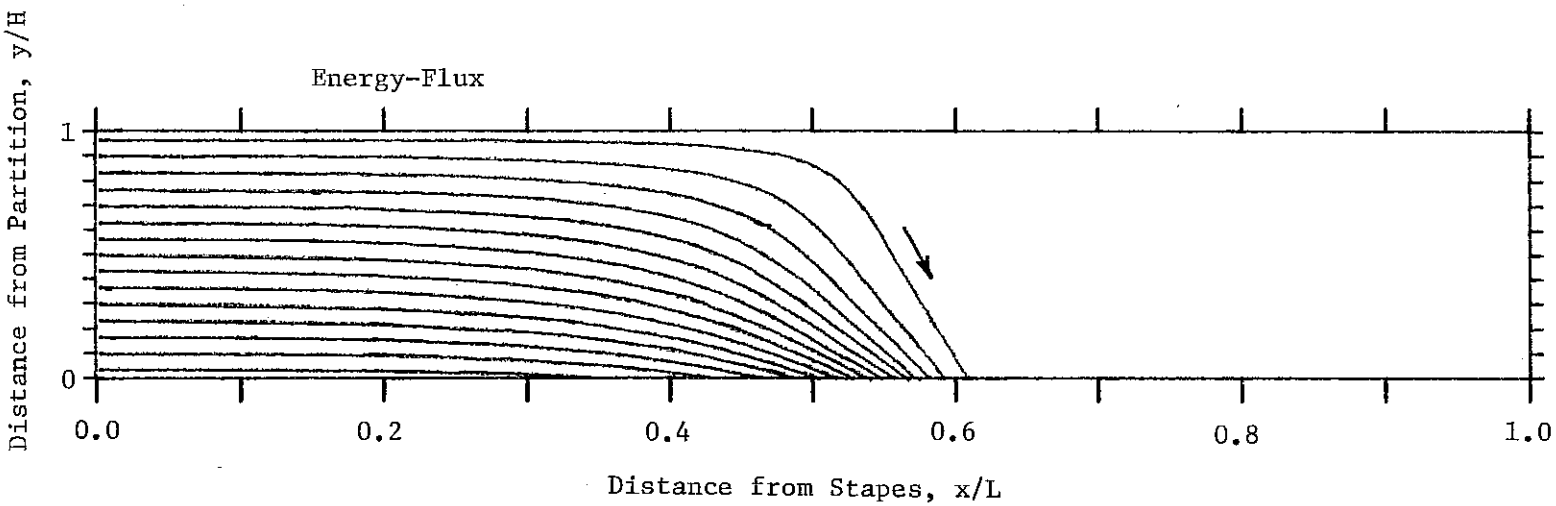

Figure 4.8. Lines of energy-flux in the two-dimensional, frequency-domain model (PSA). All flux lines start near the stapes and terminate at the partition boundary. This figure represents a solution of the frequency-domain model at 1.6 kHz and with parameter set A, except with M=16. (Model data from file A007.)

local energy-flux vector. These energy-flux lines are uniformly spaced at the stapes boundary where the energy-flux is uniformly distributed; elsewhere, the spacing of the energy-flux lines gives a qualitative indication of the relative energy-flux.

Analysis of the phase of the neural response (see section 6.2) involves some consideration of the response latency. The latency of a measured response to a "click" stimulus can be defined as the time between the onset of the stimulus and the first zero-crossing of the response; this definition of latency is illustrated in Figure 4.9 for a solution of the time-domain model. Kim and Molnar (94) used an equivalent definition in measuring the latencies of spike discharge in single nerve fibers to a click stimulus. The solid line in Figure 4.10 is a moving-window average of nerve fiber latencies in one cat versus fiber characteristic frequency.

Time-domain model latencies were determined for ξ_b and ξ_h at many positions along the partition and are also plotted in Figure 4.10. (The cochlear maps for ξ_b and ξ_h in Figure 4.2 were used to relate position to characteristic frequency.) For characteristic frequencies above 1 kHz the neural latency is about 0.7 ms more than the model ξ_h latency; the additional delay in the neural response is attributed to the time required for chemical synaptic transmission and time required for propagation of the spike discharge along the nerve fiber from the synapse to the site where the neural response is being measured. For frequencies around 0.3 kHz the model latency is about equal to the neural latency, suggesting that there is no neural propagation delay for fibers with low characteristic frequency; this must be an

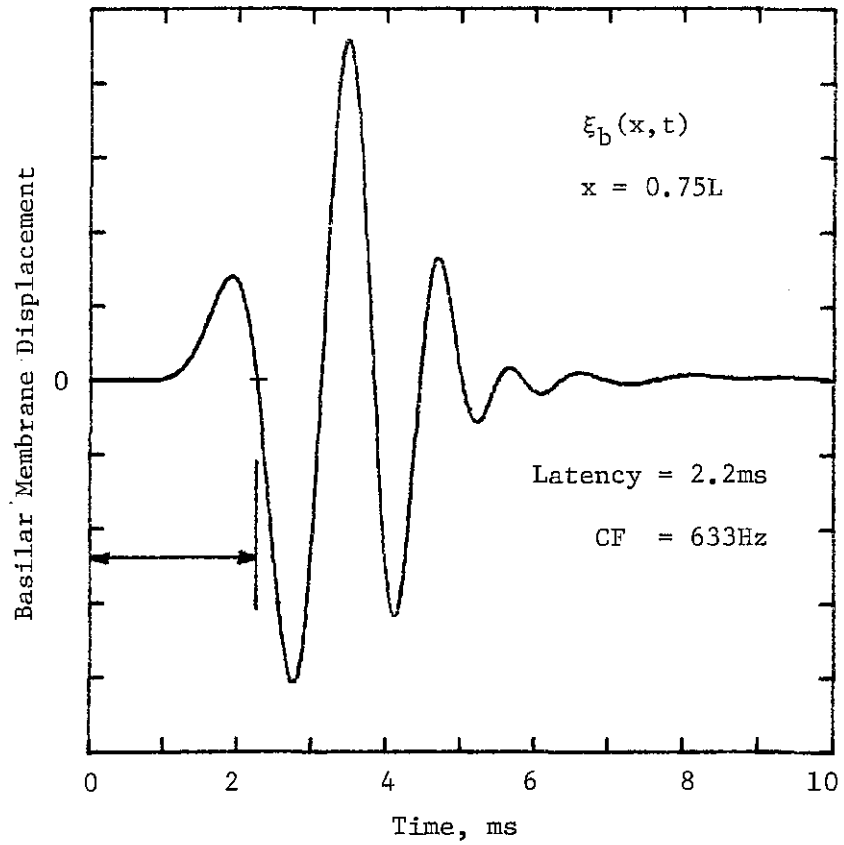

Figure 4.9. Basilar membrane displacement as a function of time. The curve shows basilar membrane displacement ξ_b at (x/L)=0.75 from the time-domain model with parameter set A. The stimulus was specified as a low-pass filtered impulse of voltage to the earphone. The latency of the basilar membrane response is defined as the time between the onset of the stimulus and the first zero-crossing of the response. The CF for this place on the basilar membrane was determined by referring to Figure 4.2. (Model data from file IM23-1.)

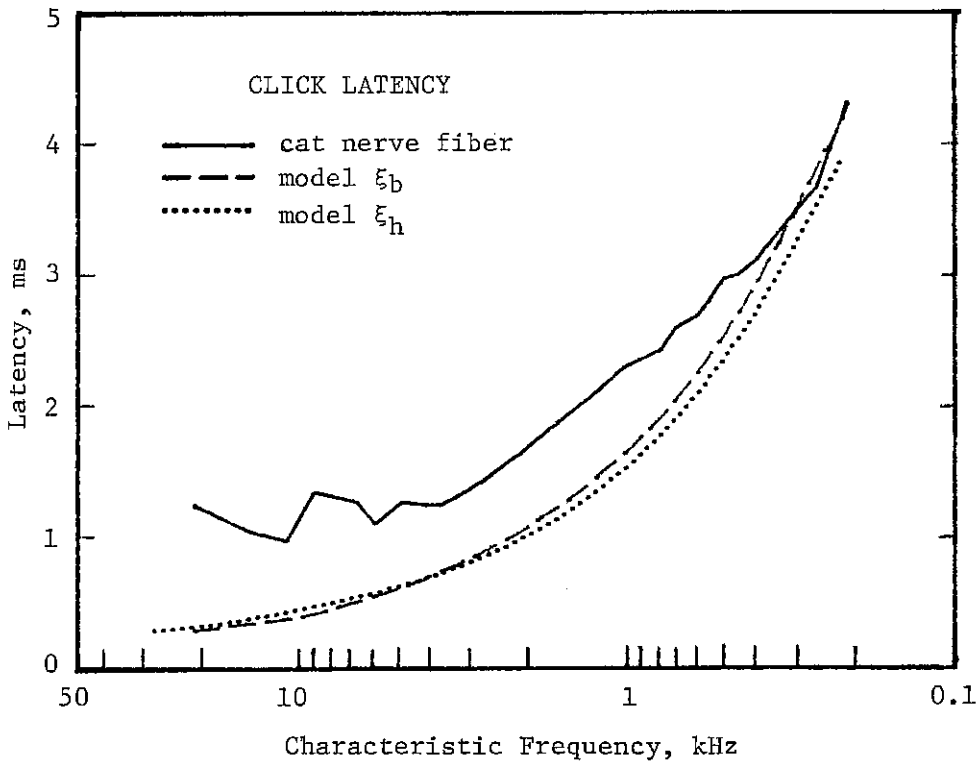

Figure 4.10. Comparison of the latency of spike discharge in cat nerve fibers with the latency of cochlear partition displacement in the time-domain model. The latency of a response to a click stimulus was defined in Figure 4.9. The solid line representing cat nerve fiber data is a moving-window average of latencies measured in many individual nerve fibers in one cat [from Kim and Molnar (94)]. The curves representing model results were obtained from a solution of the time-domain model with PSA. (Model data from file IM23-1.)

incorrect result and reflects an inadequacy of the model at low frequencies. (Additional time-domain model results with PSA are included in Appendix 9.4.)

5. NEGATIVE DAMPING IN THE COCHLEAR PARTITION

In this chapter we will investigate a second method of achieving sharper cochlear tuning with a 2-DOF partition. The most important feature of this second sharpening mechanism is its use of a damping element with a negative damping value; the purpose of this damping element is to introduce mechanical energy into the cochlear model at the expense of an assumed source of biomechanical energy. The sharpening mechanism with negative damping will be referred to as an active mechanism to emphasize its dependence on an internal source of energy. A possible physical interpretation for an active sharpening mechanism, based on assumed special properties of outer hair cell (OHC) cilia, is presented in section 5.1. A set of model parameters is chosen in section 5.2 to produce model solutions which resemble direct basilar membrane measurements of Rhode (3). Model results are presented in section 5.3 and compared with Rhode's data.

5.1 COCHLEAR PARTITION-POINT MODEL WITH RESONANT OHC CILIA

In the resonant tectorial membrane model described in section 4.1 the transfer admittance Y_h, which relates fluid pressure to hair cell shearing velocity, has a "spectral zero" at a frequency about an octave below the characteristic frequency at any given place. For a fixed frequency, the real part of the transfer impedance, $Z_h = 1/Y_h$, becomes negative in a small region basal to the characteristic place. The profile of $Re[Z_h]$ versus x is similar to the damping profile used by Kim et al. (19) to demonstrate the sharpening effect of negative damping in the cochlear partition. This similarity prompted a search

for a set of micromechanical parameters for the 2-DOF partition which would produce the same sort of profile in the real part of the partition driving-point impedance, $Z_b = 1/Y_b$, (see section 3.3 for the definition of Y_b). An essential feature of the parameter values which produce the desired driving-point impedance is that (at least) one of the damping elements must have a negative damping value.

At first, a phenomenological approach was used to find parameters for the 2-DOF partition which would produce sharper basilar membrane tuning through the use of a negative damping element. The physical interpretation of the second degree-of-freedom as the tectorial membrane is not necessarily incompatible with the incorporation of a negative damping element, however, an alternative physical interpretation will be presented in this chapter.

The outer hair cell (OHC) cilia seem to be a likely candidate for the site of generation of the experimentally observed spontaneous and evoked cochlear emissions (17). If the OHC cilia are responsible for the spontaneous emissions, they must have the capability of maintaining a state of sustained oscillation, powered by some metabolic source of energy. The physical interpretation of the 2-DOF partition which follows is based on the hypothesis that the OHC cilia are capable of generating mechanical energy at the expense of some metabolic energy source and that this capability normally acts to sharpen basilar membrane tuning without causing the cilia to go into a state of continued oscillation.

Figure 5.1 shows a schematic drawing of a cochlear partition cross-section with 2-DOF's. In this partition model, the basilar membrane (BM) and tectorial membrane (TM) are represented [Figure 5.1(a)] in the same manner as the 1-DOF partition model (Figure 2.13) which was reviewed in section 2.5. The shearing between TM and reticular lamina (RL) is completely determined by the shear lever gain $g(x)$, which is independent of time. The viscous damping r_p and partition bending stiffness k_p are also the same as in the 1-DOF partition.

The second degree-of-freedom for this 2-DOF partition model is due to the bending motion of the OHC cilia. The combined effect of the three rows of outer hair cells, each with three (or more) rows of cilia, is represented in Figure 5.1(b) by a single cilium. This cilium is assumed to pivot at its base on RL and have its top imbedded in TM (95). The displacement of the mid-portion of the cilium is represented in Figure 5.1(b) by a lateral displacement ξ_c of the lumped cilium mass m_c relative to a fixed point on TM. The bending motion of the cilium in this model is opposed by a bending stiffness k_c and a viscous damping r_c. The final (and most important) element of the active partition model is a damping element r_a associated with the base of the cilium, which will be assigned a negative damping value. This 2-DOF partition model has the property that it reduces to the traditional 1-DOF partition when the active element r_a is set to zero.

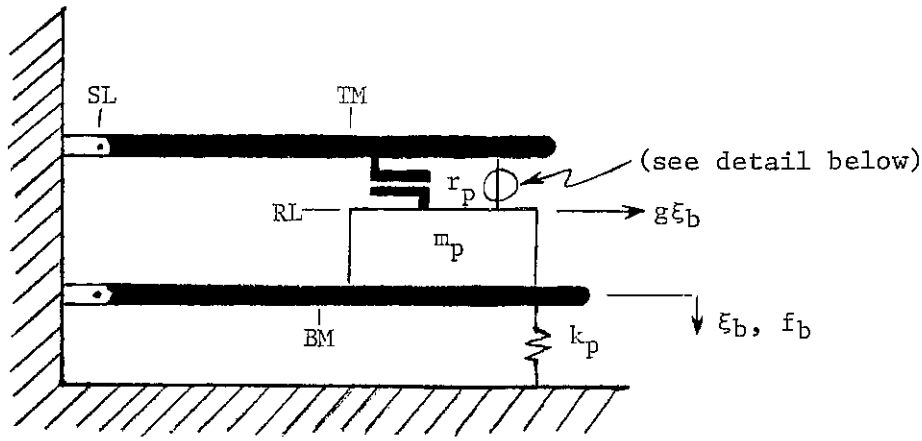

(a)

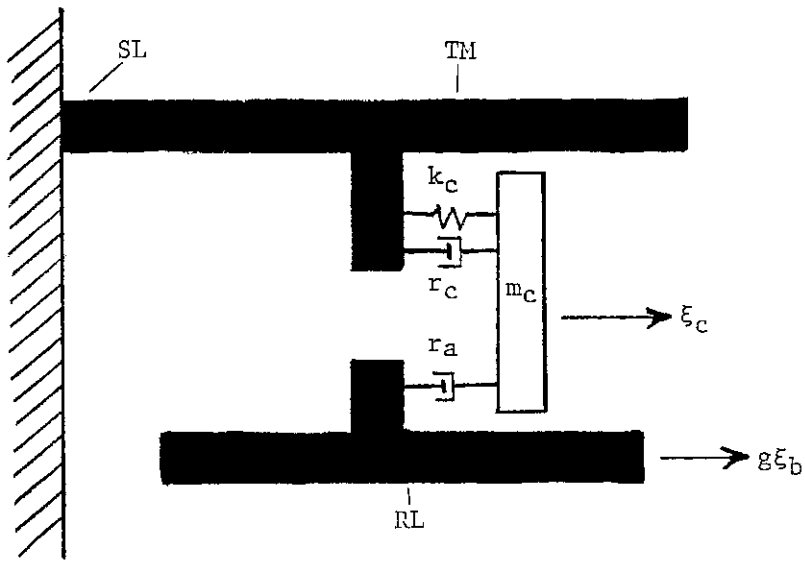

(b)

Figure 5.1. A 2-DOF partition model with resonant OHC cilia. (a) The first DOF is the same as the traditional 1-DOF partition (see Figure 2.13). (b) Detail of the sub-tectorial space shows the second DOF associated with lateral motion of the OHC cilia. TM - tectorial membrane; BM - basilar membrane; SL - spiral limbus; RL - reticular lamina. Other symbols are described in Table 5.1.

The micromechanics of the cochlear partition with resonant OHC cilia are described by the following equations of motion:

$$f_b = m_p \ddot{\xi}_b + g^2 r_p \dot{\xi}_b + k_p \dot{\xi}_b + g r_a (g \dot{\xi}_b - \dot{\xi}_c) \tag{5.1}$$

$$0 = m_c \ddot{\xi}_c + r_c \dot{\xi}_c + k_c \xi_c + r_a (\dot{\xi}_c - g \dot{\xi}_b) \quad , \tag{5.2}$$

where f_b is the vertical force (per unit length) applied to the basilar membrane at the same place where basilar membrane displacement ξ_b is measured. Both $f_b(t)$ and $\xi_b(x,t)$ are defined to be positive downward. The cilium displacement $\xi_c(x,t)$ is defined to be positive away from the spiral limbus (SL). Equations (5.1) and (5.2) are the same as the general equations of motion given by equations (3.8) and (3.9) with the following change of variables:

$$P_d = f_b / w_p \tag{5.3}$$

$$\xi_1 = -\xi_b \tag{5.4}$$

$$\xi_2 = -\xi_c / g \tag{5.5}$$

$$M_1 = m_p / w_p \tag{5.6}$$

$$M_2 = g m_c / w_p \tag{5.7}$$

$$K_1 = k_p / w_p \tag{5.8}$$

$$K_2 = g k_c / w_p \tag{5.9}$$

$$K_3 = 0 \tag{5.10}$$

$$R_1 = g^2 r_c / w_p \tag{5.11}$$

$$R_2 = g r_c / w_p \tag{5.12}$$

$$R_3 = g r_a / w_p \, , \tag{5.13}$$

where, as before, $w_p = A_s/H$ is the effective width of the cochlear partition associated with the two-dimensional model. The

micromechanical variables and parameters which characterize the partition model with resonant OHC cilia are described in Table 5.1.

5.2 MODEL PARAMETERS TO MATCH BASILAR MEMBRANE DATA

The direct experimental measurement by Rhode (3) of basilar membrane motion in squirrel monkey was reviewed in section 2.3. In this section we will use Rhode's data to help us choose values for the model parameters which demonstrate the sharpening effect of the active partition with resonant OHC cilia.

Since detailed information about the anatomy of the squirrel monkey's ear is not available, we will assume that it is similar to the cat. Therefore, the middle-ear parameters and macromechanical cochlear parameters in this chapter are the same as those used in chapter 4, except for the scala height H which will be adjusted to provide better correspondence between model solutions and Rhode's data.

As in chapter 4, we will define a set of constants to characterize the experimental data and use these constants to derive contraints on the model parameters. The first group of b-constants describe the amplitude and phase of the experimental basilar membrane to malleus response ratio at a fixed place on BM (see Figure 2.5):

b_1 - frequency of maximum response or characteristic frequency (CF), Hz.

b_2 - amplitude of the basilar membrane to malleus displacement ratio obtained by fitting a 6 dB/octave line to the low frequency data points and extending it until it reaches CF.

b_3 - slope of the low-frequency phase data, cycles/Hz.

Table 5.1. Dependent variables and parameters for the cochlear partition model with resonant OHC cilia. (See Figure 5.1).

Cochlear partition variables:

ξ_b - basilar membrane vertical displacement, cm.

ξ_c - cilium lateral displacement, cm.

f_b - vertical force applied to basilar membrane, dyn/cm.

Cochlear partition parameters:

k_p - partition bending stiffness, dyn cm^{-2}

r_p - sub-tectorial fluid space damping, dyn sec cm^{-2}.

m_p - partition mass, gm/cm.

k_c - cilium bending stiffness, dyn cm^{-2}.

r_c - cilium bending damping, dyn sec cm^{-2}.

m_c - cilium mass, gm/cm.

r_a - active damping element, dyn sec cm^{-2}.

g - radial shear lever gain.

b_4 - slope of the mid-frequency phase data, cycles/Hz.

b_5 - frequency of the beginning of the phase plateau region, Hz.

The next group of b-constants provide additional information needed to model the above basilar membrane data

b_6 - average ratio of malleus displacement to stapes displacement below CF.

b_7 - place on the basilar membrane at which the displacement data was obtained as a fraction of the total length L of the cochlea.

b_8 - natural log of the fractional change in CF which results from a small change in place on the basilar membrane (toward the apex) divided by the distance (cm) between the two places, cm^{-1}.

In order to retain some correspondence between the model parameters and the resonant OHC cilia hypothesis, we will define

b_9 - ratio of the mass of the OHC cilia to the total mass of the partition.

Estimates for the b-constants, based on experimental data, are listed in Table 5.2.

As before, the micromechanical parameters are constrained to have exponential x variation. With this in mind, the squirrel monkey cochlear (frequency-to-place) map is assumed to have an exponential form,

$$f_c(x) = b_1 \exp [\, b_8(x - b_7 L)\,] , \tag{5.14}$$

where f_c is the CF at position x.

Table 5.2. Values of b-constants chosen to characterize direct basilar membrane measurements.

From squirrel monkey basilar membrane to malleus transfer ratio [Rhode's animal 69-473, (56)]:

$b_1 = 7.4 \times 10^3$ Hz

$b_2 = 3.7$

$b_3 = -4.3 \times 10^{-4}$ cycles/Hz (1 to 6 kHz)

$b_4 = -7.7 \times 10^{-4}$ cycles/Hz (6 to 9 kHz)

$b_5 = 9.0$ Hz

Squirrel monkey malleus to stapes ratio (74):

$b_6 = 2$ (0.1 to 8 kHz)

Position of measurement on basilar membrane (74):

$b_7 = 0.25$ ("basal turn")

From squirrel monkey dual position measurements (74):

$b_8 = -1.4$ cm^{-1}

From chinchilla anatomical measurements (95, 96):

$b_9 = 10^{-4}$

In the remainder of this section the b-constants are related to the micromechanical model parameters in a manner similar to that used in section 4.2. Unfortunately, the parameter relationships which are presented in this chapter are not as well developed as those in the chapter 4; accordingly, it was much more difficult to find suitable parameter values.

First consideration was given to the selection of parameter values for partition stiffness K_1 and scala height H. Initially, these parameter values were determined by approximate formulas based on a one-dimensional model, similar to the formulas derived in Appendix 9.2. The initial parameter values were modified to improve the agreement between model solutions and Rhode's direct measurements. The approximate formulas were useful in indicating the type of change in parameter values that was needed to achieve a desired effect on the model solution; however, quantitative evaluation of the formulas in Appendix 9.2 does not yield the same parameter values as listed in Table 5.3.

In the model, the transition to the plateau region occurs approximately at the natural resonance of the (unloaded) partition. The loading of the fluid mass on the partition and the second degree-of-freedom have an effect on the location of the plateau transition. The value of partition mass, as represented by M_1, was chosen by starting at a value which assumed 1-DOF and no fluid loading and then decreasing this value (by trial-and-error) in order to shift the plateau transition (in the frequency-domain solutions) toward the apex.

$$M_{1o} < (2\pi b_5)^{-2} K_{1o} \exp(2 b_7 b_8 L) \tag{5.15}$$

$$M_{1e} = K_{1e} - 2 b_8 . \tag{5.16}$$

The mass of the OHC cilia m_c can be related to the mass of the partition m_p. For simplicity, we assume that the shear lever gain is equal to 1 for all x,

$$g(x) = 1 , \tag{5.17}$$

so that,

$$M_{2o} = b_9 M_{1o} \tag{5.18}$$

$$M_{2e} = M_{1e} . \tag{5.19}$$

The natural resonance of the OHC cilia determines the frequency of the spectral zero in the partition driving-point impedance, Z_b. At a given place, the active behavior of the OHC cilia will have its greatest effect at the frequency of this spectral zero. The spectral zero is possibly related to the break in slope of both the magnitude and phase of Rhode's basilar membrane data, which typically occurs about half an octave below CF (see Figure 2.5). The value for cilia stiffness in the model, as represented by K_2, was chosen to place the spectral zero about half an octave below CF.

Because the cilia mass is much smaller than the partition mass, the effect of the second degree-of-freedom will only be significant when

$$\left| \frac{R_3^2}{R_2 + R_3} \right| \approx R_1 . \tag{5.20}$$

This condition was achieved by choosing

$$R_3 \approx -R_2 , \tag{5.21}$$

so that the denominator in equation (5.20) becomes relatively small.

(The value of R_2 is chosen to be positive and the value of R_3 is chosen to be negative.) Together, R_2 and R_3 make the OHC cilia a source of energy which is capable of boosting the response of the partition. Extreme care must be taken in choosing these cilia damping values in order to avoid dynamic instability in the time-domain model. Dynamic instability is identified in the time-domain model by solutions which continue to grow in amplitude until some time-domain variable exceeds the limits of floating-point representation on the computer. The subject of model stability will be discussed further in chapter 6.

The values of the model parameters chosen to demonstrate the active sharpening mechanism and to simulate Rhode's basilar membrane data (animal 69-473) are listed in Table 5.3. This set of parameters will be referred to as parameter set B (PSB) to distinguish it from other sets of parameters used in this dissertation.

5.3 MODEL RESULTS FOR PARAMETER SET B (PSB)

In this section we present a collection of model results obtained by using parameter set B (PSB) in the two-dimensional cochlear model (see Table 5.3). The model solutions included in this section are intended to characterize an active sharpening mechanism and to provide comparison with experimental data.

The partition driving-point impedance, $Z_b = 1/Y_b$, describes the mechanical properties of the partition boundary for the frequency-domain model (see section 3.3). The real and imaginary parts of $Z_b(x)$ are shown in Figure 5.2 for four different frequencies: 1, 2, 4, and 8 kHz. The real part of Z_b determines

Table 5.3. Values for the cochlear model parameters (PSB).

Macromechanical parameters:

$L = 2.25$ cm

$H = 0.3$ cm

$\rho = 1.0$ gm cm^{-3}

$A_s = 0.0126$ cm^2

$w_p = 0.042$ cm

Micromechanical parameters:

$K_{1o} = 1.32 \times 10^{8}$ dyn cm^{-3},	$K_{1e} = -3.1$ cm^{-1}
$R_{1o} = 500$ dyn sec cm^{-3},	$R_{1e} = -1.4$ cm^{-1}
$M_{1o} = 5.0 \times 10^{-3}$ gm cm^{-2},	$M_{1e} = -0.3$ cm^{-1}
$K_{2o} = 3.30 \times 10^{3}$ dyn cm^{-3},	$K_{2e} = -3.1$ cm^{-1}
$R_{2o} = 5.000$ dyn sec cm^{-3},	$R_{2e} = -1.7$ cm^{-1}
$M_{2o} = 5.0 \times 10^{-7}$ gm cm^{-3},	$M_{2e} = -0.3$ cm^{-1}
$K_{3o} = 0$ dyn cm^{-3},	$K_{3e} = 0$ cm^{-1}
$R_{3o} = -4.960$ dyn sec cm^{-3},	$R_{3e} = -1.7$ cm^{-1}

Helicotrema parameters:

$L_h = 0.05$ cm

$R_h = 50$ dyn sec cm^{-3}

Spatial discretization parameters:

$M = 4$

$N = 240$

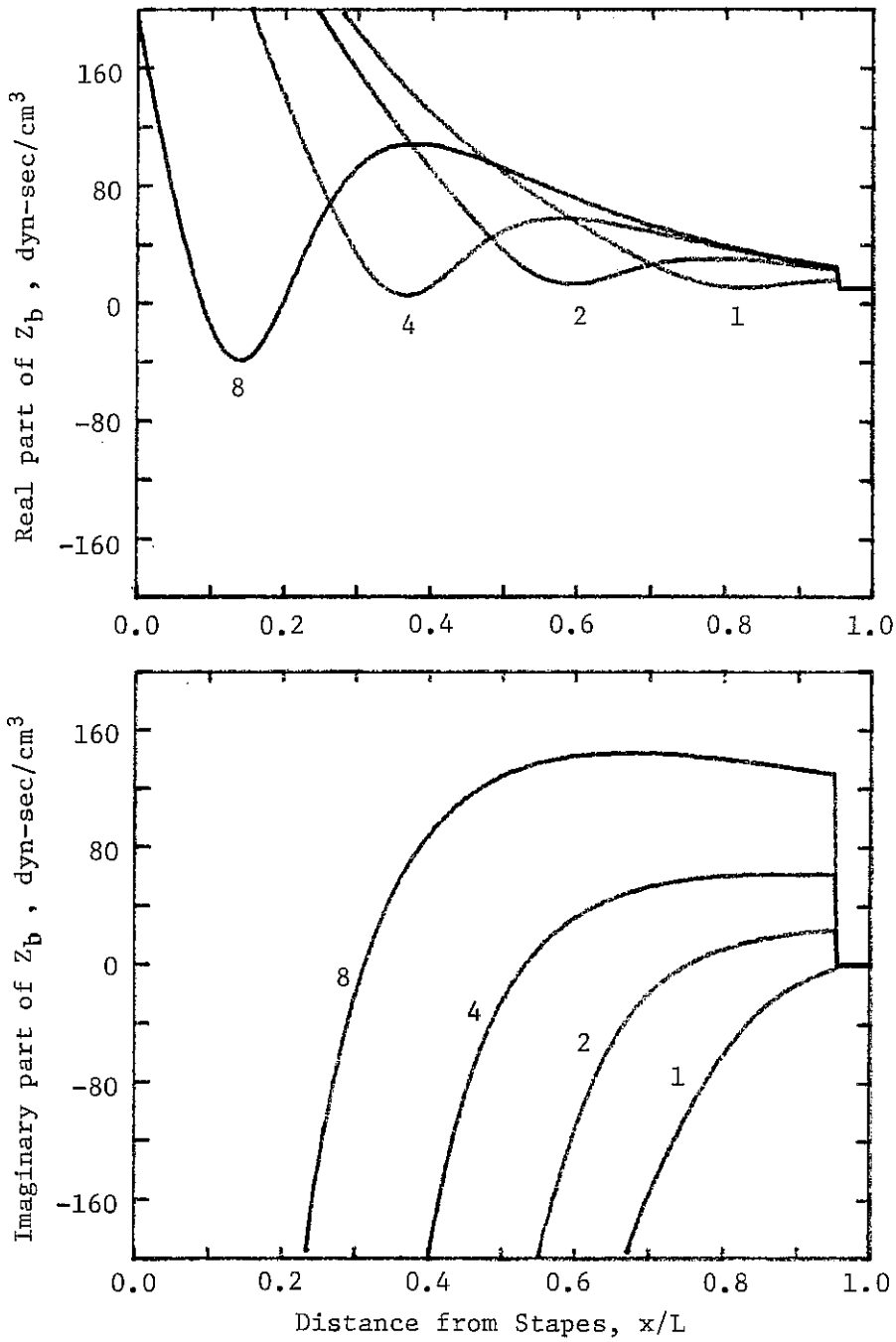

Figure 5.2. Driving-point impedance of the cochlear partition (PSB). (a) Real part of $Z_b(x)$. (b) Imaginary part of $Z_b(x)$. Four frequencies are shown superimposed. The numerals indicate frequency in kHz.

whether the partition absorbs or emits energy at a given place and frequency. In Figure 5.2(a) only the 8 kHz curve has a region where $Re[Z_b]$ becomes negative [(x/L) = 0.09 to 0.20]. The (unloaded) resonant place is identified by the zero-crossing of the imaginary part of Z_b. For a frequency of 8 kHz the resonant place is at (x/L) = 0.31.

Solutions of the frequency-domain model for basilar membrane displacement are shown in Figure 5.3. Both magnitude and phase of basilar membrane displacement are shown re stapes displacement for the same four frequencies as in Figure 5.2. The transition to the plateau region in the 8 kHz solution is just slightly nearer the stapes [(x/L) = 0.29 to 0.30] than the resonant place determined from Figure 5.2. The phase plateau at most frequencies tends to be at an integer multiple of 2π. At certain frequencies (for example at 8 kHz in Figure 5.3) the phase plateau appears to change abruptly by 2π and the magnitude curve acquires a prominent notch.

Figures 5.4 and 5.5 show two-dimensional views of the cochlear fluid duct based on solutions of the frequency-domain model at 2 kHz. For these two figures the value of the discretizing variable M was increased to 16 in order to provide better spatial resolution in the y dimension. Also, the x and y dimensions have been scaled differently in order to provide a better view of the y dimension.

Fluid pressure $P_d(x,y)$ is shown in Figure 5.4 by means of (a) iso-magnitude contours and (b) iso-phase contours. The magnitude contours are separated by 10 dB and the phase contours are separated by one-quarter cycle. As in the previous chapter, one can identify a

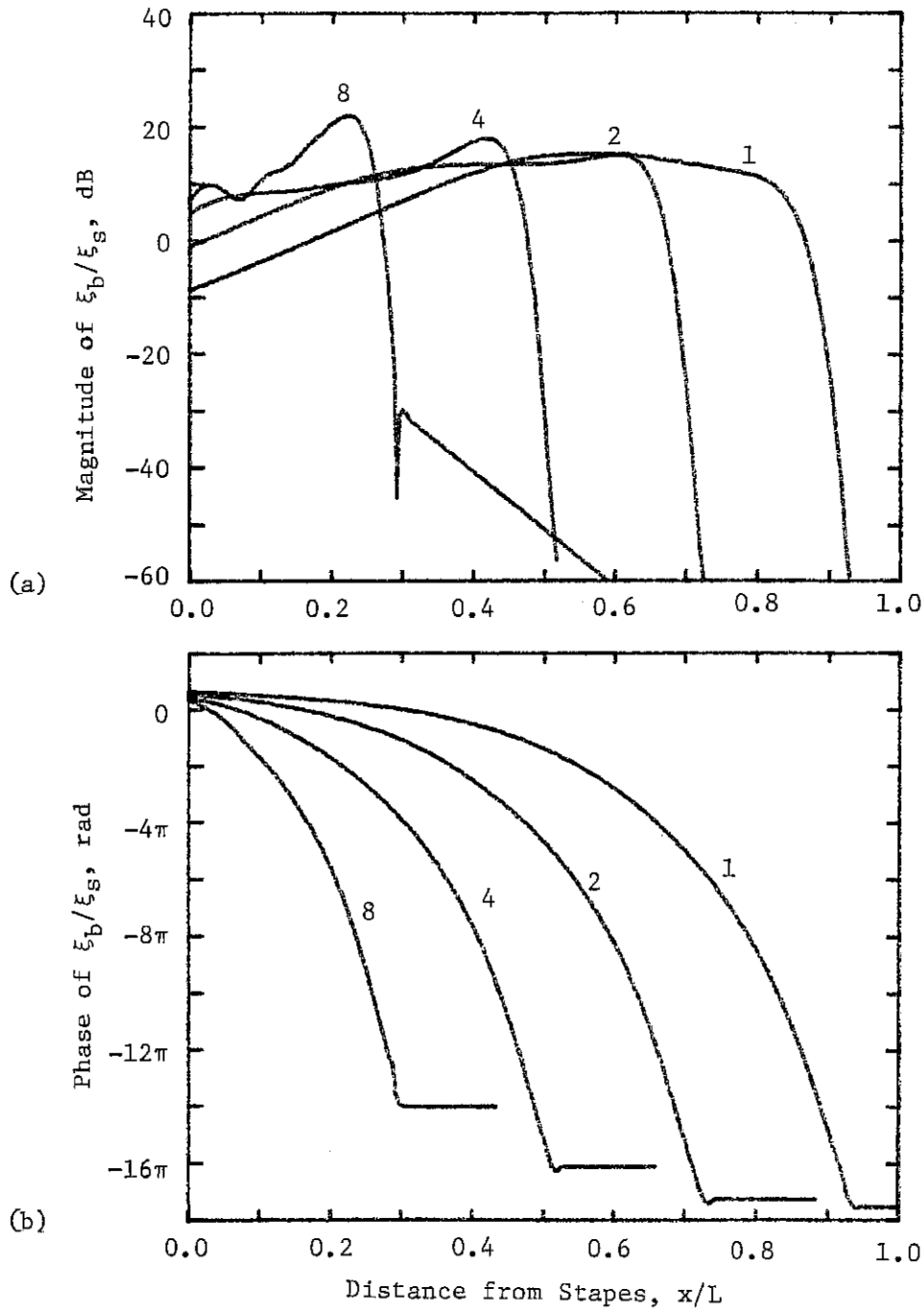

Figure 5.3. Basilar membrane displacement as a function of distance from the stapes (PSB). The curves show the ratio of basilar membrane displacement ξ_b to stapes displacement ξ_s from the frequency-domain model at four frequencies. (a) Magnitude. (b) Phase. The numerals denote frequency in kHz. (Model data from files B001, B002, B003, and B004.)

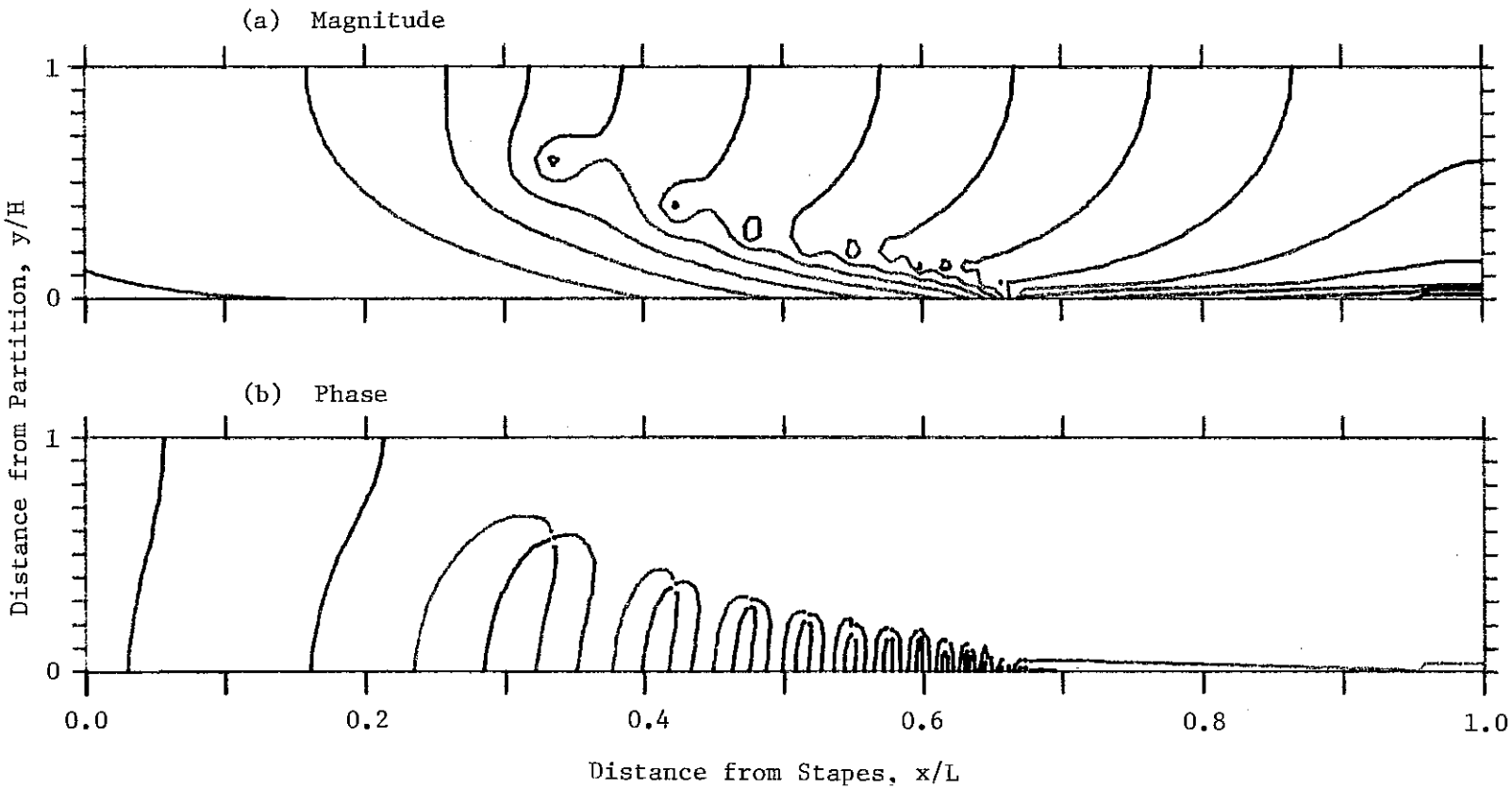

Figure 5.4. Iso-pressure contours in the two-dimensional, frequency-domain model (PSB). (a) Iso-magnitude contours with 10 dB separation between contours. (b) Iso-phase contours with a quarter cycle separation between contours. This figure represents a solution of the frequency-domain model at 2 kHz and with parameter set B, except with M=16. (Model data from file B005.)

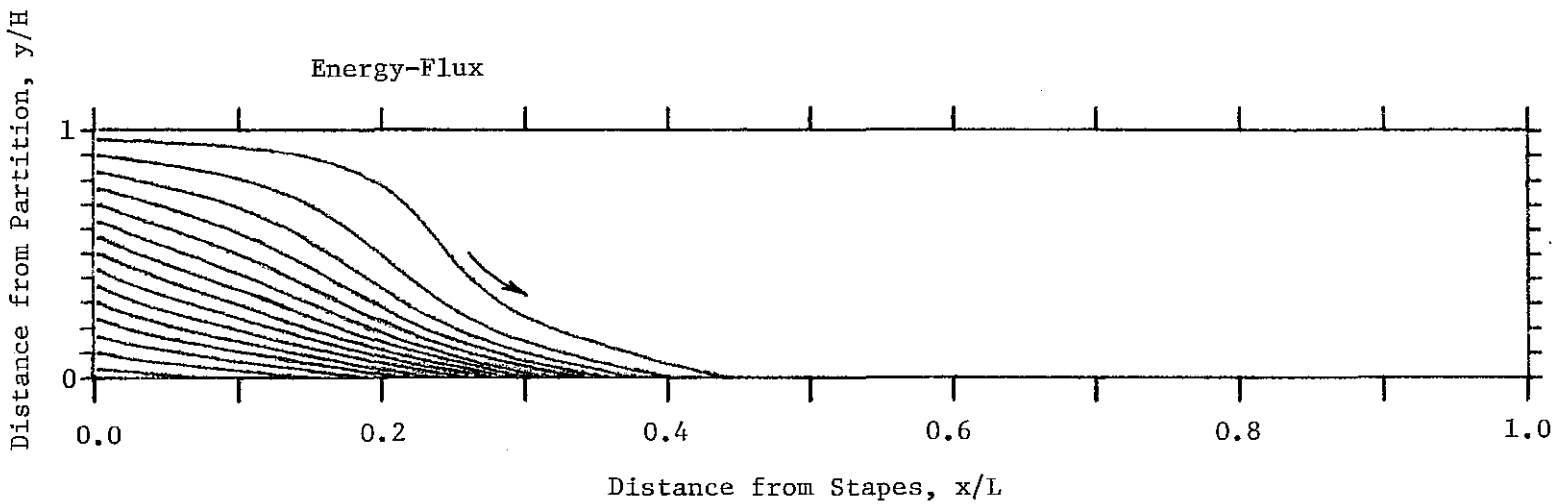

Figure 5.5. Lines of energy-flux in the two-dimensional, frequency-domain model (PSB) All flux lines start near the stapes and terminate at the partition boundary. This figure represents a solution of the frequency-domain model at 2 kHz and with parameter set B, except with M=16. (Model data from file B005.)

"long-wave" region [(x/L)=0.00 to 0.2], a "short-wave" region [(x/L)=0.2 to 0.67], and a "plateau" region [(x/L)=0.67 to 1.00]. In this case, 12 pressure "nodes" can be identified within the short-wave region.

Figure 5.5 illustrates energy flow in the two-dimensional fluid. Each path was drawn by starting at a location near the stapes boundary and following the direction of the energy-flux vector [see equation (4.42)] until reaching the partition boundary. The real part of the driving-point impedance was positive everywhere at 2 kHz; thus, no energy enters the fluid from the partition for this frequency.

The remaining figures show results from the time-domain model. The time-domain stimulus was a 16 kHz low-pass impulse of voltage to the earphone (8 pole Butterworth low-pass filter). The earphone, acoustic coupler, and middle-ear parameters were the same as in chapter 4 (see appendix 9.2). The time-step was $\Delta t = 2\times10^{-6}$ sec. At every tenth time step the basilar membrane displacement at selected positions was stored, until 2048 sets of displacement values had been collected. The basilar membrane response as a function of frequency was obtained by taking a Fourier transform of the time-domain values of basilar membrane displacement ξ_b and dividing the frequency components by the Fourier transform of the reference variable, which was either malleus displacement ξ_m or stapes displacement ξ_s.

Figure 5.6 shows the model results for basilar membrane displacement re stapes displacement at 3 positions [(x/L)=0.25, 0.50, and 0.75]. The time-domain solutions in Figure 5.6 are plotted as a

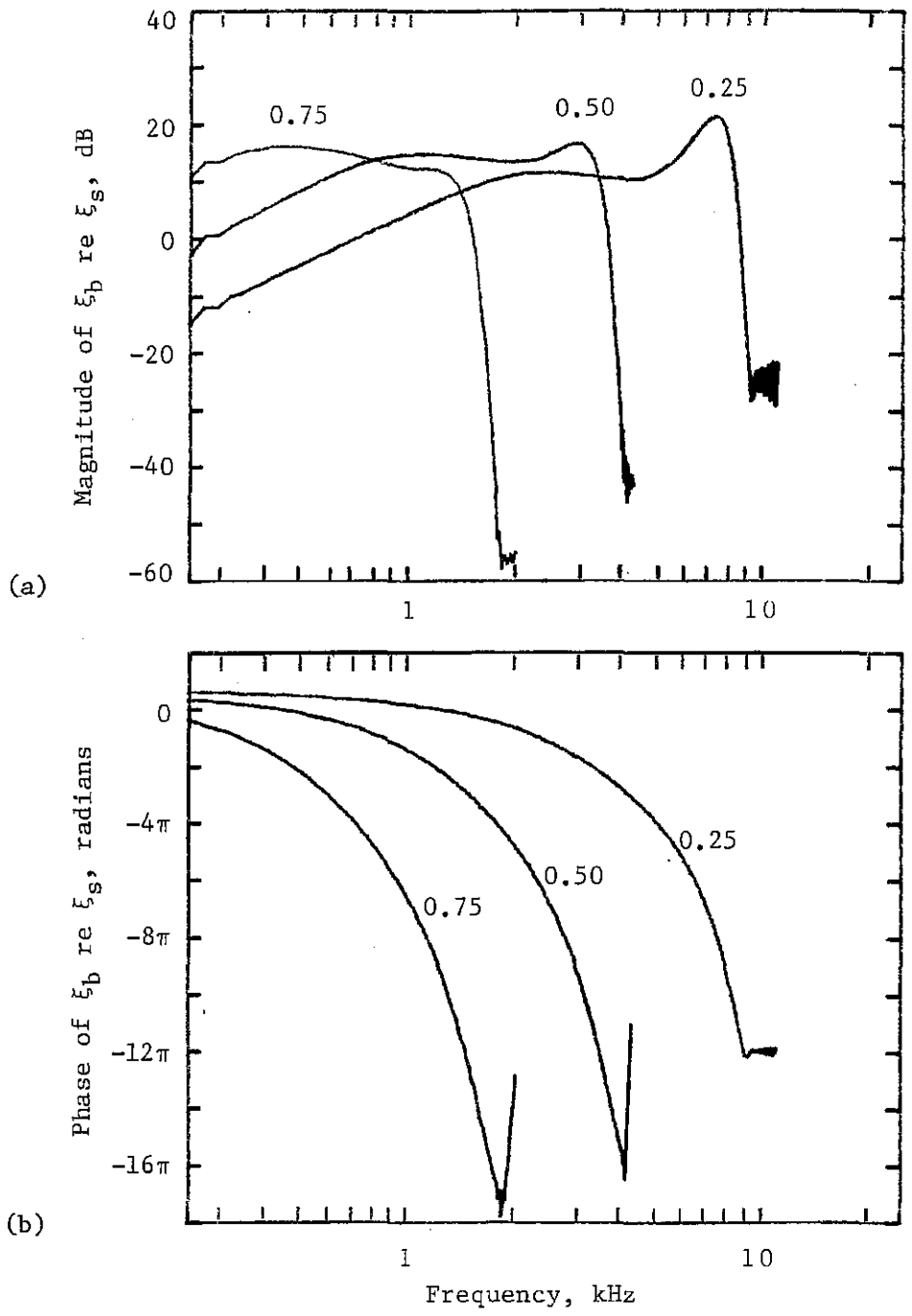

Figure 5.6. Basilar membrane displacement as a function of frequency (PSB). The curves show the ratio of basilar membrane displacement to stapes displacement in the time-domain model at three positions. (a) Magnitude. (b) Phase. The numerals indicate distance from the stapes as a fraction, x/L. [Model data from file IM22-2.]

function of frequency, whereas, the frequency-domain solutions in Figure 5.3 were plotted as a function of place.

The model solution for basilar membrane displacement ξ_b at (x/L)=0.25 re malleus displacement ξ_m is compared with Rhode's data (animal 69-473) in Figure 5.7 and 5.8. [Rhode's data was taken from Zweig et al. (56) Fig. 4.] The middle-ear transfer function which relates ξ_m to ξ_s in the model is given in Appendix 9.1.

Figure 5.8 shows the same results as Figure 5.7 except that the frequency scale is linear instead of logarithmic. The linear frequency scale makes it possible to see that the slope of the phase (of both Rhode's data and the model) is approximately constant between 1 and 6 kHz and between 6 and 9 kHz. In the model, the resonant frequency of the OHC cilium at this position (5.9 kHz) was approximately equal to the frequency where the phase changes slope.

The phase plateau of the basilar membrane displacement at (x/L)=0.25 is at -12π when referenced to stapes displacement and at -13π when referenced to malleus displacement; the difference is due to a $-\pi$ phase shift in the malleus to stapes transfer ratio (see Appendix 9.1). Rhode (97) often observed the phase plateau to be at an integer multiple of π.

The next two figures demonstrate the changes in the model solutions which result from changes in the negative damping parameter R_3. Figure 5.9 compares model solutions with slight changes in the negative damping (R_{3o}=-4.955, -4.960, and -4.965). The effect of small changes in negative damping is similar to the non-linear effect which Rhode observed with changes in stimulus level (see Figure 2.6).

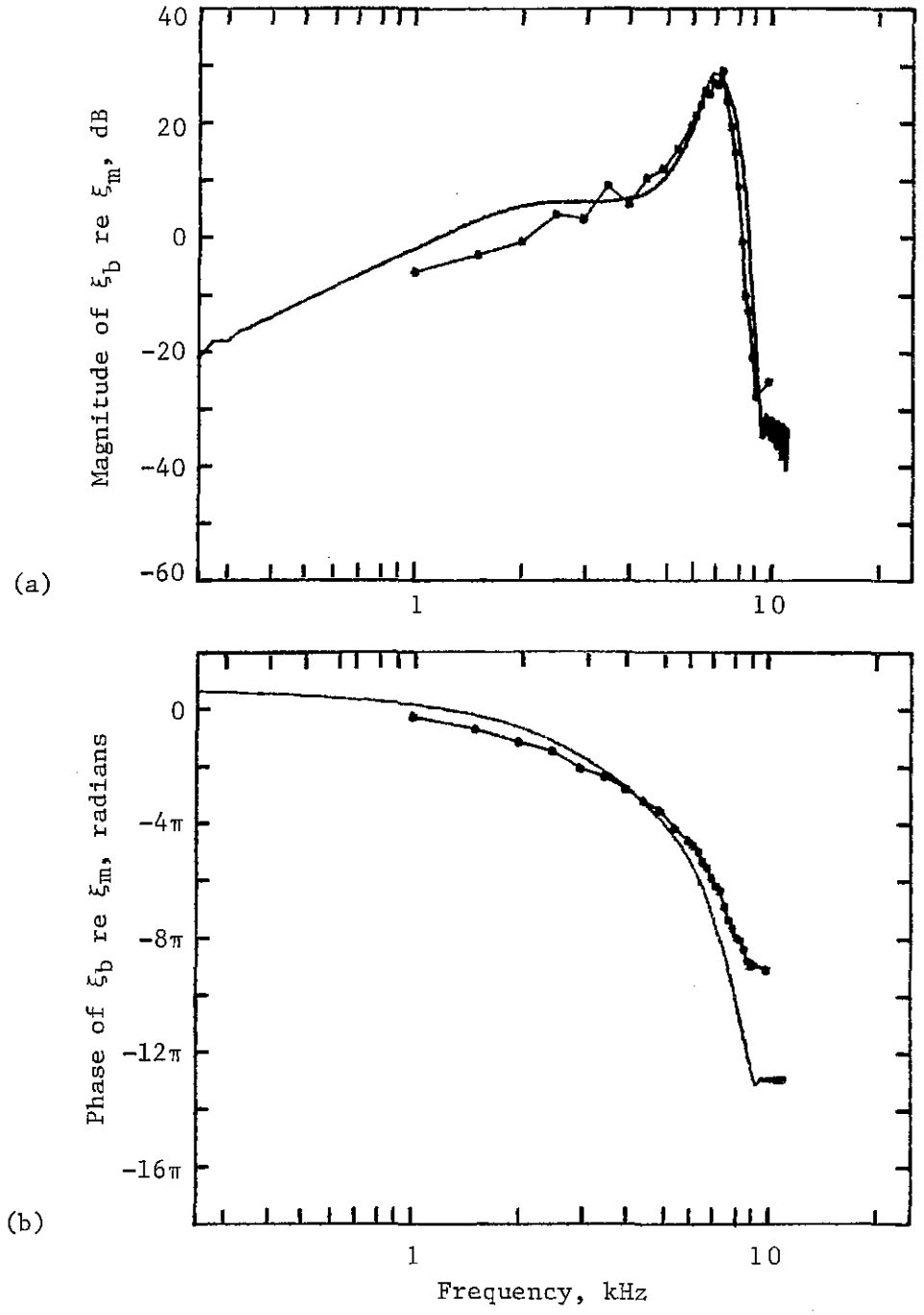

Figure 5.7. Comparison between model results with PSB and Rhode's data for basilar membrane displacement (log frequency scale). The curves show basilar membrane displacement at (x/L)=0.25 re malleus displacement from the time-domain model (solid line) and Rhode's Mössbauer measurements (circles) as a function of frequency. (a) Magnitude. (b) Phase. [Rhode's data from animal 69-473 (56) and model data from file IM22-2.]

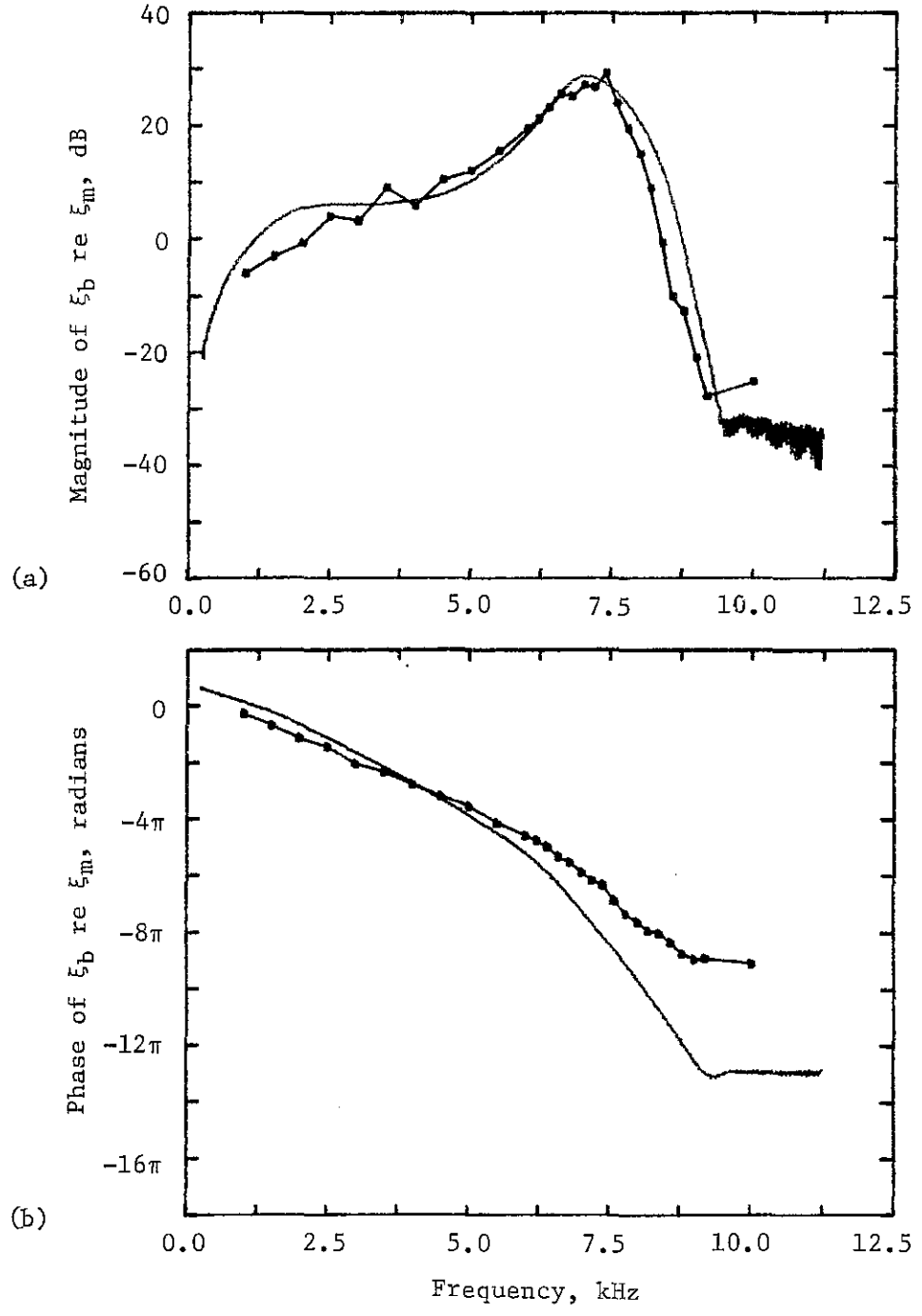

Figure 5.8. Comparison between model results with PSB and Rhode's data for basilar membrane displacement (linear frequency scale). The curves show basilar membrane displacement at (x/L)=0.25 re malleus displacement from the time-domain model (solid line) and Rhode's Mössbauer measurements (circles) as a function of frequency. (a) Magnitude. (b) Phase. [Rhode's data from animal 69-473 (56) and model data from file IM22-2.]

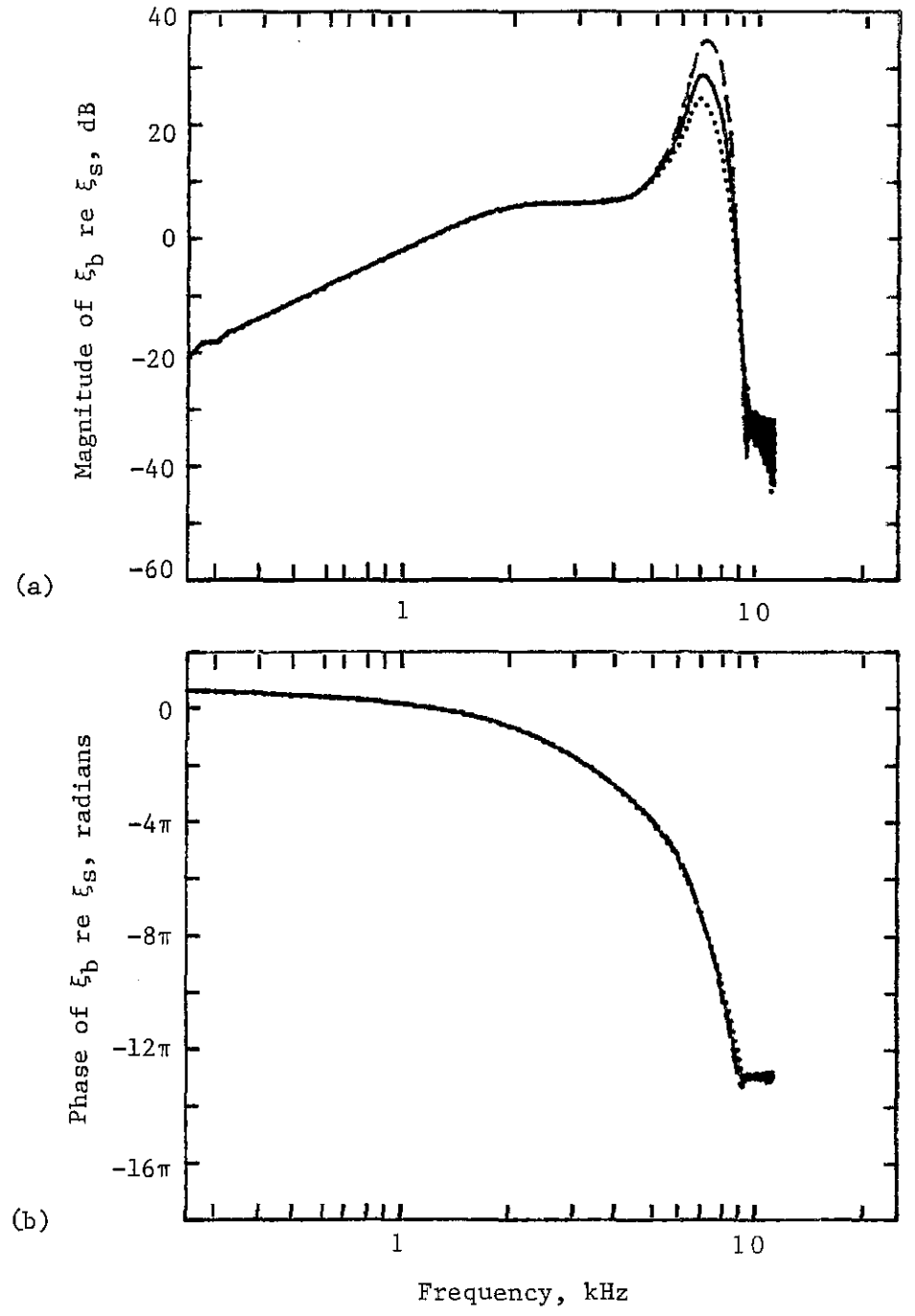

Figure 5.9. Sensitivity of the model solution to small changes in the negative damping. The curves show the ratio of basilar membrane displacement to malleus displacement in the time-domain model with R_{3o} = -4.955 (dotted line), -4.960 (solid line), and -4.965 (dashed line). (a) Magnitude. (b) Phase. (From data files IM22-1, IM22-2, and IM22-3.)

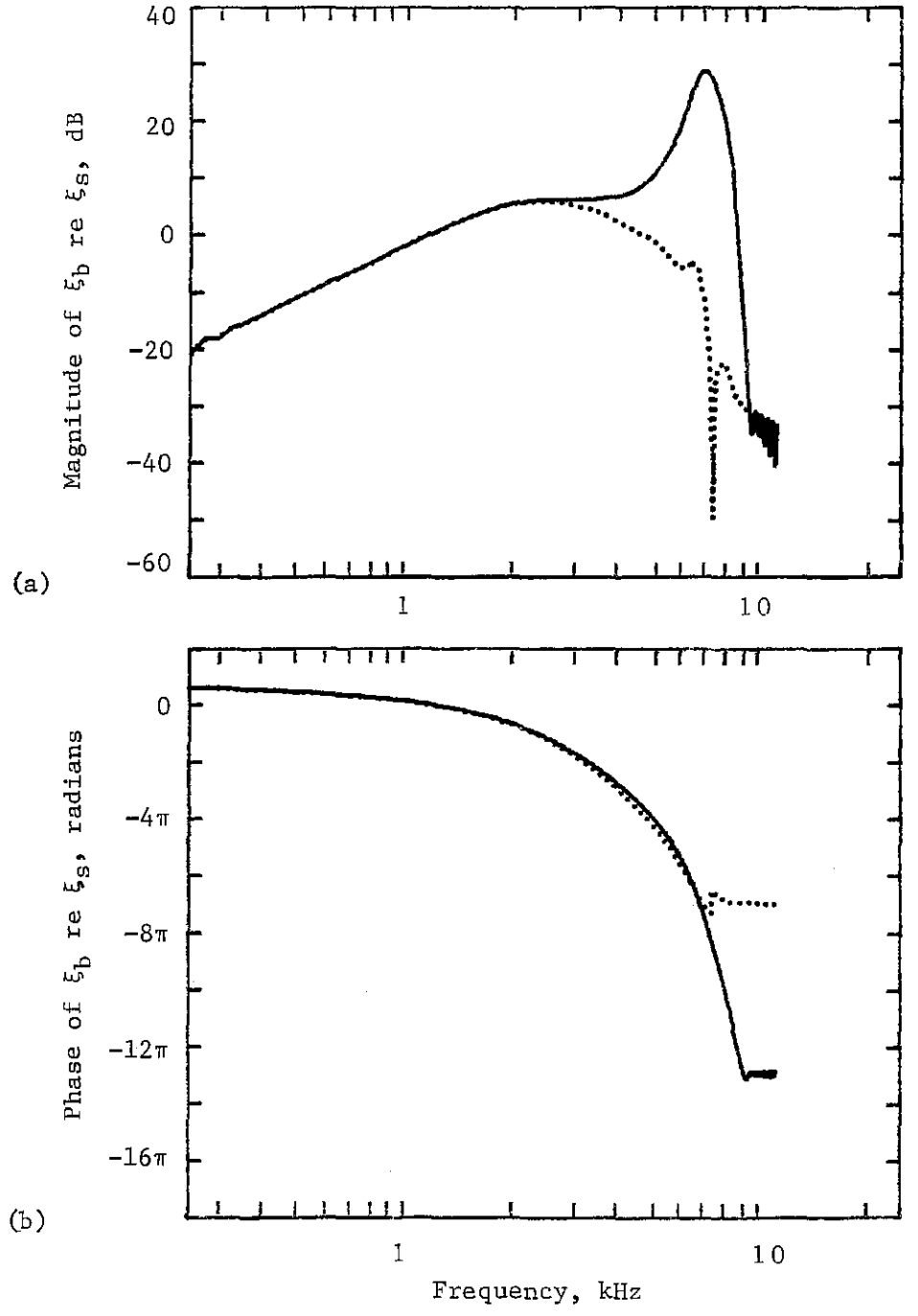

Figure 5.10. Effect on model solutions of setting negative damping to zero. The curves show basilar membrane displacement at (x/L)=0.25 re stapes displacement from the time-domain model with R_{3o}=-4.960 (solid line) and 0.00 (dotted line). (a) Magnitude. (b) Phase. (From data files IM22-2 and IM22-4.)

Figure 5.10 shows the effect of setting the negative damping to zero (R_{3o}=-4.960 and 0.00). The effect of setting the negative damping to zero is similar to the effect that Rhode observed when the animal died (see Figure 2.7). When R_3 is zero the 2-DOF partition model reduces to the traditional 1-DOF partition model.

6. DISCUSSION

The model results presented in chapters 4 and 5 demonstrate two ways of using fourth-order partition dynamics to extend the traditional two-dimensional cochlear model. In this chapter, we will discuss some of the important features and implications of these extensions to the model. Section 6.1 reviews the methods used to obtain solutions to the model equations. The use of a 2-DOF partition to implement a "second-filter" by means of a resonant tectorial membrane is discussed in section 6.2. Implementation of an "active" sharpening mechanism by means of a 2-DOF partition is discussed in section 6.3. In section 6.4, we will consider the possible role of an active sharpening mechanism in the generation of spontaneous and evoked acoustic emissions from the cochlea. Certain topics that are thought to be important areas for future research are identified in section 6.5.

6.1 MODEL IMPLEMENTATION

6.1.1 Numerical methods

In chapter 3, both frequency-domain and time-domain model equations were derived by using a spatial finite-difference approximation and expressed in a form suitable for matrix representation. In both cases the resulting matrix equation is block-tridiagonal and suitable for a Gaussian block-elimination solution technique (89). This solution method has been applied successfully to the frequency-domain model in previous work

(62, 63, 21). The application of the finite-difference approximation to the time-domain model has not been previously reported.

The time-domain model used in this research represents a significant advance toward providing a comprehensive model of the mechanics of the peripheral auditory system. The use of a finite-difference spatial-approximation made it possible to obtain simultaneous solution of a model of the cochlea and a model for the middle ear, acoustic coupler, and dynamic earphone (see Appendix 9.1). The use of fourth-order partition dynamics made it possible to simultaneously represent a shearing-displacement of the sensory hair cells which was not exactly proportional to basilar membrane displacement. This time-domain model implementation permits the stimulus to be specified as (a) fluid pressure at the stapes, (b) acceleration of the stapes, (c) air pressure at the eardrum, or (d) electrical voltage to the earphone. The response of fluid pressure, basilar membrane displacement, or hair cell shearing-displacement along the partition can be examined at any desired time-step in the model solution. The incorporation of nonlinear elements in the cochlear partition of the time-domain model could generate distortion products which would be seen in model solutions as far back as the displacement of the earphone diaphragm.

The complex pattern of fluid pressure in the y dimension, including the presence of pressure nodes, makes it necessary to question the appropriateness of the finite-difference spatial approximation. Viergever's (15) finite-element method has the advantage of being more easily adapted for a non-uniform discretizing

grid; this makes solutions more efficient by allowing points to be concentrated where spatial wavelengths are short. This type of non-uniform grid has not yet been applied to a time-domain cochlear model. The Green's function time-domain models of Allen and Sondhi (14) or Matthews (21) eliminate the need for discretizing the y dimension, at the expense of certain restrictions on allowable boundary conditions. One potential advantage of the Green's function model is the possible representation of a three-dimensional model without requiring additional computation time. Also, the inclusion of fluid viscosity in a time-domain model may be somewhat easier with the Green's function approach.

The main advantage of the finite-difference solution method over a Green's function solution method is the wider range of allowable boundary conditions. Efficient solution of a Green's function time-domain model is possible when the integral equation is in convolutional form, but this requires that the basilar membrane mass be constant with distance from the stapes. The simultaneous solution of middle-ear mechanics in a Green's function time-domain model is, at best, difficult in a linear model and no known simultaneous solution method is applicable when nonlinearities are present.

6.1.2 Computational considerations

The numerical solution methods were coded in FORTRAN and executed on a Texas Instruments 980B minicomputer. Narrative descriptions of some of the more useful FORTRAN programs are included in Appendix 9.3.

The model results included in this dissertation were subject to certain practical restrictions imposed by available memory and computation speed of the computer. The TI 980B is a 16 bit computer with about 60,000 words of fast, random-access memory available to the user. It does not have special hardware for floating-point operations; a single-precision (32 bit) floating-point multiply-and-add operation requires about 700 microseconds. The main attractions of the TI 980B were its accessibility and facility for high-resolution CRT graphic displays.

The computer implementation of the frequency-domain model utilized disk memory in order to store the large matrix generated by spatial discretization with M=16. The frequency-domain solutions each require about $3N(M^3+M^2)$ complex multiply-and-add operation which were all done with single-precision arithmetic. The trial-and-error evaluation of the model parameters was facilitated by using a small value for M (e.g. M=4) in order to obtain model solutions in a reasonable amount of time. The computation time for each parameter set was about 40 seconds with M=4 and about 40 minutes with M=16.

The computer implementation of the time-domain model used only fast memory for matrix storage and, consequently, was limited to spatial discretization with M=4. It is because of this limitation that all parameter sets in this dissertation are defined with M=4. Floating-point numbers were represented in "double-precision" (40 bits) in the time-domain model because the multiply-and-add time was only half as long as for single-precision (350 microseconds). Still, the time-domain model ran very slowly. With a 2 microsecond model

time-step, the time-domain model took about 16 hours to compute 20 milliseconds of model time.

6.1.3 Validity of model solutions

When one considers the complicated pattern of fluid pressure in two dimensions (see Figures 4.7 and 5.4), it is surprising how well the model performed with only 4 points to discretize the y-dimension. The accuracy of frequency-domain model solutions was checked in two ways: First, the model solutions with M=4 and M=16 were compared to judge the sensitivity of the model solutions to spatial discretization. Second, the energy-flux vector (see equation 4.42) was integrated over the stapes boundary and the partition boundary in order to obtain an energy input-output transfer ratio. The cochlear fluid was assumed, in chapter 3, to be inviscid and so should not absorb energy. The net amount of energy absorbed by the partition should be equal to the amount of energy which enters the fluid at the stapes; thus, the energy transfer ratio should always be equal to one.

Figure 6.1 shows the sensitivity of the model solution for PSA at 1.6 kHz to spatial discretization. There is a noticeable difference between the model solutions with M=4 and M=16; however, the qualitative features of the solution do not change much. The energy transfer ratio was computed to be 1.000 for all model solutions with PSA. It appears that the solutions for PSA with M=4 are reasonably accurate.

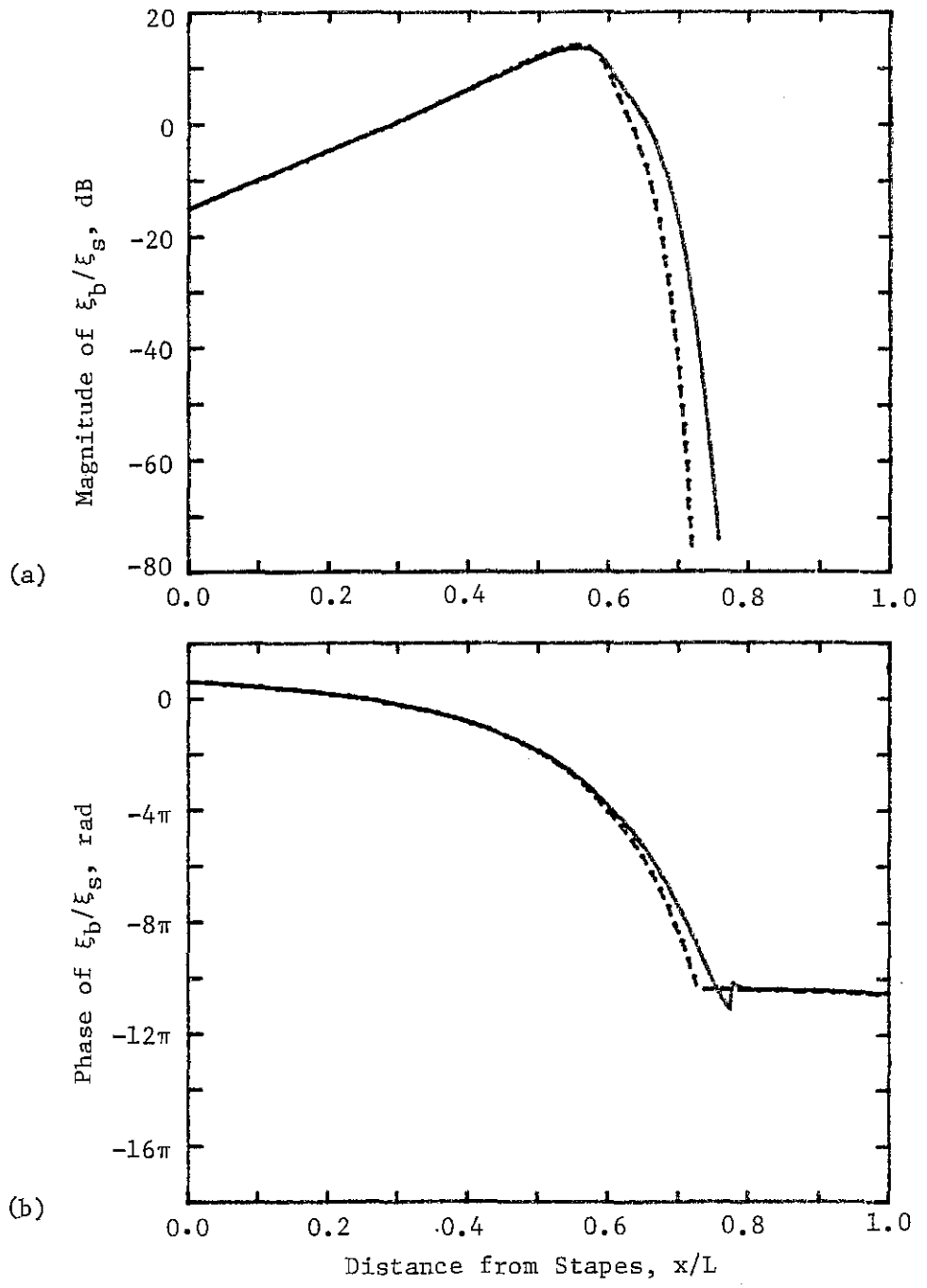

Figure 6.1. Sensitivity of model solution to spatial discretization (PSA). Solution of the frequency-domain model for a frequency of 1.6 kHz with M=4 (solid line) and M=16 (dashed line). (Model data from files A002 and A007).

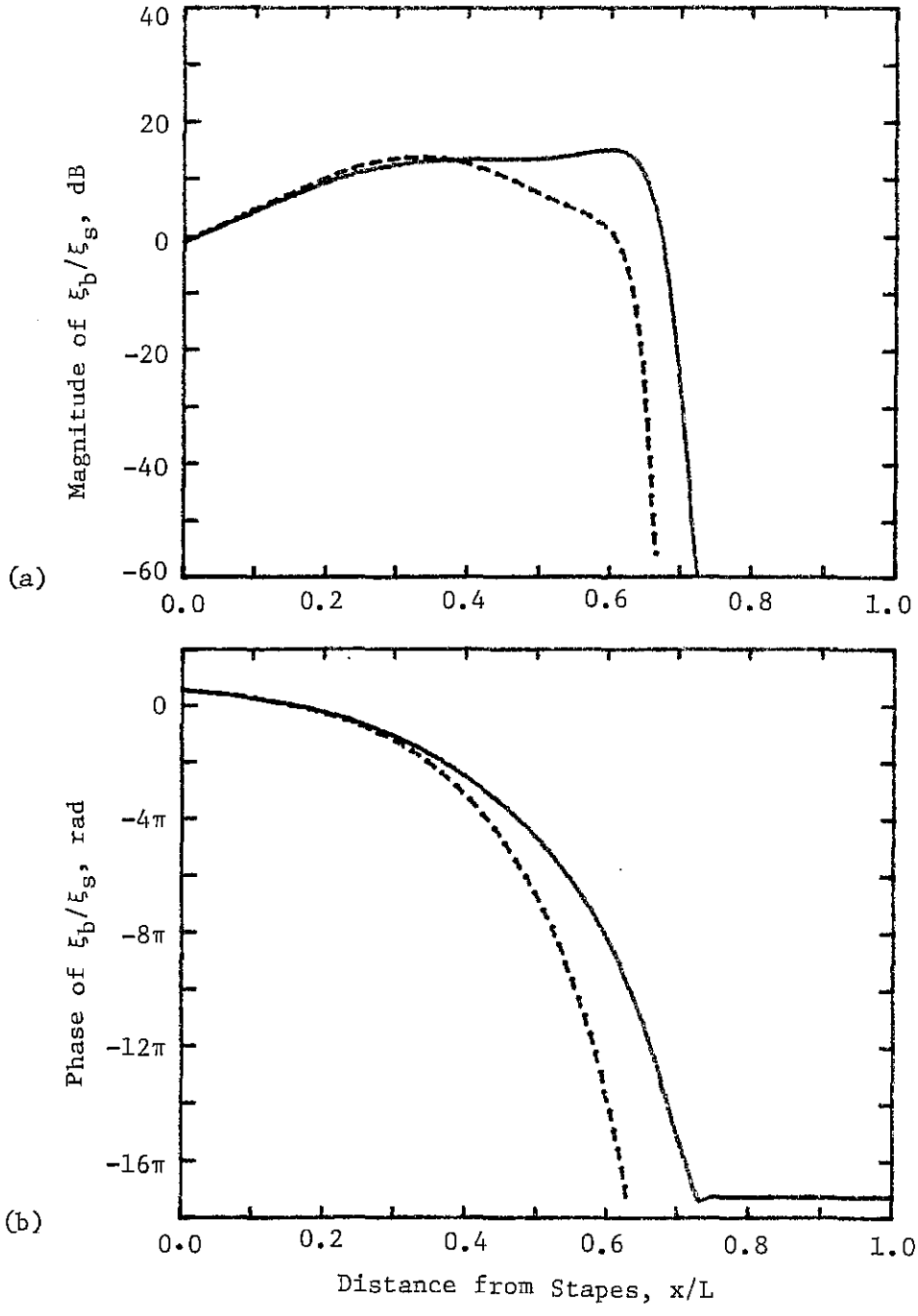

Figure 6.2. Sensitivity of model solution to spatial discretization (PSB). Solution of the frequency-domain model for a frequency of 2 kHz with M=4 (solid line) and M=16 (dashed line). (Model data from files B002 and B005).

Figure 6.2 shows the sensitivity of the model solution for PSB at 2.0 kHz to spatial discretization. The difference between the model solutions with M=4 and M=16 is more significant for PSB than for PSA; the phase plateau drops by about four more cycles with M=16. Considering the presence of the 12 pressure whirls in the cochlear fluid (see Figure 5.4), it is likely that the fluid pressure is not accurately represented even with M=16. On the other hand, the variation of model solutions with M is gradual and somewhat predictable and the model solutions with M=4 are thought to be adequate to provide model results which illustrate the methods and concepts of chapter 5. The energy transfer ratio was computed to be 1.000 for all model solutions with PSB.

6.2 COCHLEAR PARTITION WITH SECOND-FILTER

The concept of a second-filter being interposed between basilar membrane response and neural excitation was reviewed in chapter 2. The desire to implement a second-filter mechanism in the model which would retain bidirectional coupling between basilar membrane motion and hair cell transduction was part of the motivation for the 2-DOF partition presented in chapter 5.

6.2.1 Tectorial membrane as a second-filter

The idea that the lateral motion of the tectorial membrane (TM) provides a second-filtering of mechanical excitation to the hair cells has been suggested previously by Allen (12) and Zwislocki (11). A cochlear second-filter has often been hypothesized to account for the discrepancy between experimental measurements of basilar membrane motion and single nerve fiber responses (see section 2.2). Allen

showed that the TM second-filter is capable of accounting for much of the discrepancy between model results for basilar membrane displacement and experimental neural responses.

The term "second-filter" may be misleading because it has been used previously in the context of cochlear mechanics with various interpretations. A "filter" is usually characterized by its frequency-domain properties. For the purpose of this discussion, the cochlear second-filter will be defined as the ratio of the basilar membrane driving-point admittance to the hair cell transfer admittance

$$H_s = Y_h / Y_b = g Z_2 / (Z_2 + Z_3) \qquad (6.1)$$

(see sections 3.3 and 4.2 for the definitions of Y_b, Y_h, g, Z_2, and Z_3). (Allen defines a second-filter in the same way and calls it a "transduction filter"). In terms of classical filter theory (88) H_s has a single pair of complex poles and a single pair of complex zeros in the (Laplace transform) s plane ($s=\tau+i\omega$). In chapter 4, parameter set A was chosen to place the poles of H_s at the characteristic frequency (CF) and the zeros of H_s about an octave below CF. For PSA, the magnitude of H_s at low frequencies is about 0.2 and for high frequencies is about 1.0.

The partition driving-point impedance of the basilar membrane, $Z_b=1/Y_b$, can be expressed in terms of the second-filter

$$Z_b = Z_1 + Z_3 H_s / g \qquad (6.2)$$

The effect of H_s on the driving-point impedance is evidence of the bidirectional coupling of the second-filter. The ratio of the first term to the second term in equation (6.2) at a given frequency is about 15 near the base and about 3 near the apex. The model solutions

presented in chapter 4 include the effect of the second-filter in computing basilar membrane displacements. This is an important point when considering whether nonlinearities in the transduction process might be responsible for nonlinear motion of the basilar membrane (98).

The second-filter implementation used by Allen (12) did not preserve bidirectional coupling, because it was not important for the particular model parameters used by Allen. However, for our parameter set A the bidirectional coupling is important. In fact, the TM resonance has a greater influence on the place of maximum basilar membrane displacement for sinusoidal stimuli than does the resonance of the basilar membrane.

The 2-DOF partition with resonant TM represents the TM as a series of tuned mechanical resonators along the length of the partition which are not directly coupled to each other. This representation of TM is not supported by its anatomical structure (95). von Békésy (1) lifted the edge of TM with a hooked needle and described its behavior as similar to the cover of a book, being hinged to the spiral limbus and relatively stiff across its width and length. The effect of longitudinal stiffness of TM on the second-filter deserves further attention [see Zwislocki (11)].

The comparison of the model solution for hair cell shearing with the neural response data of Kim et al. (4) in Figure 4.6 is one of the important results of this dissertation. Certain quantitative features of the neural data were used in the selection of model parameters: the place of maximum response, the phase slope, the location of the

spectral zero, and the relative damping of the spectral zero. Other features of the neural data which were not used in the selection of model parameters also seem to be present in the model data: the phase increase of about pi radians between the spectral zero and CF, the slopes of the magnitude near the place of maximum response, the relatively constant magnitude region on the basal side of the spectral zero, and the difference in magnitude between the basal region and the place of maximum response. In general, the combined magnitude and phase effects of the spectral zero seem to be present in the neural data. This result supports the presence of a spectral zero in the hair cell transfer admittance Y_h; however, it does not exclude the possibility that it might also be present in the driving-point admittance Y_b.

The magnitude of the neural response data in Figure 4.6 was not shifted vertically to bring it into agreement with the magnitude of the model solutions. The close agreement without this shift must be regarded as fortuitous. The neural response magnitude was computed as the magnitude of the stimulus frequency component of the Fourier transform of a period histogram of a single nerve fiber response, divided by the spontaneous rate of the nerve fiber (4). The model solution magnitude was determined from the frequency-domain model as the magnitude of the (complex) ratio of basilar membrane displacement to stapes displacement. There is no apparent reason why these magnitude definitions should coincide with each other.

The phase of the neural response data was shifted vertically to bring it into closer agreement with the phase of the model solutions. The phase of the 1550 Hz data was shifted upward by 0.42π and the phase of the 620 Hz data was shifted upward by 0.58π. (Phase shifts of multiples of 2π are ignored, since they are equivalent to no shift at all.) In the remainder of this section we will analyze the various contributions to the neural response phase.

6.2.2 Analysis of the phase of the neural response

The model phase component $\phi_0(f)$ was defined in section 4.2 as the vertical shift needed to bring the sum of the exponential phase component $\phi_1(x;f)$ and the phase jump $\phi_2(x;f)$ into agreement with the neural phase data. We can further analyze the sub-components of ϕ_0 by considering

$$\phi = 2\pi f \tau_0 + \phi_{00} + \phi_{01} + \phi_{02} + \phi_{03} , \qquad (6.3)$$

where the sub-components are defined as follows:

ϕ_0 - total neural delay due to synaptic delay at the hair cell and propagation delay along the nerve fiber.

ϕ_{00} - phase of hair cell depolarization re hair cell shearing-displacement ξ_h.

ϕ_{01} - phase of hair cell shearing-displacement ξ_h at x=0 re stapes displacement ξ_s.

ϕ_{02} - phase of stapes displacement ξ_s re eardrum pressure P_e.

ϕ_{03} - phase of eardrum pressure P_e which coincides with zero phase of period histogram.

The phase of the neural response data was defined to be zero when rarefaction of eardrum pressure coincided with increase in probability

of nerve spike discharge (4), thus $\phi_{03} = \pi$ rad by definition. We assume that depolarization of the hair cell coincides with increase in probability of nerve spike discharge (99).

The neural delay τ_0 can be estimated from Figure 4.10 as the difference in latency between the model solution for ξ_h and the neural transient response data. This latency difference varies with CF, but the delay appears to be about 0.7 ms in the frequency range from 0.5 to 2 kHz.

The phase sub-component ϕ_{00} contributes to the neural phase, but is not a part of the model solution. Hudspeth and Corey (100) have determined that deflection of the stereocilia of a vertebrate hair cell toward the kinocilium causes depolarization of the hair cell. The kinocilium is not present in cochlear hair cells, but the associated "basal body" is located on the side of the stereocilia away from the spiral limbus. The value of ϕ_{00} will also depend on whether the (stereo-) cilia of the hair cell with which the nerve fiber synapses makes contact with the tectorial membrane. The nerve fiber probably synapses with an inner hair cell (IHC) (101) and the contact of IHC cilia with tectorial membrane is still a controversial issue (102). If the IHC cilia are attached to TM, then IHC depolarization would coincide with an upward <u>displacement</u> of the partition. If the IHC cilia do not make contact with TM, then they would be deflected by viscous drag of the subtectorial fluid and IHC depolarization would coincide with an upward <u>velocity</u> of the partition. [See Billone (102).] We would expect $\phi_{00} = \pi$ if the IHC cilia contact TM and $\phi_{00} = 1.25\ \pi$ if they do not.

The phase sub-components ϕ_{01} and ϕ_{02} can be determined from the cochlear model and the middle-ear model. The values of ϕ_{01} and ϕ_{02} are listed in Table 6.1 for PSA with frequencies of 620 Hz and 1550 Hz. (The vertical shift of the neural phase data in Figure 4.6 is equal to the difference between ϕ_{01} and ϕ_{0}.)

The "known" quantities in Table 6.1, together with equation (6.3), make it possible to compute estimates for ϕ_{00}, which are also listed in Table 6.1. There are too many sources of error in this computed estimate to make a valid judgment about whether the IHC cilia contact TM, but with refinement of the model and a larger set of data such a judgment might be possible (see section 6.5).

6.3 COCHLEAR PARTITION WITH NEGATIVE DAMPING

In chapter 5, we looked at an example of a 2-DOF partition in which the second degree-of-freedom was associated with bending displacements of the cilia of the outer hair cell (OHC). The damping element which coupled the base of the OHC cilia with the reticular lamina was given a negative damping value in order to make the OHC cilia a source of mechanical energy.

6.3.1 Outer hair cells as active mechanical devices

Spontaneous acoustic emissions have been objectively measured in a large percentage of otherwise normal human ears (48, 47). This observation provides strong support for the presence of some type of active mechanical device within the cochlea, capable of spontaneous, sustained oscillation and powered by a metabolic source of energy. The physical nature of such an active device has been a subject of speculation for many years (16, 17).

Table 6.1. Values of the sub-components of neural response phase.

	620 Hz	1550 Hz
ϕ_0	0.1 π	0.2 π
τ_0	0.7 ms	0.7 ms
ϕ_{00} *	1.68 π	1.07 π
ϕ_{01}	0.68 π	0.62 π
ϕ_{02}	-0.13 π	-0.66 π
ϕ_{03}	π	π

* Values on this line were computed using equation (6.3) and the other values in this table.

Recent anatomical observations provide support for the mechanical tuning of OHC cilia. The height of the OHC cilia in chinchilla increases gradually from base to apex by about a factor of 5 (95). The shorter cilia located near the base, presumably, have less mass, greater bending stiffness, and resonate at a higher frequency than the longer cilia located toward the apex.

The possible active nature of the OHC cilia is speculative. One possibility is that transduction molecules associated with the cell membrane of the OHC cilia might be capable of exerting a mechanical force (103). The interior of the cilia consists of packed actin filaments which form a fairly rigid structure (104). The base of the cilia of each hair cell is embedded in a "cuticular plate" which is situated at the top of the hair cell much like a loose stopper in a test tube (104, 102). Lateral forces within the hair cell might be capable of moving the cuticular plate relative to the reticular lamina (105). Both of these possibilities are consistent with the 2-DOF partition model of chapter 5.

An interesting consequence of the partition model with resonant OHC cilia is that lateral displacements of the cilia may be much greater than vertical displacements of the basilar membrane, due to the presence of negative damping. Let a quantity called G(x) be defined as the maximum ratio of cilia displacement ξ_c to basilar membrane displacement ξ_b at a given place over frequency in the frequency-domain model. This maximum will occur at the spectral zero frequency and can be computed from model parameters

$$G(x) = g(x)\, R_2(x) \,/\, \left[R_2(x) + R_3(x)\right] . \qquad (6.4)$$

For parameter set B, G(x) has a value of 125 for all x. Rhode (3) measured basilar membrane displacements of about 10^{-6} cm for stimuli at 80 dB SPL (see Figure 2.5). With the above value of G(x), we would expect cilia displacements of about 10^{-4} cm, for stimuli at 80 dB SPL. The quanitity G(x) might be thought of as representing an "active gain" in ξ_c over ξ_b. The existence of this active gain might be helpful in explaining how neural excitation is possible when basilar membrane vibrations are extremely small.

It is important to check whether the amount of energy required from the model cilia is compatible with the physiological capabilities of such a system. For a sinusoidal stimulus, we will compute the energy output of the negative damping element during each stimulus cycle per unit distance along the partition.

$$e_1 = -D^2 f R_3 w_p, \tag{6.5}$$

where D is the root-mean-square (RMS) value of $(\xi_h - \xi_c)$, f is the stimulus frequency, R_3 is the negative damping element, and w_p is the effective width of the partition. For example, a model solution with a sinusoidal stimulus of f=7.4 kHz, an RMS relative cilia displacement of 10^{-4} cm, and parameter set B, will produce an energy output at position x=0 of e_1=10-5 erg/cm/cycle.

In order to obtain a physiological estimate for energy output, we can consider all of the OHC hair cells to have flagellar motility. It has been estimated that a single flagellating cilia (in Sabellaria) is capable of generating as much as 5×10^{-9} erg of mechanical energy per stroke (106). In chinchilla there are about 20 cilia per OHC and about 4×10^{3} OHC per cm (95, 96). If all of the cilium were capable of

generating 10^{-9} erg each cycle of a 7.4 kHz stimulus, we could expect a combined energy output from the cilia of $e_2=10^{-4}$ erg/cm/cycle.

The amount of electrical energy available to the hair cell provides another estimate of the physiological capability of the system. In a vertebrate hair cell Corey and Hudspeth (107) measured a receptor current of 10^{-10} amp in response to cilia displacements which followed a 10 Hz triangle wave with 10^{-4} cm amplitude. During this measurement, a holding potential of -60 mV was applied to the hair cell. This result implies a flow of electrical energy into the hair cell of about 6×10^{-5} erg/sec. At 7.4 kHz and with 4×10^{3} OHC/cm, we might expect an energy flow into the cochlear partition of about $e_3=3\times10^{-5}$ erg/cm/cycle.

The amount of energy required of the model cilia e_1 appears to be within the range of energy (e_2, e_3) which might be expected from such a physiological system.

6.3.2 Negative damping

The incorporation of negative damping elements in the cochlear partition provides a means of modeling controlled energy sources in the partition. Within the constraints of a linear, time-invariant, 2-DOF mechanical system (such as assumed in section 3.2), this is the most obvious way to introduce a local source of mechanical energy. The partition model with negative damping can be considered to be a first approximation of some more general mechanical system which might possibly have nonlinear, time-varying elements.

One might expect the presence of negative damping in the partition to produce instability and cause oscillations even in the absence of any acoustic stimulus. Indeed, one of the important results of this dissertation is the demonstration that negative damping in the partition does not necessarily lead to dynamic instability. For the model conditions presented in chapter 5, the loading of the cochlear fluid on the partition keeps the partition from becoming unstable. The fluid is able to channel the energy output of the partition into more apical regions where it can again be absorbed by the partition.

The dynamic stability of the model was determined by observing time-domain model solutions with an impulsive stimulus. The impulsive stimulus was computed as the impulse response of a low-pass filter, except that it was identically zero after about 4 ms. (The stimulus file name was "IM6.STIM".) The model was considered stable if the amplitudes of all observed velocity and displacement variables continued to approach zero 10 to 20 ms after the onset of the stimulus. Usually, the parameter sets which produced unstable time-domain solutions had frequency-domain solutions for some frequency in which the phase of the pressure had positive slope at x=0. Positive phase slope indicates a traveling wave going toward the stapes (see section 6.4). In certain other parameter sets unstable behavior could be made stable by decreasing the size of the time-step Δt. For example, PSA is unstable with a 2 microsecond time-step, but is stable with a 1 microsecond time-step.

As an alternative to negative damping, one attractive possibility is a time-varying, nonlinear stiffness which has an energy producing "hysteresis". If the stiffness of the OHC cilia varied with the potential difference between scala media and the interior of the hair cell, than such a hysteresis might be produced.

6.3.3 Fitting Rhode's data

Parameter set B produces time-domain solutions which match Rhode's data better than any other model solutions known to this author. However, this particular set of parameters is not felt to be optimally suited for representing the squirrel monkey cochlea or even for matching Rhode's data. The computation time required for obtaining time-domain model solutions made the trial-and-error search for parameters very time consuming; consequently, optimization of the parameter set was very difficult. Improvements in the present parameter search strategy are needed.

It should be noted that the middle-ear response of the model has a significant effect on the comparison between model solutions and Rhode's data in Figures 5.7 and 5.8. The middle-ear parameter values were taken from Matthews (21) and were selected to fit experimental data from cat. Unfortunately, the ratio of malleus displacement to stapes displacement in the model (see Figure 9.2) does not agree with Rhode's (3) direct measurements. If the middle-ear transfer ratio had been more realistic, the agreement between model solutions and Rhode's data would have been equally as good with slight adjustment of the amount of negative damping. The "active" sharpening mechanism has

a strong influence on the tip segment of the basilar membrane tuning curve. (This was demonstrated in section 5.3.)

The resemblance of the model results with small changes in the negative damping (Figure 5.9) to the nonlinear experimental results of Rhode (Figure 2.6) suggest that the negative damping value should be nonlinear. A nonlinear damping element generates distortion products with two-tone stimulation which are similar to those observed experimentally (4, 21). The current time-domain model is capable of handling such nonlinear elements, but the computation time makes the use of sinusoidal stimuli impractical

The change in model solution for basilar membrane displacement which results from setting R_{3o} to zero (see Figure 5.7) is similar to the change in experimental measurements of basilar membrane displacement when the animal dies (see Figure 2.7). Similar changes in response are seen when comparing normal threshold tuning curves of spiral ganglion cells with the tuning curves of spiral ganglion cells in a region devoid of outer hair cells (108). [See also Steele and Taber (66)]. It is often observed that the "tip" segment of cochlear tuning curves is vulnerable to a wide range of physiological insults to the cochlea (109, 110).

6.3.3 Alternative parameter set with negative damping (PSC)

In section 6.1, we saw that solutions for PSB were sensitive to changes in spatial discretization. This undesirable aspect of the model solution was attributed to short wavelengths in the fluid pressure, rather than the presence of negative damping. In order to substantiate this claim, an alternative parameter set will be

presented which has negative damping, but is not very sensitive to changes in the spatial discretization. This alternative parameter set is also better suited for demonstrating the effect of energy flow out of the partition on the two-dimensional views of the cochlea.

Values of the model parameters for parameter set C (PSC) are listed in Table 6.2. The cochlear-partition driving-point impedance is shown in Figure 6.3 as a function of place for four frequencies. Figure 6.4 shows the sensitivity of a frequency-domain model solution for PSC at 1.6 kHz to spatial discretization. Time-domain solutions are stable with PSC and resemble Rhode's data, though not as closely as with PSB (see Figure 6.5).

The next two figures show two-dimensional views of the cochlear fluid for PSC with M=16. The iso-pressure contours in Figure 6.6 show a transition from long-wave region to plateau region with no short-wave region. The lines of energy-flux in Figure 6.7 show a region [near (x/L)=0.6] where energy from the stapes is not absorbed by the partition; this is due to emission of energy from the partition which is channeled through the fluid a short distance toward the apex, where it is absorbed by the partition. The energy transfer ratio for PSC was computed to be 1.000 for both solutions (with M=4 and M=16).

6.4 COCHLEAR ECHOES AND SPONTANEOUS EMISSIONS

In section 2.2 the experimental observations of evoked cochlear mechanical responses (cochlear echoes) and spontaneous cochlear acoustic emissions were reviewed. In this section we will suggest a means of simulating these phenomena in a cochlear model which has negative damping in the cochlear partition.

Table 6.2. Values for the cochlear model parameters (PSC).

Macromechanical parameters:

$L = 2.25$ cm

$H = 0.1$ cm

$\rho = 1.0$ gm cm^{-3}

$A_s = 0.0126$ cm^2

$w_p = 0.126$ cm

Micromechanical parameters:

$K_{1o} = 2.0 \times 10^9$ dyn cm^{-3}, $K_{1e} = -5.0$ cm^{-1}

$R_{1o} = 6600$ dyn sec cm^{-3}, $R_{1e} = -2.0$ cm^{-1}

$M_{1o} = 2.0 \times 10^{-2}$ gm cm^{-2}, $M_{1e} = 0.0$ cm^{-1}

$K_{2o} = 1.0 \times 10^8$ dyn cm^{-3}, $K_{2e} = -5.0$ cm^{-1}

$R_{2o} = 3600$ dyn sec cm^{-3}, $R_{2e} = -2.5$ cm^{-1}

$M_{2o} = 1.0 \times 10^{-2}$ gm cm^{-3}, $M_{2e} = 0.0$ cm^{-1}

$K_{3o} = 0$ dyn cm^{-3}, $K_{3e} = 0$ cm^{-1}

$R_{3o} = -3000$ dyn sec cm^{-3}, $R_{3e} = -2.5$ cm^{-1}

Helicotrema parameters:

$L_h = 0.05$ cm

$R_h = 50$ dyn sec cm^{-3}

Spatial discretization parameters:

$M = 4$

$N = 240$

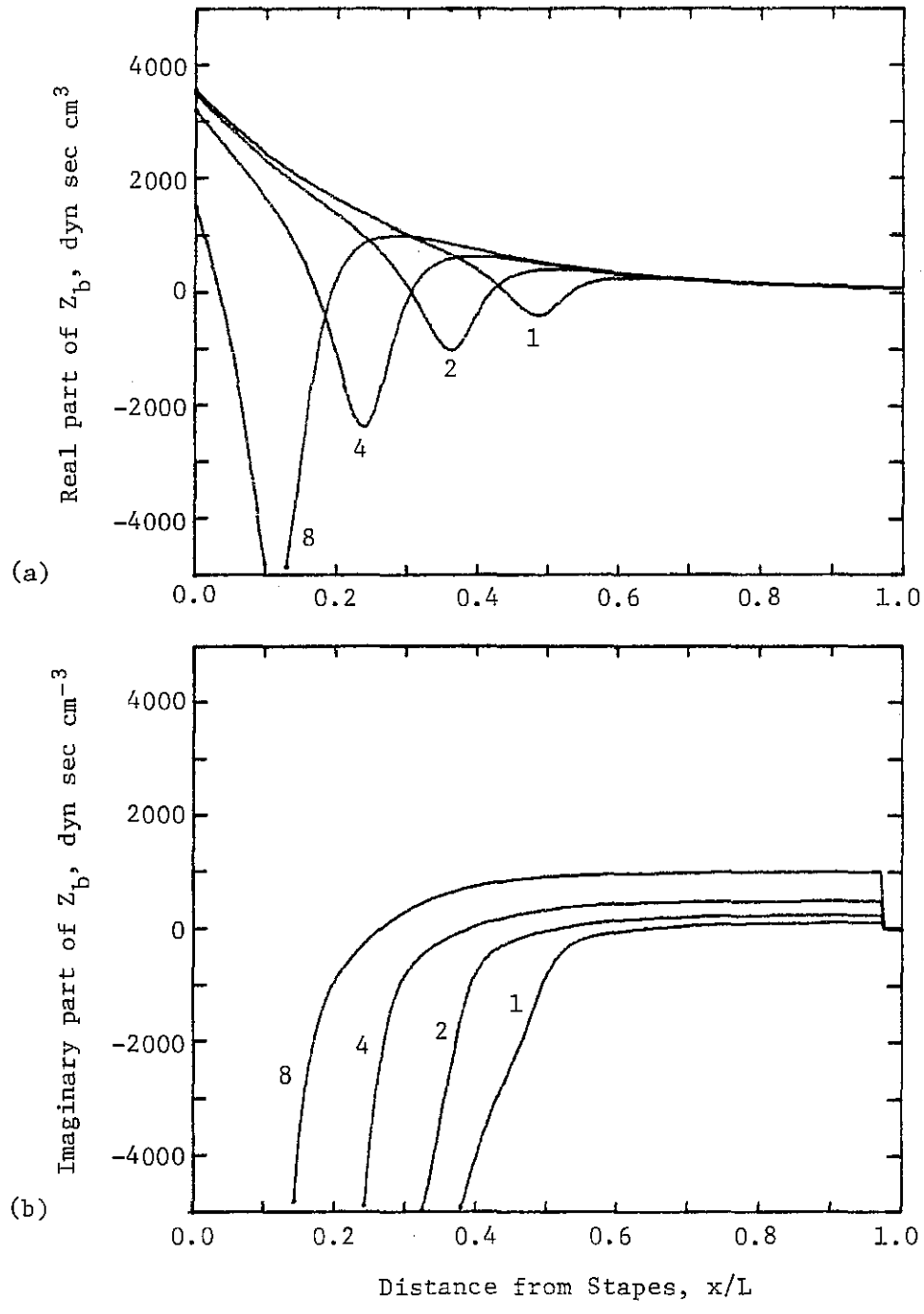

Figure 6.3. Driving-point impedance of the cochlear partition (PSC). (a) Real part of $Z_b(x)$. (b) Imaginary part of $Z_b(x)$. Four frequencies are shown superimposed; the numerals indicate frequency in kHz.

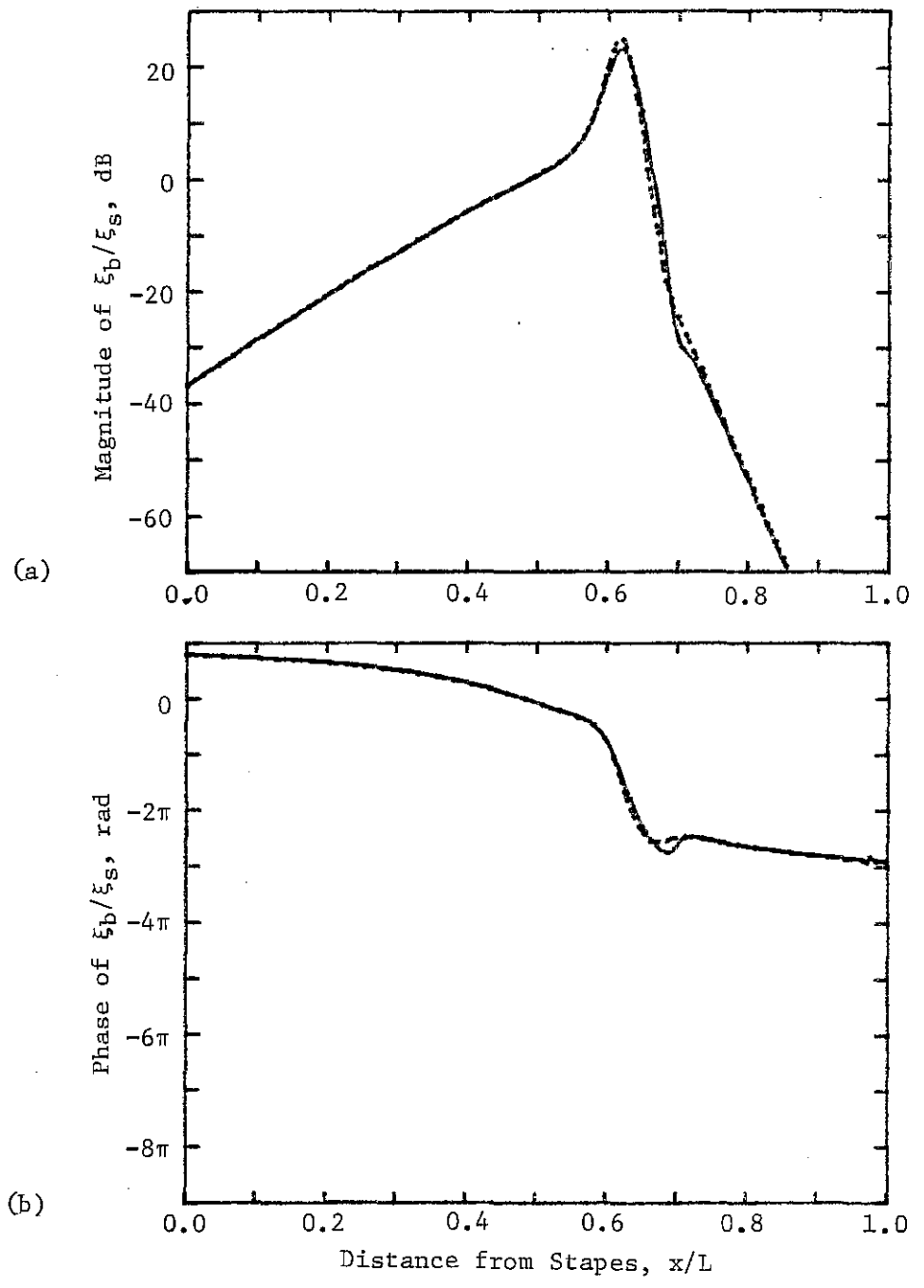

Figure 6.4. Sensitivity of model solution to spatial discretization (PSC). Solution of the frequency-domain model for a frequency of 620 Hz with M=4 (solid line) and M=16 (dashed line). (Model data from files C001 and C002).

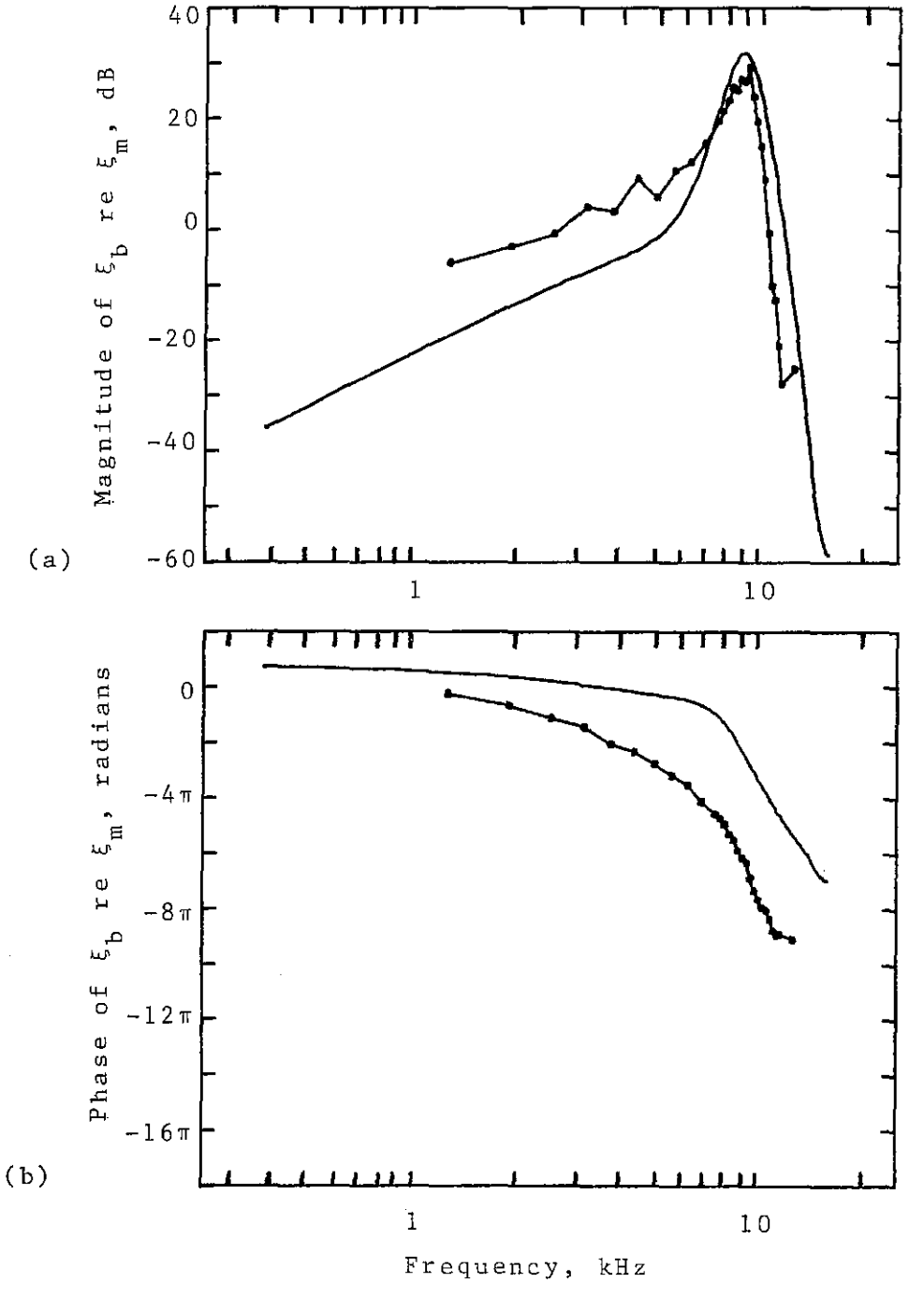

Figure 6.5. Comparison between model results with PSB and Rhode's data for basilar membrane displacement. The curves show basilar membrane displacement at (x/L)=0.22 re malleus displacement (solid line) and Rhode's Mössbauer measurements (circles) as a function of frequency. (a) Magnitude. (b) Phase. [Rhode's data from animal 69-473 (56) and model data from file IM14-1.]

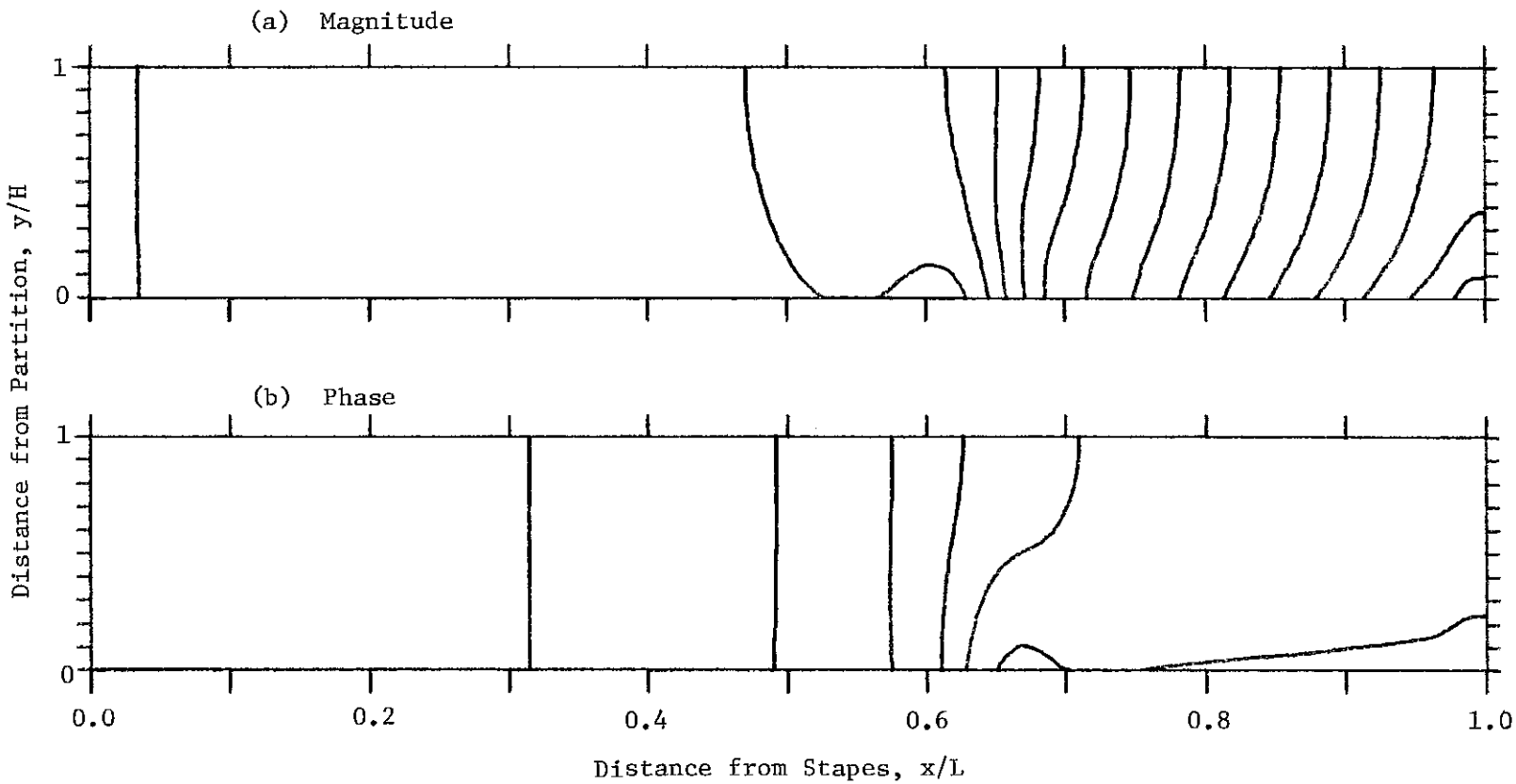

Figure 6.6. Iso-pressure contours in the two-dimensional frequency-domain model (PSC). (a) Iso-magnitude contours with 10 dB separation between contours. (b) Iso-phase contours with a quarter cycle separation between contours. Solution for frequency of 620 Hz and parameter set C, except with M=16. (Model data from file C002).

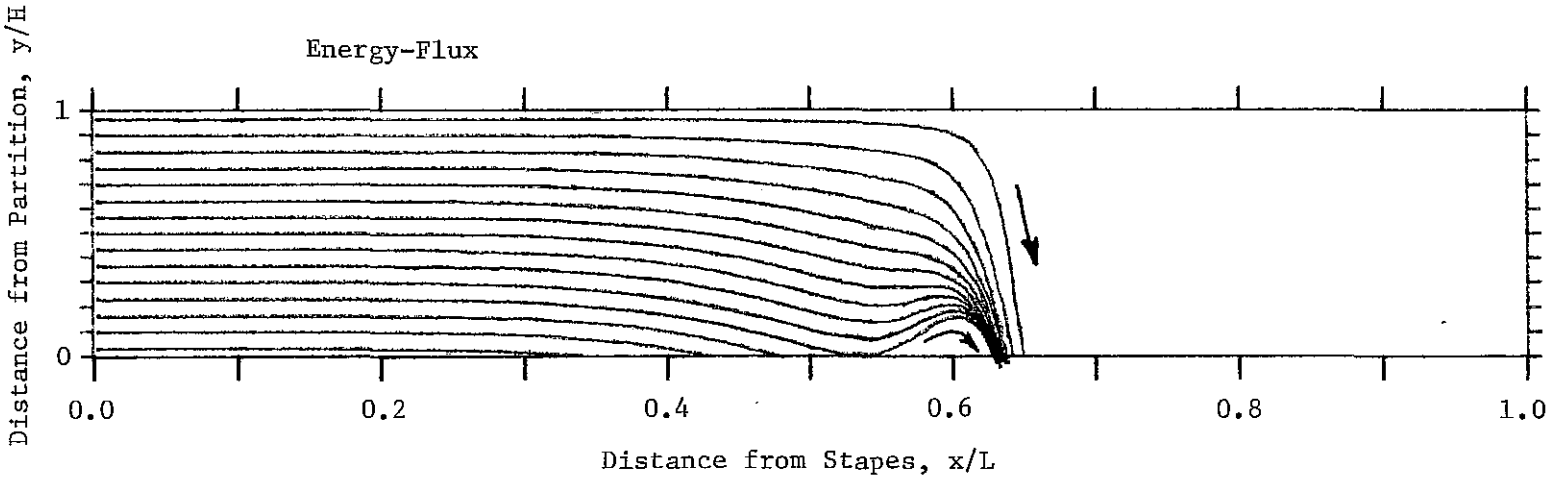

Figure 6.7. Lines of energy-flux in the two-dimensional frequency-domain model (PSC). Solution for frequency of 620 Hz and parameter set C, except with M=16. All flux lines shown in this figure originate near the stapes boundary and terminate at the partition boundary. (Model data from file C002).

Table 6.3. Values for the cochlear model parameters (PSD).

Macromechanical parameters:

$L = 3.5$ cm

$H = 1.0$ cm

$\rho = 1.0$ gm cm^{-3}

$A_s = 0.0126$ cm^2

$w_p = 0.0126$ cm

Micromechanical parameters:

$K_{1o} = 1.0 \times 10^8$ dyn cm^{-3},	$K_{1e} = -3.0$ cm^{-1}
$R_{1o} = 200$ dyn sec cm^{-3},	$R_{1e} = -1.5$ cm^{-1}
$M_{1o} = 0$ gm cm^{-2},	$M_{1e} = 0$ cm^{-1}
$K_{2o} = 3.3 \times 10^3$ dyn cm^{-3},	$K_{2e} = -3.1$ cm^{-1}
$R_{2o} = 5.000$ dyn sec cm^{-3},	$R_{2e} = -1.7$ cm^{-1}
$M_{2o} = 5.0 \times 10^{-7}$ gm cm^{-3},	$M_{2e} = -0.3$ cm^{-1}
$K_{3o} = 0$ dyn cm^{-3},	$K_{3e} = 0$ cm^{-1}
$R_{3o} = -4.980$ dyn sec cm^{-3},	$R_{3e} = -1.7$ cm^{-1}

Helicotrema parameters:

$L_h = 0.05$ cm

$R_h = 50$ dyn sec cm^{-3}

Spatial discretization parameters:

$M = 4$

$N = 240$

In Table 6.3 we introduce parameter set D (PSD). This set of model parameters includes a negative damping element (R_3) and is similar to PSB. The most significant change from PSB is the increase in scala height to H = 1 cm. The scala height was increased in order to increase the magnitude of the response in the plateau region (on the apical side of the resonant place). The increase in scala length L put the 1 kHz place in a mid-position in the cochlea. The elimination of partition mass M_1 had qualitatively little effect.

The partition driving-point admittance Y_b for PSD is shown in Figure 6.8 for a frequency of 1 kHz. The spectral zero at (x/L)=0.5 has a pronounced effect on both magnitude and phase of the admittance. The admittance has a negative real part between (x/L)=0.43 and 0.61; consequently, the partition emits energy in this region.

The frequency-domain solution for PSD at 1 kHz is shown in Figure 6.9. The displacement of the basilar membrane in the vicinity of the characteristic place is greatly increased by the existence of the energy emitting region. The model solution in Figure 6.9 (with R_{3o}=-4.980) shows no sign of any significant reflection of the forward traveling wave. (The forward direction is defined to be from base to apex.)

The amount of backward traveling wave can be increased by adjusting the negative damping R_3 so that it more nearly cancels the positive damping R_2. Figure 6.10 shows the effect of letting R_{3o}=-4.983. The prominent dips in magnitude and abrupt pi phase shifts indicate the presence of a backward traveling wave of

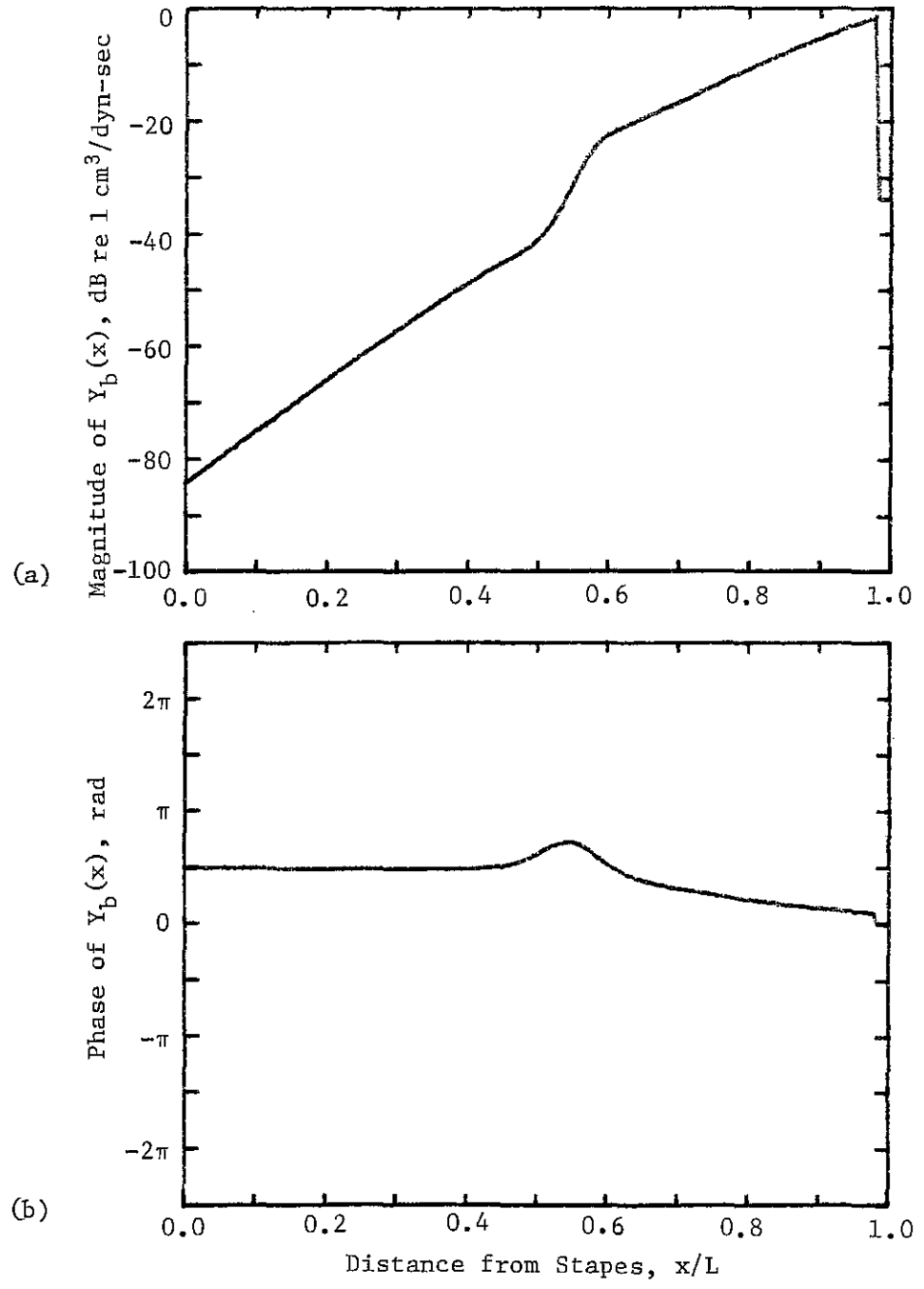

Figure 6.8. Driving-point admittance of the cochlear partition (PSD). Partition admittance Y_b for a frequency of 1 kHz as a function of distance from the stapes. (a) Magnitude. (b) Phase. The real part of $Y_b(x)$ is negative in the region (x/L)=0.43 to 0.61.

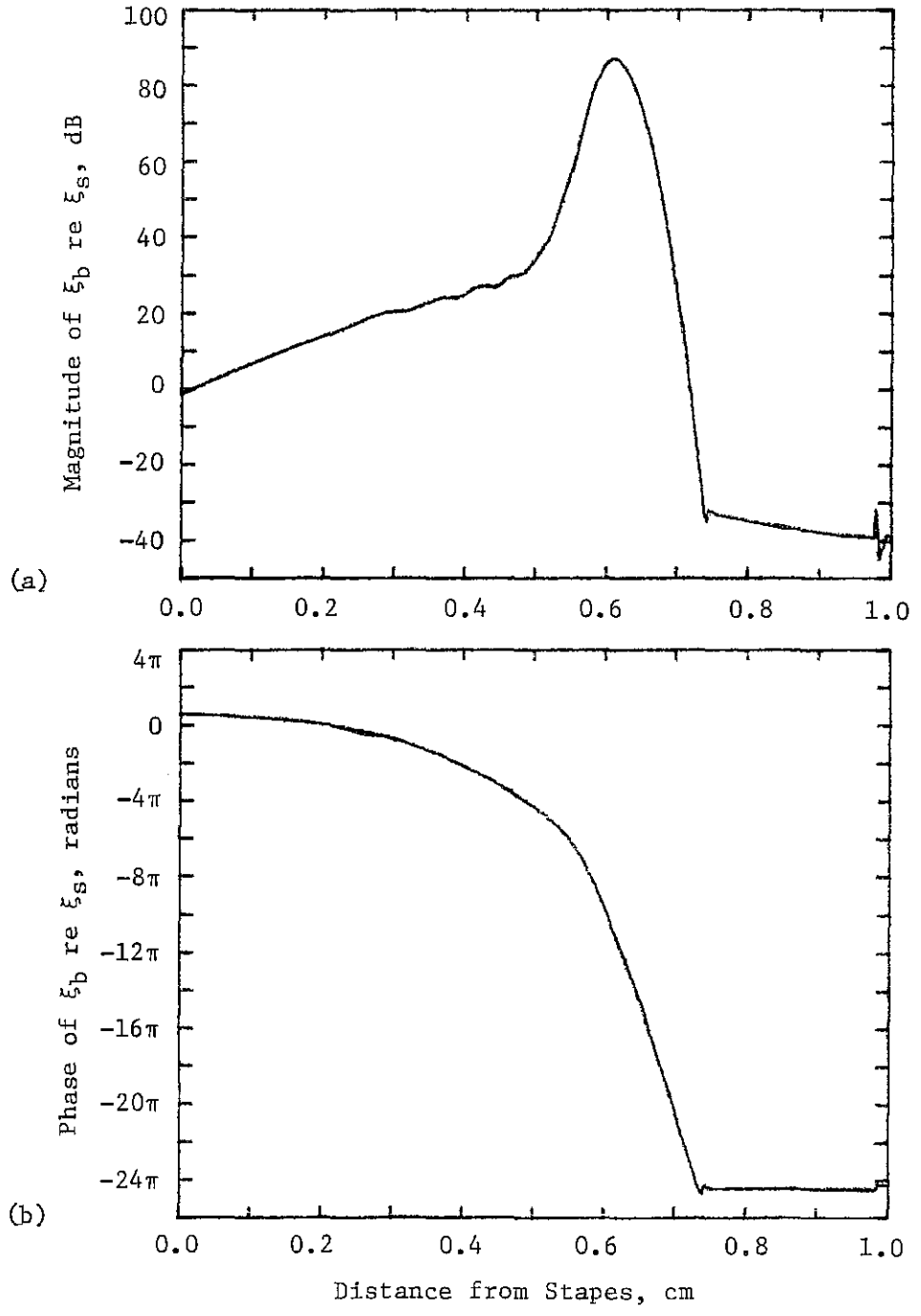

Figure 6.9. Active partition without noticeable reflections. Frequency-domain solution for a frequency of 1 kHz and parameter set D, with R_{3o}=-4.980. (Model data from file D001).

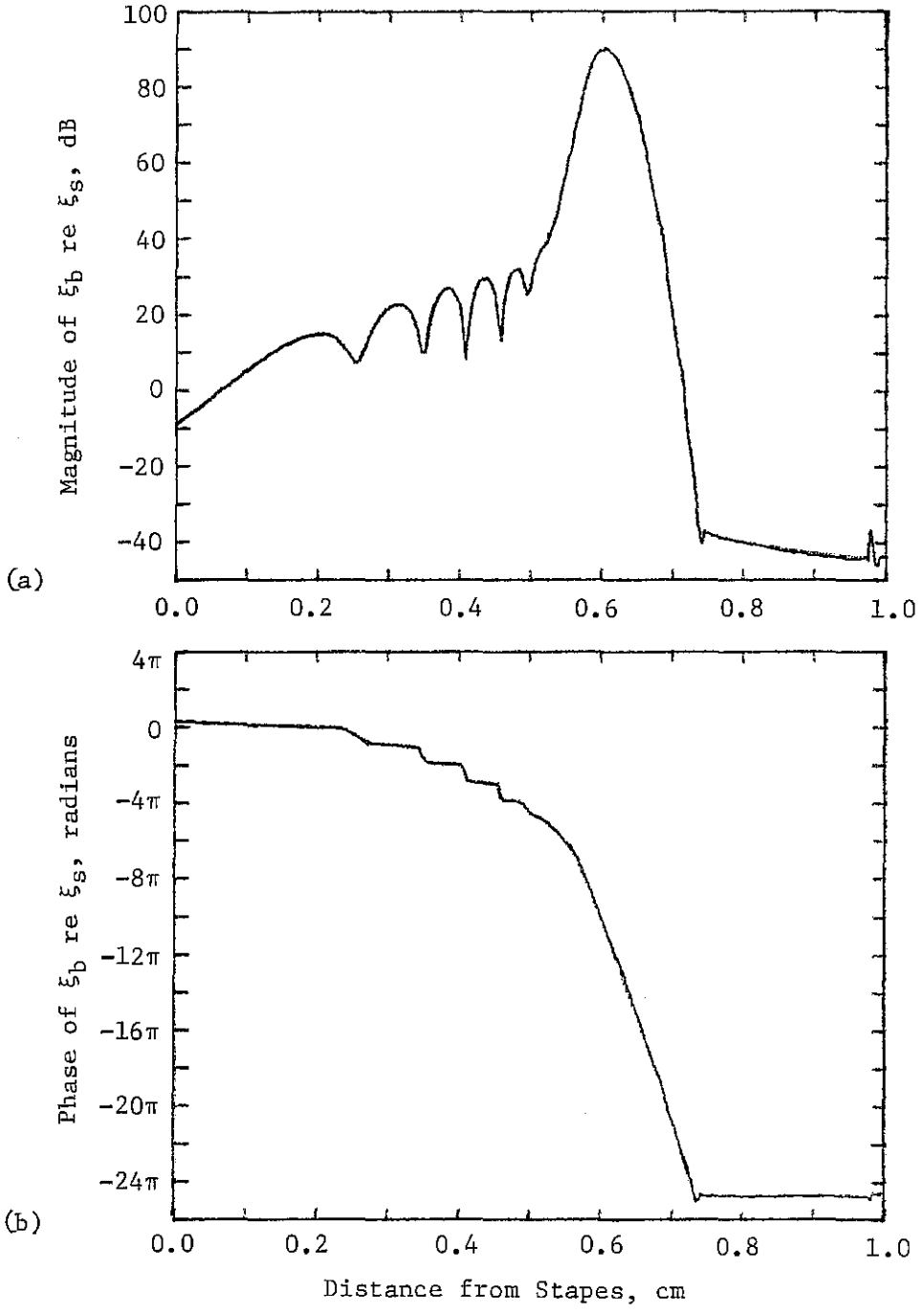

Figure 6.10. Active partition with prominent reflections. Frequency-domain solution for a frequency of 1 kHz and parameter set D, except with R_{3o}=-4.983. (Model data from file D002).

comparable magnitude to the forward traveling wave. The phase slope at the basal end is negative, indicating that the forward traveling wave still dominates; the stapes driving-point impedance still has a positive real-part and energy flows into the cochlea from the stapes at this frequency. This amount of backward traveling wave is thought to correspond with the state of the cochlea when prominent evoked cochlear emissions (cochlear echoes) are observed without the presence of spontaneous emissions. The cochlea appears to be in a "marginally stable" state.

The amount of backward traveling wave can easily exceed the amount of forward traveling wave if the value of R_3 is sufficiently close to $-R_2$. In Figure 6.11 we see a solution for PSD with $R_{3o}=-4.985$. The phase slope at the base indicates that energy is flowing out of the stapes at this frequency. This amount of backward traveling wave seems to correspond with the state of the cochlea which produces spontaneous cochlear emissions. Note that the magnitude of the solution in Figure 6.9 is not much different in appearance from the magnitude in Figure 6.10.

Attempts at simulating cochlear echoes in the time-domain model without also generating spontaneous emissions have been largely unsuccessful. The various constraints of the present model implementation made it difficult to maintain stability in the time-domain model. In particular, the exponential constraint on x variation of the micromechanical parameters made it impossible to set up marginally stable conditions in the mid-portion of the cochlea without also creating an unstable condition at one or both ends.

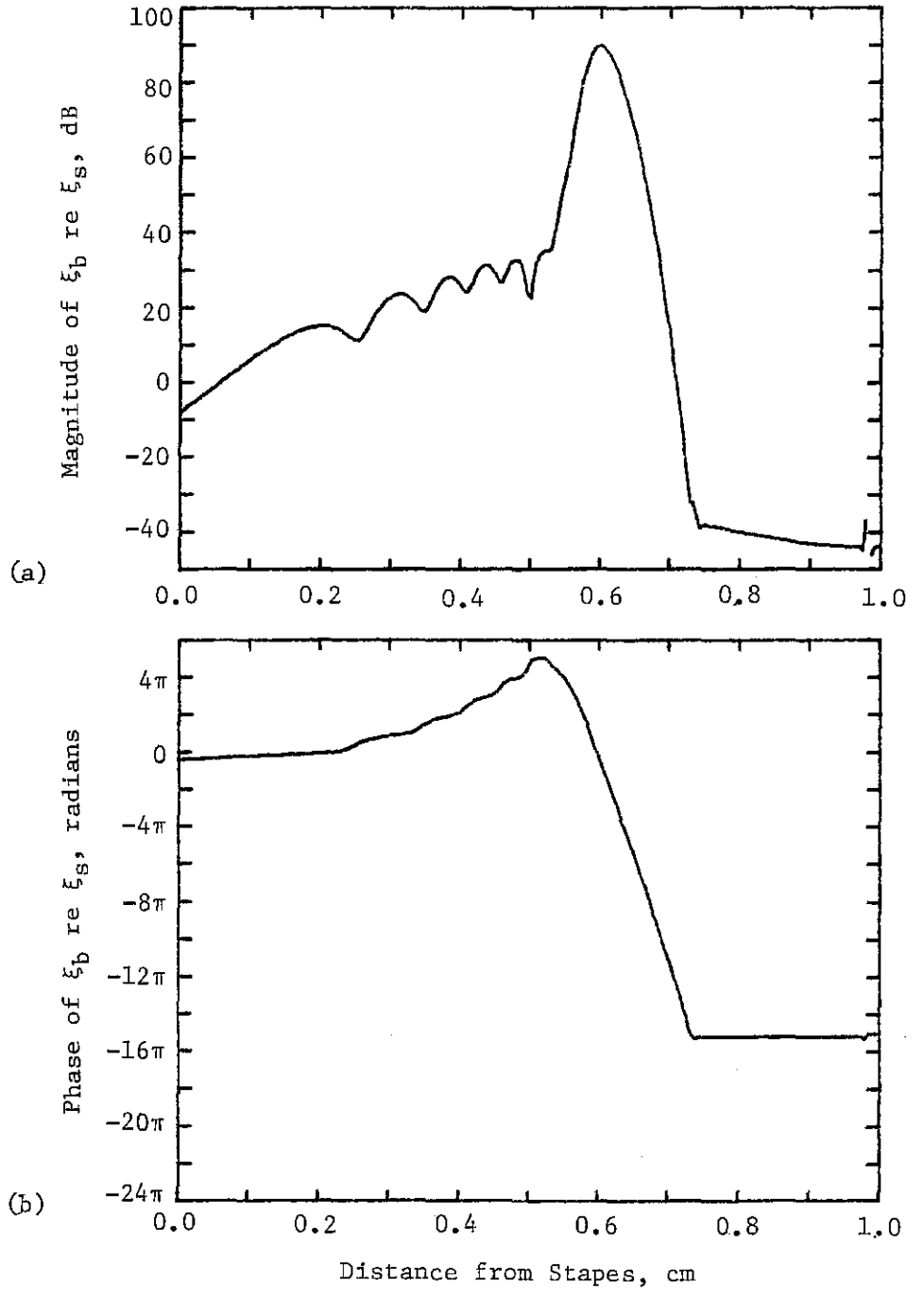

Figure 6.11. Active partition with spontaneous emission. Frequency-domain solution for a frequency of 1 kHz and parameter set D, except with R_{3o}=-4.985. (Model data from file D003).

Time-domain model solutions for PSD were not stable. The few stable cases wherein the model solutions showed energy flow directed outward at the stapes and the malleus for a limited time interval were either ambiguous, because of short latencies (less than 1 ms), or else not convincing because of apparent numerical accuracy problems in the spatial discretization. Cochlear echoes, of the type observed by Kemp (17), could not be reproduced in the time-domain model within the constraints of the current model implementation.

6.5 ITEMS FOR FUTURE RESEARCH

The following paragraphs describe topics which are thought to be promising areas for future research.

a. One problem with the current finite-difference time-domain model implementation is its inability to accurately represent solutions with very short wavelengths. Increasing the number of points in the spatial discretization would be possible on a larger computer, but the computation time would soon become prohibitive. Using a Green's function time-domain model eliminates the need to discretize the y dimension at the expense of certain restrictions on allowable boundary conditions. Current implementations of Green's function time-domain models (14, 21) do not allow basilar membrane mass to vary with x and do not allow simultaneous solution of middle-ear mechanics; it may be possible to remove these restrictions in future implementations. One potential advantage of the Green's function approach is the possibility of finding a Green's function to represent a three-dimensional model. A 3-D Green's function would make it possible to obtain solutions to a 3-D time-domain model with

practically no increase in computation time over the 2-D time-domain model. Another potential advantage is the possibility of a convenient means of including the effects of fluid viscosity.

b. It would not be difficult to incorporate a nonlinear element in the 2-DOF partition with resonant tectorial membrane. With this extension one could obtain a refined version of Matthews' (21) model results concerning propagation of two-tone distortion products (provided one could deal with the problem of computation time in the current model implementation). The nonlinear element could be one of the damping elements as proposed by Kim et al. (69, 98) or the cilia stiffness as proposed by Allen (12).

c. The simulation of cochlear echoes in a two-dimensional, time-domain cochlear model still presents a significant challenge. The model solutions in section 6.4 suggest that simulation of the echoes should be possible with a linear, 2-DOF partition which includes a negative damping element. The removal of the exponential constraint on partition parameters might be helpful in generating stable model solutions. Reflections at the apical boundary of the cochlea may be more prominent in a three-dimensional model and these reflections may have a significant influence on the cochlear echoes.

d. The development of a model for hair cell transduction which has the capability of bidirectional mechanical-electrical transduction might help to support the physical interpretation of the 2-DOF partition with resonant OHC cilia. Other work on the hydrodynamic aspects (106) and mechanics (111) of ciliary motion could be helpful in improving this physical interpretation. [See also Steele (67).]

It may be possible to show that the nonlinearity of intracellular potential versus cilia displacement (100) is sufficient to account for the observed mechanical nonlinearities. It has been proposed that cilia bending stiffness could be variable and somehow affected by partition motion (12, 29). The idea of cilia stiffness with an energy producing "hysteresis" offers one possible alternative to negative damping.

e. Careful analysis of the phase of the neural response data might provide useful information as to whether the inner hair cells are in contact with the tectorial membrane. An example of this type of analysis was discussed in section 6.2.2. Refinement of the model and a larger set of neural data are needed.

f. An attempt should be made to reconcile the differences in the resonant tectorial membrane and resonant OHC cilia interpretations of the 2-DOF partition. (Comparisons between PSA and PSB model solutions are included in Appendix 9.4.) If desired, the features of both could be included in a 3-DOF partition. Perhaps an alternative physical interpretation could consolidate these features into a single 2-DOF partition.

g. The time-domain cochlear model with fourth-order partition and parameters chosen to match neural data may be useful in the design of a sound spectrograph which could graphically simulate the neural output of the cochlea as a function of time.

7. SUMMARY AND CONCLUSIONS

The main objective of this dissertation was to present methods and motivation for the inclusion of fourth-order partition dynamics in a two-dimensional cochlear model for the purpose of modifying cochlear tuning. Two types of sharpening mechanisms were demonstrated in both time-domain and frequency-domain models of the cochlea with fourth-order partition dynamics.

The time-domain and frequency-domain cochlear models presented in this dissertation use a finite-difference approximation to discretize their two spatial dimensions. The finite-difference method permits simultaneous solution of mathematical models for the cochlea, middle-ear, acoustic coupler, and dynamic earphone mechanics in the time-domain model. The application of the finite-difference approximation to a time-domain model of the cochlea had not previously been demonstrated.

A "second-filter" sharpening mechanism was modeled by letting the lateral motion of the tectorial membrane (TM) become a second degree-of-freedom in cochlear partition-point mechanics. Model parameters chosen according to this resonant TM hypothesis were used to obtain model solutions which resemble the neural spatial-mapping data of Kim et al (4). The presence of a pi phase jump in the neural data and an abrupt change in the slope of the magnitude basal to the characteristic place provide support for the presence of a "spectral zero" in the transfer admittance which relates fluid pressure to hair cell shearing velocity.

An "active" sharpening mechanism was modeled by letting lateral motion of the outer hair cell (OHC) cilia become a second degree-of-freedom in cochlear partition-point mechanics and coupling the cilia to the reticular lamina with a negative damping element. This resonant OHC cilia hypothesis was used to obtain model solutions which resemble the direct basilar membrane measurements of Rhode (3) obtained in live squirrel monkeys. The change in slope of both magnitude and phase of the direct measurements at a frequency below the characteristic frequency provides support for the presence of a "spectral zero" in the driving-point admittance which relates fluid pressure to basilar membrane velocity. The effects of changes in stimulus level and of death of the animal on basilar membrane motion observed by Rhode are simulated in the model by making the negative damping parameter less negative or zero.

The presence of negative damping does not necessarily cause instability in the cochlear model. Both time-domain and frequency-domain results in this dissertation show that a small amount of negative damping can provide a means of sharpening basilar membrane tuning without causing reflections or spontaneous emissions. Frequency-domain results suggest that a larger amount of negative damping may create a marginally stable state in the model wherein reflections are significant, but no spontaneous emissions are present; a still larger amount of negative damping in the frequency-domain model creates an unstable state in which there is a net flow of energy out of the cochlea.

The marginally stable state of the cochlea (mentioned above) may be related to the existence of cochlear echoes as observed by Kemp (17). An attempt was made to simulate cochlear echoes in the time-domain model, but such echoes were not observed for any of the linear, stable parameter sets for which valid model solutions have been obtained.

In both the "second-filter" and "active" sharpening mechanisms, the addition of a second degree-of-freedom in the partition-point mechanics leads to fourth-order equations of motion. The presence of fourth-order equations in the model increases the difficulty of selecting appropriate parameters for the cochlear partition. Also, the computation time required for obtaining solutions to the cochlear model is increased with the fourth-order equations, especially in the time-domain model. However, the agreement between the model solutions and experimental data appears to be significantly improved with the addition of these second degrees-of-freedom. In addition, the 2-DOF partition-point model allows more detailed physical interpretations of cochlear micromechanics. These advantages make the 2-DOF partition a useful extension to the two-dimensional cochlear model over the traditional 1-DOF partition.

8. ACKNOWLEDGMENTS

I am indebted to many people for providing me with the opportunity for pursuing my doctoral studies and for contributing ideas and insights which have become a part of this dissertation.

My research advisor, Professor J. R. Cox, has patiently provided thoughtful and objective guidance to my research. He has helped me to improve the scientific quality of my research, while allowing me to choose my own direction. My academic advisor, Professor C. E. Molnar, has a knack for identifying relevant issues which are too important to be ignored or treated lightly. His insights have helped me to strengthen the presentation of my research. Many of the ideas presented in this dissertation reflect the content of numerous conversations with my third advisor, Professor D. O. Kim. I appreciate his enthusiasm toward my research and his willingness to share with me his understanding of controversial topics in cochlear mechanics, especially concerning the active behavior of the cochlea.

I have enjoyed many discussions of cochlear modeling issues with John Matthews and cochlear physiology with John Siegel. Both persons have provided me with insights and much needed encouragement.

I would like to thank J. R. Pierce, J. B. Allen, C. E. Molnar, R. H. Cannon, T. R. Turner, and my family for encouraging me to continue my doctoral studies at times when it was very difficult for me to do so.

My wife, Donna, has generously given emotional and financial support throughout the period of my graduate studies. In addition,

she has provided helpful suggestions and secretarial assistance in the preparation of this dissertation.

Financial support was provided by an NIH training grant [GM-07564] and NIH research grants [NS-07498] and [RR-00396].

9. APPENDICES

APPENDIX 9.1

MATHEMATICAL MODELS FOR MIDDLE EAR, ACOUSTIC COUPLER AND DYNAMIC EARPHONE MECHANICS

This appendix describes the mathematical models which are used to represent the mechanics of the middle ear, acoustic coupler, and dynamic earphone in this dissertation. The inclusion of these three items in a comprehensive model of the peripheral auditory system allows the stimulus to be specified as air pressure at the eardrum or voltage to the earphone. In such a comprehensive model acoustic signals are allowed to propagate both into and out of the cochlea.

The mathematical models described in this appendix are based on the presentation of an acoustic stimulus to a cat by a method used in the Sensory Biophysics Laboratory at Washington University. A dynamic earphone is attached to an acoustic coupler which is placed near the eardrum of the cat. Mathematical models for middle ear, acoustic coupler, and dynamic earphone are presented as equations of motion in this appendix. These equations have been incorporated into the time-domain model for cochlear mechanics which is described in section 3.4.

The description of the middle ear, acoustic coupler, and dynamic earphone models requires the introduction of additional variables and parameters. Model variables used in the middle ear, acoustic coupler, and dynamic earphone models are described in Table 9.1; model parameters are described in Table 9.2 and values for these parameters are listed in Table 9.3.

Table 9.1. Model variables for middle ear, acoustic coupler and dynamic earphone.

Cochlea

P_s - fluid pressure at stapes, dyn cm^{-2}.

Middle ear

ξ_s - displacement of stapes, cm.

ξ_m - displacement of mallues, cm.

ξ_e - displacement of eardrum with ξ_m=0, cm.

P_e - air pressure at eardrum, dyn cm^{-2}.

Acoustic coupler

ξ_a - dislacement of air in coupler tube, cm.

P_a - air pressure at earphone diaphragm, cm.

Dynamic earphone

ξ_d - displacement of earphone diaphragm, cm.

V_p - electrical voltage delivered to earphone, volts.

Table 9.2. Model parameters for middle ear, acoustic coupler and dynamic earphone.

Middle ear

K_m - stiffness of malleus attachment, dyn cm^{-1}.

R_m - damping of malleus attachment, dyn sec cm^{-1}.

M_m - effective mass of malleus, gm.

A_m - effective area of eardrum associated with ξ_m, cm^2.

K_e - stiffness of "eardrum" attachment, dyn cm^{-1}.

R_e - damping of "eardrum" attachment, dyn sec cm^{-1}.

M_e - effective mass of "eardrum", gm.

A_e - effective area of eardrum associated with ξ_e, cm^2.

K_s - stiffness of stapes and round window attachment, dyn cm^{-1}.

R_s - damping of stapes attachment, dyn sec cm^{-1}.

M_s - effective mass of stapes, gm.

A_s - effective area of stapes footplate, cm^2.

K_i - stiffness of incudo-malleolar joint, dyn cm^{-1}.

G_m - gain of middle ear lever.

Table 9.2. (continued)

Acoustic coupler

K_a - stiffness due to air compression in coupler cone, dyn cm^{-1}.

R_a - damping due to air compression and fuzz in coupler cone, dyn sec cm^{-1}.

M_a - mass of air in coupler tube, gm.

A_a - cross-sectional area of coupler tube, cm^2

R_b - damping due to air motion and fuzz relative to coupler walls, dyn sec cm^{-2}.

τ_a - acoustic propagation delay through coupler, sec.

Dynamic earphone

K_d - stiffness of diaphragm suspension, dyn cm^{-1}.

R_d - damping of diaphragm suspension, dyn sec cm^{-1}

M_d - effective mass of diaphragm, gm.

A_d - effective area of diaphragm, cm^2.

R_p - damping due to voice coil motion through magnetic field, dyn sec cm^{-1}.

C_p - force on voice coil due to stimulus voltage, dyn $volt^{-1}$.

B - magnetic flux density surrounding voice coil, gauss.

ℓ - length of wire in voice coil winding, cm.

R_v - electrical resistance of voice coil winding with $\xi_d=0$, ohm.

Table 9.3. Values of model parameters for middle ear, acoustic coupler and dynamic earphone.

Middle ear

$K_m = 3.44 \times 10^5$ dyn cm^{-1}.

$R_m = 6.65$ dyn sec cm^{-1}

$M_m = 4.82 \times 10^{-3}$ gm

$A_m = 0.347$ cm^2

$K_e = 3.13 \times 10^4$ dyn cm^{-1}

$R_e = 3.25$ dyn sec cm^{-1}

$M_e = 0.135 \times 10^{-3}$ gm

$A_e = 0.05$ cm^2

$K_s = 4.41 \times 10^5$ dyn cm^{-1}

$R_s = 31.8$ dyn sec cm^{-1}

$M_s = 4.27 \times 10^{-3}$ gm

$A_s = 0.0126$ cm^2 (also a cochlear model parameter)

$K_i = 1.32 \times 10^7$ dyn cm^{-1}

$G_m = 0.5$

Table 9.3. (continued)

Acoustic coupler

$K_a = 2.19\times10^{3}$ dyn cm^{-1}

$R_a = 0.1$ dyn sec cm^{-1}

$M_a = 0.217\times 10^{-3}$ gm

$A_a = 0.0707$ cm^2

$R_b = 0.6$ dyn sec cm^{-2}

$\tau_a = 0.21\times10^{-3}$ sec

Dynamic earphone

$K_d = 7.72\times10^{6}$ dyn cm^{-1}

$R_d = 100$ dyn sec cm^{-1}

$M_d = 57\times10^{-3}$ gm

$A_d = 2.5$ cm^2

$R_p = 144$ dyn sec cm^{-1}

$C_p = 2.69\times10^{3}$ dyn $volt^{-1}$

$B = 7.5\times10^{3}$ gauss

$\ell = 716$ cm

$R_v = 200$ ohm

9.1.1 MIDDLE EAR

The middle ear model described in this section is essentially the same as the one developed by Matthews (21) for cat middle ear with bulla widely opened. The displacement of air at the end of the coupler tube ξ_a creates a pressure at the eardrum P_e which deflects the eardrum in two modes ξ_m and ξ_e. Compression of air between the end of the coupler tube and the eardrum is not considered in the model so that

$$A_a\xi_a = A_m\xi_m + A_e\xi_e \ , \tag{9.1.1}$$

where A_a, A_m, and A_e are the effective areas associated with the respective displacements. Only one of the eardrum defection modes ξ_m contributes to displacement of the malleus; the other deflection mode ξ_e reflects the inefficiency of the eardrum. The stapes and incus are assumed to move together as a single lumped mass M_s. Displacement of the stapes (and incus) ξ_s is coupled to malleus displacement by means of a stiff, incudo-malleolar joint K_i. There is also a lever gain G_m between malleus and stapes displacements. The middle ear interacts with the cochlea at the footplate of the stapes where there is an average fluid pressure P_s over the effective area of the footplate A_s. The middle ear model is illustrated in Figure 9.1.

The middle ear model has three degrees-of-freedom. Associated with each degree-of-freedom is a mass which is attached to the temporal bone by means of a viscous damping and a stiffness. The equations of motion for the middle ear model are

$$A_eP_e = M_e\ddot{\xi}_e + R_e\dot{\xi}_e + K_e\xi_e \tag{9.1.2}$$

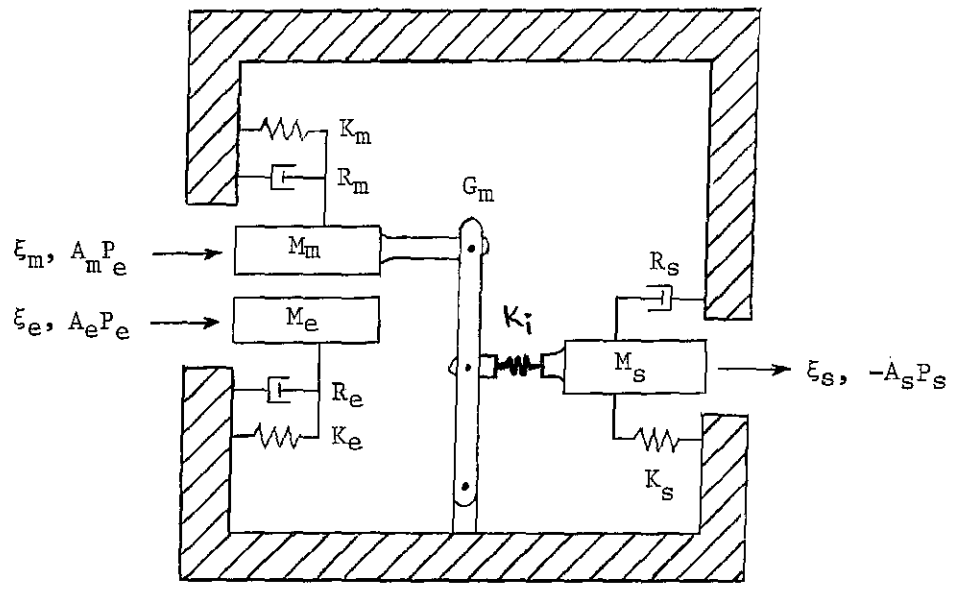

Figure 9.1. Mechanical model of the middle ear.

$$A_m P_e = M_m \ddot{\xi}_m + R_m \dot{\xi}_m + K_m \xi_m + G_m K_i (G_m \xi_m - \xi_s) \qquad (9.1.3)$$

$$-A_s P_s = M_s \ddot{\xi}_s + R_s \dot{\xi}_s + K_s \xi_s + K_i (\xi_s - G_m \xi_m) \ . \qquad (9.1.4)$$

The model parameters in the above equations are described in Table 9.2.

Matthews (21) used experimental measurements of middle ear response in cat to determine values for middle ear model parameters. The middle ear parameters values listed in Table 9.3 are based on those obtained by Matthews.

The middle ear has an effect on the time-domain model results presented in chapter 5. Figure 9.2 shows the ratio of the frequency response of stapes displacement ξ_s to malleus displacement ξ_m with the stimulus defined as voltage to the earphone and PSB used in the cochlear model.

9.1.2 ACOUSTIC COUPLER

A simplified diagram of the acoustic coupler used by Kim (5) and others is shown in Figure 9.3. The acoustic coupler is basically a funnel; it has a rigid-walled conical cavity which is attached to a small diameter tube. The larger end of the coupler is attached to a dynamic earphone (as illustrated in Figure 9.2) and the smaller end is placed near to the eardrum of the experimental animal.

The model for the acoustic coupler described in this section is essentially the same as the one used by Matthews (21). The air in the coupler tube is treated as a lumped mass which has some displacement ξ_a relative to the walls of the coupler. A force is exerted on this air mass by the pressure at the end of the tube P_e which is assumed to

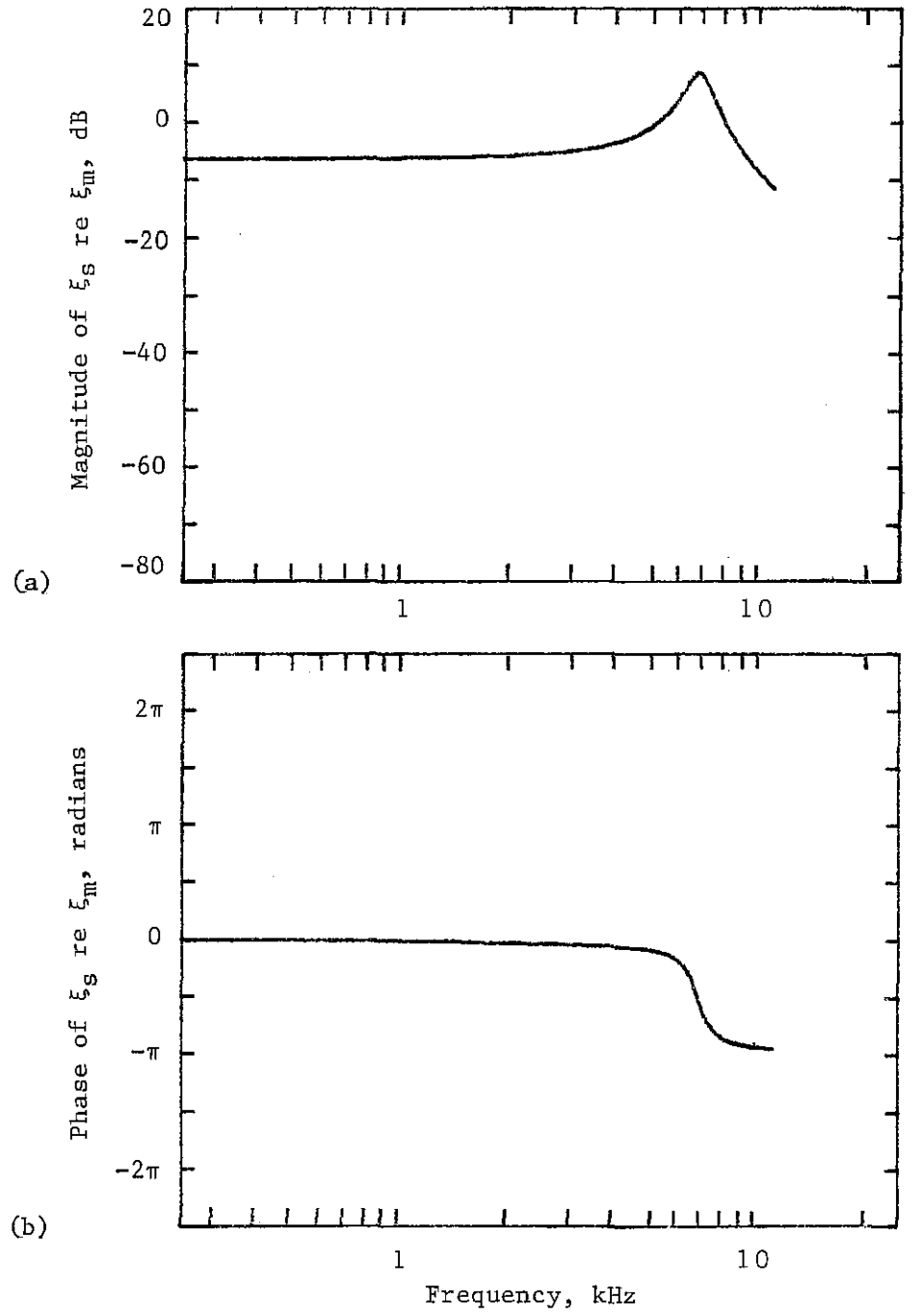

Figure 9.2. Ratio of stapes displacement ξ_s to malleus displacement ξ_m as a function of frequency. (a) Magnitude. (b) Phase. Curves are from a solution of the time-domain model with middle ear, acoustic coupler, dynamic earphone and PSB in the cochlea. (Data from file IM22-1.)

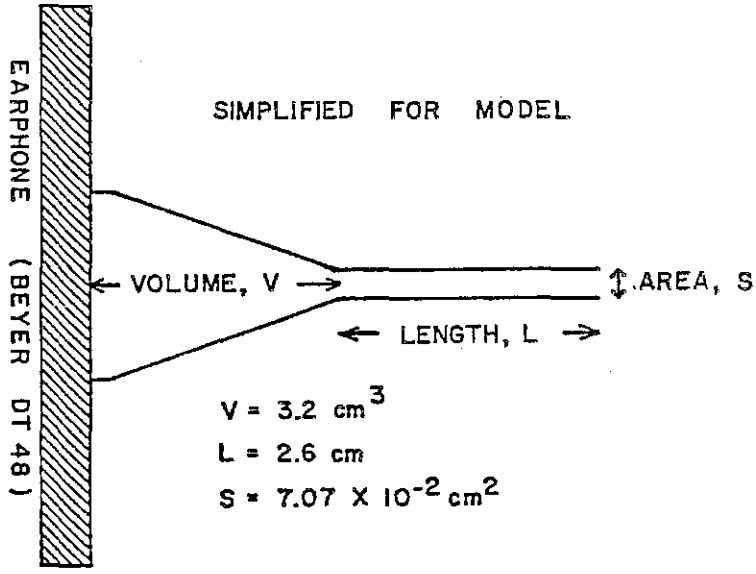

Figure 9.3. Simplified diagram of the acoustic coupler. The dynamic earphone (Beyer DT-48) is coupled to the eardrum of the experimental animal by this device. [Figure from Matthews (21). Diagram prepared by D. O. Kim.]

be the same as the pressure at the eardrum. The air in the conical cavity is treated as a spring K_a which couples the air in the tube to the diaphragm of the earphone. The force exerted by the earphone diaphragm is represented by an average pressure P_a over the effective area of the earphone diaphragm A_d. Cotton fills the conical cavity and the tube and is responsible for damping of air motion. This fuzz-damping is represented in the model by two parameters, R_a and R_b. The model of the acoustic coupler is illustrated in Figure 9.4.

The acoustic coupler model described briefly above has a single degree-of-freedom associated with movement of the air mass in the coupler tube. The equation of motion which describes the acoustic coupler model is

$$-A_a P_e = M_a \ddot{\xi}_a + R_b \dot{\xi}_a + R_a [\dot{\xi}_a - (A_d/A_a)\, \dot{\xi}_d] + K_a [\xi_a - (A_d/A_a)\, \xi_d] \ , \qquad (9.1.5)$$

where ξ_d is the displacement of the earphone diaphragm and the parameters for the acoustic coupler are described in Table 9.2. The parameter values listed in Table 9.3 are based on those obtained by Matthews.

The acoustic coupler also has an acoustic propagation delay τ_a of about 0.21 milliseconds (see Figure 9.5). This propagation delay is not included in the acoustic coupler model.

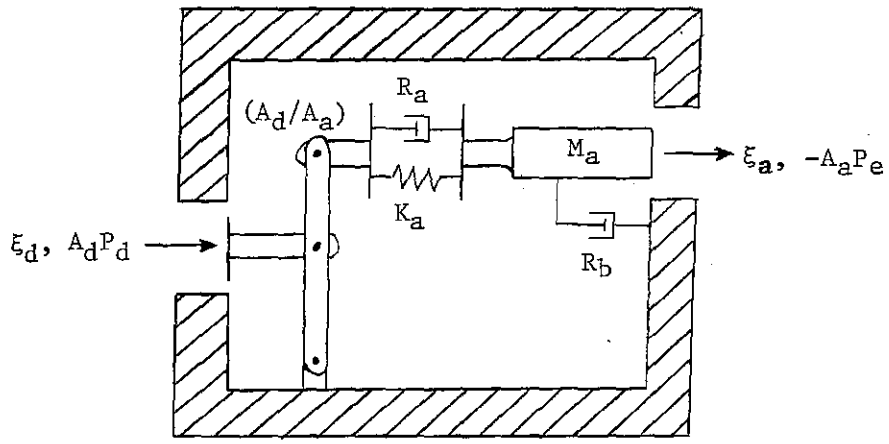

Figure 9.4. Mechanical model of the acoustic coupler.

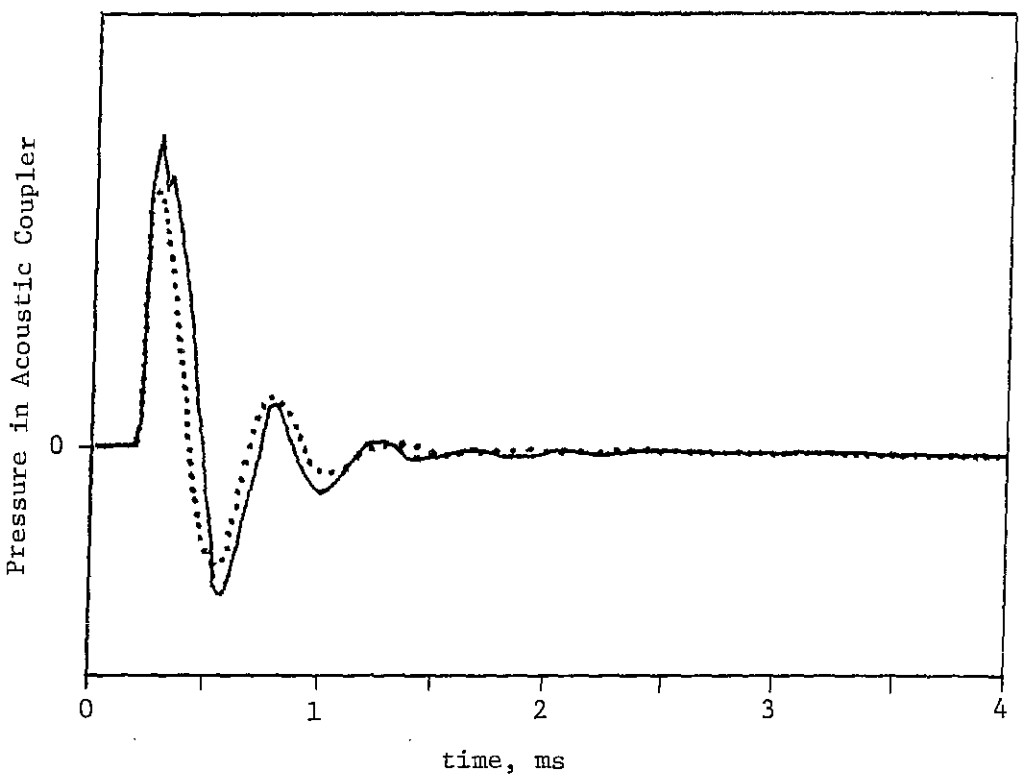

Figure 9.5. Comparison of measured response and model response of dynamic earphone. The experimentally measured response (solid line) represents pressure in the coupler tube in response to a 75 microsecond voltage pulse to the earphone. The model response $P_e(t)$ was shifted by 0.2 milliseconds to compensate for acoustic propagation delay in the coupler. [Earphone response measured by D. O. Kim.]

9.1.3 DYNAMIC EARPHONE

The acoustic transducer used as a stimulus source for most of the animal experiments in the Sensory Biophysics Laboratory is a Beyer DT-48, 200 ohm dynamic earphone. The model for the DT-48 earphone described in this section was adapted from a simple, low-frequency earphone model developed by Beranek (112). The input to the earphone is an ideal voltage source V_p. The output of the earphone is represented by a displacement ξ_d and air pressure P_a over the effective area of the diaphragm A_d. The dynamic earphone model is illustrated in Figure 9.6. The equation of motion for the dynamic earphone model is

$$C_p V_p - A_d P_d = M_d \ddot{\xi}_d + (R_d + R_p)\,\dot{\xi}_d + K_d \xi_d \quad . \tag{9.1.6}$$

The dynamic earphone parameters are described in Table 9.2.

According to Beranek, the parameters C_p and R_p may be computed from the magnetic flux density B which surrounds the voice coil, the length of wire ℓ in the voice coil winding, and the electrical resistance R_v of the voice coil winding with the diaphragm blocked.

$$C_p = 0.1\ B\ell / R_v \tag{9.1.7}$$

$$R_p = 10^{-9}\ (B\ell)^2 / R_v \tag{9.1.8}$$

(The numerical constants in the above equations are a result of conversion between electrical units and cgs mechanical units.) The values of B, ℓ, and R_v have been obtained from the manufacturer of the earphone (113) and are listed in Table 9.3.

Schlemmer (114) has analyzed an acoustic system which included a Beyer DT-48, 8 ohm dynamic earphone. The values of the model parameters for effective area A_d, effective mass M_d, and stiffness K_d

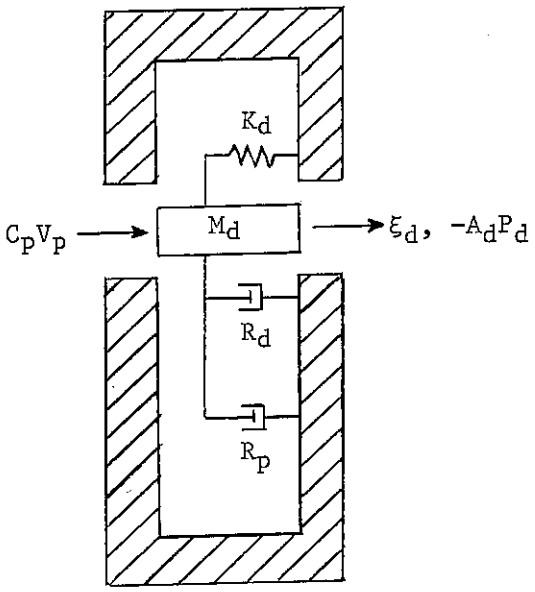

Figure 9.6. Mechanical model of the dynamic earphone.

of the earphone diaphragm which are listed in Table 9.3 are based on the work of Schlemmer.

The value of the parameter for damping of the diaphragm attachment was chosen to match an experimentally measured impulse response. The DT-48 earphone was attached to the acoustic coupler which was terminated with a rigid plug. A 75 microsecond rectangular pulse of voltage was delivered to the earphone while monitoring the pressure in the coupler tube. Figure 9.5 shows a comparison between the model response and the measured response.

APPENDIX 9.2

APPROXIMATE FORMULAS

FROM A ONE-DIMENSIONAL COCHLEAR MODEL

The first portion of this appendix follows Allen (12) in deriving approximate formulas for traveling-wave delay $\tau_d(x)$ and stapes driving-point impedance Z_s from a one-dimensional, frequency-domain cochlear model. These approximate formulas are then used to obtain the relationships between model parameters and quantitative features of experimental data that are needed in chapters 4 and 5.

For frequencies below resonance the partition driving-point impedance is dominated by the basilar membrane stiffness and can be approximated by

$$Z_b(x) = K_1(x) / i\omega \ . \tag{9.2.1}$$

With this approximation, the one-dimensional model equation which describes pressure difference P(x) across the partition is (56)

$$\frac{d^2}{dx^2} P(x) + \left[\frac{\omega}{c}\right]^2 P(x) = 0 \ , \tag{9.2.2}$$

where

$$c(x) = \left[\frac{H K_1(x)}{2\rho} \right]^{1/2} , \tag{9.2.3}$$

and, as before,

$$K_1(x) = K_{1o} \exp(K_{1e} x) \ . \tag{9.2.4}$$

The WKB-approximate solution to equation (9.2.2) [as shown by Zweig et al. (56)] is

$$P(x) = P(0) \left[\frac{c(x)}{c(0)} \right]^{1/2} \exp[-i\omega\tau_d(x)] \ , \tag{9.2.5}$$

where

$$\tau_d(x) = \int_0^x \frac{du}{c(u)} \tag{9.2.6}$$

is the traveling-wave delay at position x.

The stapes velocity V_s can be determined from equation (9.2.5) and the stapes boundary condition

$$\begin{aligned} -2i\omega\rho V_s &= \frac{d}{dx} P(0) \\ &= [c'(0)/2 - i\omega] P(0)/c(0) , \end{aligned} \tag{9.2.7}$$

where

$$c'(0) = K_{1e}\, c(0)/2 . \tag{9.2.8}$$

The stapes input impedance is the ratio of stapes pressure to stapes velocity

$$\begin{aligned} Z_s &= P(0) / V_s \\ &= -2i\omega\rho\, c(0) / [K_{1e}\, c(0)/4 - i\omega] . \end{aligned} \tag{9.2.9}$$

In chapter 4, we need a relationship between the stiffness K_1 and the slope of the phase of the pressure $\phi_1(x)$ with respect to x. According to equations (9.2.5) and (9.2.6)

$$\begin{aligned} \frac{d}{dx}\phi_1(x) &= -\omega \frac{d}{dx} \tau_d(x) \\ &= -\omega(2\rho/H)^{1/2} [K_1(x)]^{-1/2} . \end{aligned} \tag{9.2.10}$$

Solving for K_1 in equation (9.2.10) gives

$$K_1(x) = \left(\frac{2\omega^2\rho}{H}\right) \left[\frac{d}{dx}\, \phi(x)\right]^{-2} . \tag{9.2.11}$$

If we let $\omega=2\pi f$, then equation (9.2.11) is the same as equation (4.17).

In chapter 5, we need a relationship between the stiffness K_1 and the slope of the phase of the pressure with respect to frequency. According to equations (9.2.5) and (9.2.6)

$$\frac{d}{d\omega}\,\phi_1(x;\omega) = -\tau_d(x)$$
$$= \left(\frac{2}{K_{1e}}\right)\left(\frac{2\rho}{H K_{1o}}\right)^{1/2}\left[1 - \exp(-K_{1e}\,x/2)\right]. \qquad (9.2.12)$$

For small x, the exponential term in equation (9.2.12) can be approximated

$$\frac{d}{d\omega}\,\phi_1(x;\omega) = -x\left(\frac{2\rho}{HK_{1o}}\right)^{1/2}\exp\left(-K_{1e}\,x/4\right) . \qquad (9.2.13)$$

In terms of the b-constants of chapter 5

$$b_3 = \frac{d}{d\omega}\,\phi_1(b_7 L;\omega)$$
$$= -b_7 L\left(\frac{2\rho}{H K_{1o}}\right)^{1/2}\exp\left(-K_{1e}\,b_7 L\right) . \qquad (9.2.14)$$

We also need a relationship between the stiffness K_1 and the magnitude of the ratio of basilar membrane displacement to stapes displacement. In the model this ratio can be expressed as

$$\left[\frac{D_b(x)}{D_s}\right] = \left[\frac{P(x)\,Z_s}{P(0)\,Z_b(x)}\right] , \qquad (9.2.15)$$

where D_s is stapes displacement and $D_b(x)$ is basilar membrane displacement at position x. Experimental measurements show that the stapes impedance is approximately real for frequencies above 1000 Hz in cat (115). Assuming that stapes impedance is real over the range of frequencies used to determine the phase slope in chapter 5, we will let

$$Z_s \approx 2\rho\, c(0)\,. \tag{9.2.16}$$

With this additional approximation the magnitude of the displacement ratio becomes

$$\left| \frac{D_b(x)}{D_s} \right| = 2\omega\rho\, [\, c(0)c(x)\,]^{1/2} / K_1(x)$$

$$= \omega \left(\frac{2\rho H}{K_{1o}} \right)^{1/2} \exp\,(-3K_{1e}\, x/4)\,. \tag{9.2.17}$$

Or, in terms of the b-constants of chapter 5

$$b_1^{-1} b_2 b_6 = \frac{1}{f} \left| \frac{D_b(x)}{D_s} \right|$$

$$= 2\pi (2\rho H / K_{1o})^{1/2} \exp\,(-3K_{1e}\, x/4)\,. \tag{9.2.18}$$

We can use equations (9.2.14) and (9.2.18) to obtain formulas for K_{1o} and H

$$K_{1o} = -b_1 b_2^{-1} b_3^{-1} b_6^{-1} b_7\, (2\pi\rho L) \exp\,(-K_{1e}\, b_7\, L) \tag{9.2.19}$$

$$H = -b_1^{-1} b_2 b_3^{-1} b_6 b_7\, (L/\pi) \exp\,(K_{1e}\, b_7\, L/2)\,. \tag{9.2.20}$$

Approximate equations similar to equations (9.2.19) and (9.2.20) were used to obtain initial values for K_{1o} and H to match Rhode's data for chapter 5. The initial parameter values were subsequently modified to obtain better agreement with the data.

APPENDIX 9.3

DESCRIPTION OF COMPUTER PROGRAMS

Much of the research effort for this dissertation was devoted to the development of FORTRAN computer programs for the purpose of computing and examining solutions of cochlear models. The capabilities of some of the most useful computer programs will be summarized in this appendix. These computer programs represent some of the cochlear modeling tools which made it possible to obtain model results for this dissertation.

BMADMIT handles specification of model parameters for the frequency-domain model and computes the necessary fourth-order admittance functions. The program accepts model parameters from the console and displays (on an oscilloscope) the partition driving-point admittance and the hair cell shearing transfer admittance. The program writes model parameters and computed admittances to a parameter file on disk.

DM12 is a two-dimensional, frequency-domain cochlear model implementation. The program uses the finite-difference method to discretize spatial dimensions (as described in section 3.3) and solves the resulting equations by a Gaussian block-elimination method. This program is similar to the one used by Neely (62). DM12 reads model parameters and admittances from a parameter file (as written by BMADMIT). The program allows spatial discretization up to M=16 and N=256 by using a temporary disk file to store the elements of the large matrix. The program writes admittance, two-dimensional

pressure, and partition displacement to a frequency-domain data file on disk.

DISPLAY reads the frequency-domain data file as written by DM12 and displays the magnitude and phase of admittance, displacement, and pressure on an oscilloscope. The program has an option of producing "hard-copy" graphs on a pen-plotter.

CONTOUR reads the two-dimensional pressure from a frequency-domain data file and plots contour lines of iso-magnitude or iso-phase on a pen-plotter. Values of magnitude or phase are accepted from the console. Contours are drawn using linear interpolation between data points.

NRGYFLUX reads the two-dimensional pressure from a frequency-domain data file and plots lines of energy-flux on a pen-plotter. The starting points of these lines are distributed near the stapes boundary. Flux lines are drawn in small segments by locating each succeeding point a small fixed distance away, in the direction of the current energy-flux vector. [See equation (4.43) for a definition of the energy-flux vector.] The program has an option of integrating the energy-flux over the stapes and partition boundaries to determine the net energy-flux through these boundaries.

MSTIMGEN computes stimuli for the time-domain cochlear model. The program interactively accepts stimulus parameters from the console and has the capability of producing various types of stimuli. (The time-domain model results in this dissertation use only the low-pass impulse stimuli.) Output is written to a stimulus file on disk in the

same format as used by Matthews (21) for his time-domain cochlear model.

TDM2 is a two-dimensional, time-domain model implementation. The program uses the finite-difference method to discretize the spatial dimensions (as described in section 3.2) and a Gaussian block-elimination procedure to solve the equations. The key to efficient solution of the equations is that only a small portion of the block-elimination procedure needs to be repeated each time step. The time discretization method is similar to that used by Allen and Sondhi (14). TDM2 accepts model parameters from the console and reads the stimulus from a stimulus file. The stimulus can be specified as stapes pressure, stapes acceleration, eardrum pressure, or earphone voltage. Various output formats are available to allow output of selected quantities to a time-domain data file at each time-step. A useful feature of the program is the capability of stopping the computation at any intermediate time-step to examine the partial solution and then resuming computation at the current state of the model.

TDM2LOOK reads the time-domain data file, performs various data processing functions, and displays the data on an oscilloscope. The program does the re-ordering of the data necessary for examining quantities as a function of time. The program computes Fourier transforms and permits the display of the frequency response of one quantity relative that of some other quantity. The program can produce "hard-copy" graphs of these displays on a pen-plotter.

APPENDIX 9.4

ADDITIONAL MODEL RESULTS WITH PSA AND PSB

The model parameter sets A and B were chosen to illustrate two different ways of using the 2-DOF partition model to implement possible cochlear sharpening mechanisms (see chapters 4 and 5). There are still many discrepancies between the model results presented in this dissertation and experimental observations of the cochlea. It may be possible to resolve some of these discrepancies by further adjustment of model parameters in the present model. There are differences between PSA and PSB with regard to physical interpretation and model results. Additional model results have been included in this appendix in order to facilitate comparisons between PSA and PSB.

In Figure 9.7 basilar membrane displacement from the time-domain model has been plotted as a function of frequency for PSA, similar to Figure 5.6 for PSB. The time-domain model results with PSA are compared with Rhode's data in Figure 9.8, similar to Figure 5.7 for PSB. Frequency-domain model results with PSA and PSB are compared in Figure 9.9.

According to the physical interpretation of resonant OHC cilia which led to PSB, the hair cell shearing-displacement ξ_h is identical to the basilar membrane displacement ξ_b. In Figure 9.10, basilar membrane displacement from the frequency-domain model with PSB is compared with the neural spatial-mapping data of Kim et al. (4), similar to Figure 4.6 for PSA.

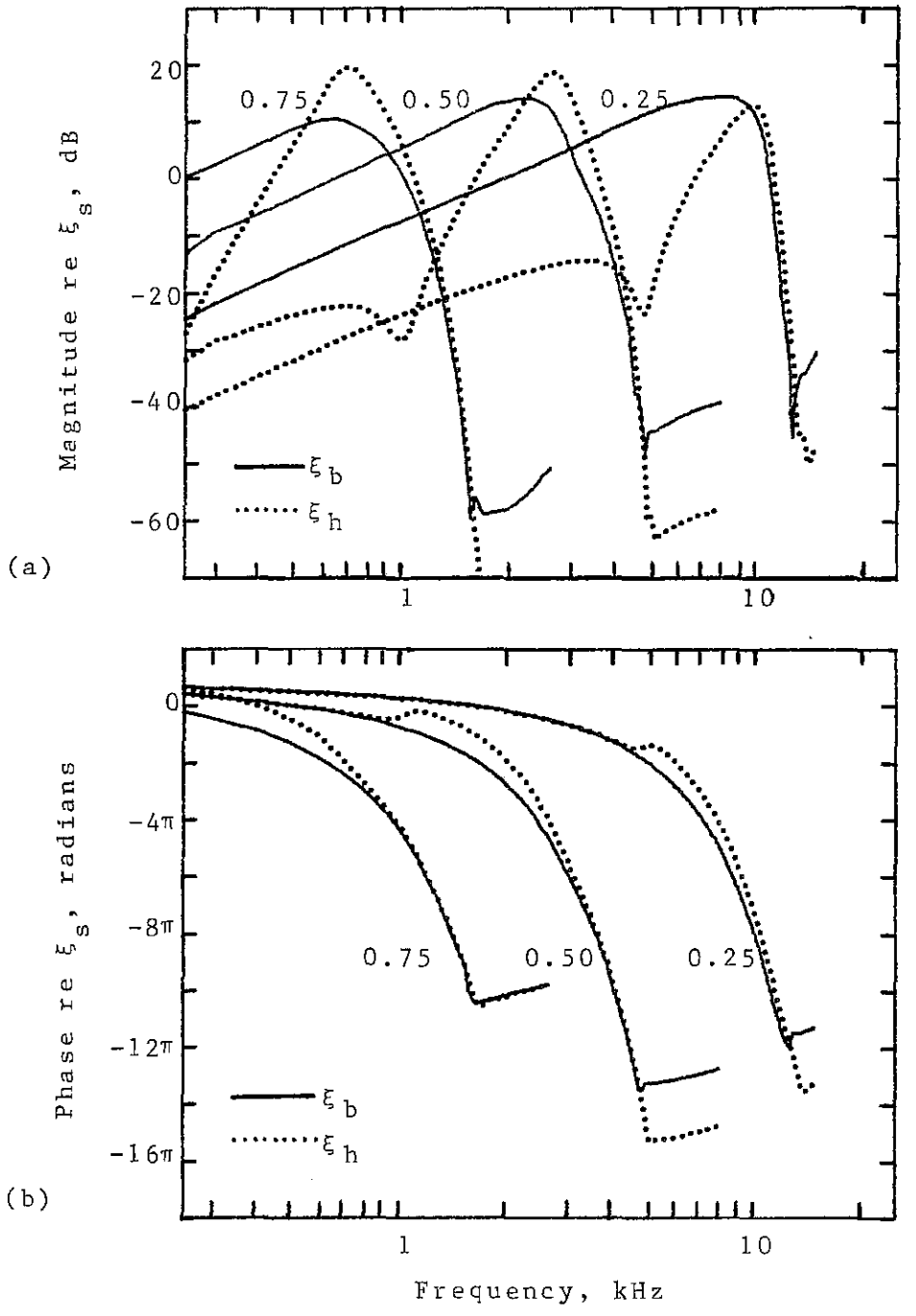

Figure 9.7. Cochlear partition displacement as a function of frequency (PSA). The curves show basilar membrane displacement (solid line) and hair cell shearing-displacement ξ_h (dashed line) re stapes displacement at three positions on the cochlear partition. (a) Magnitude. (b) Phase. The numerals indicate distance from the stapes as a fraction, x/L. (Model data from file IM23-1.).

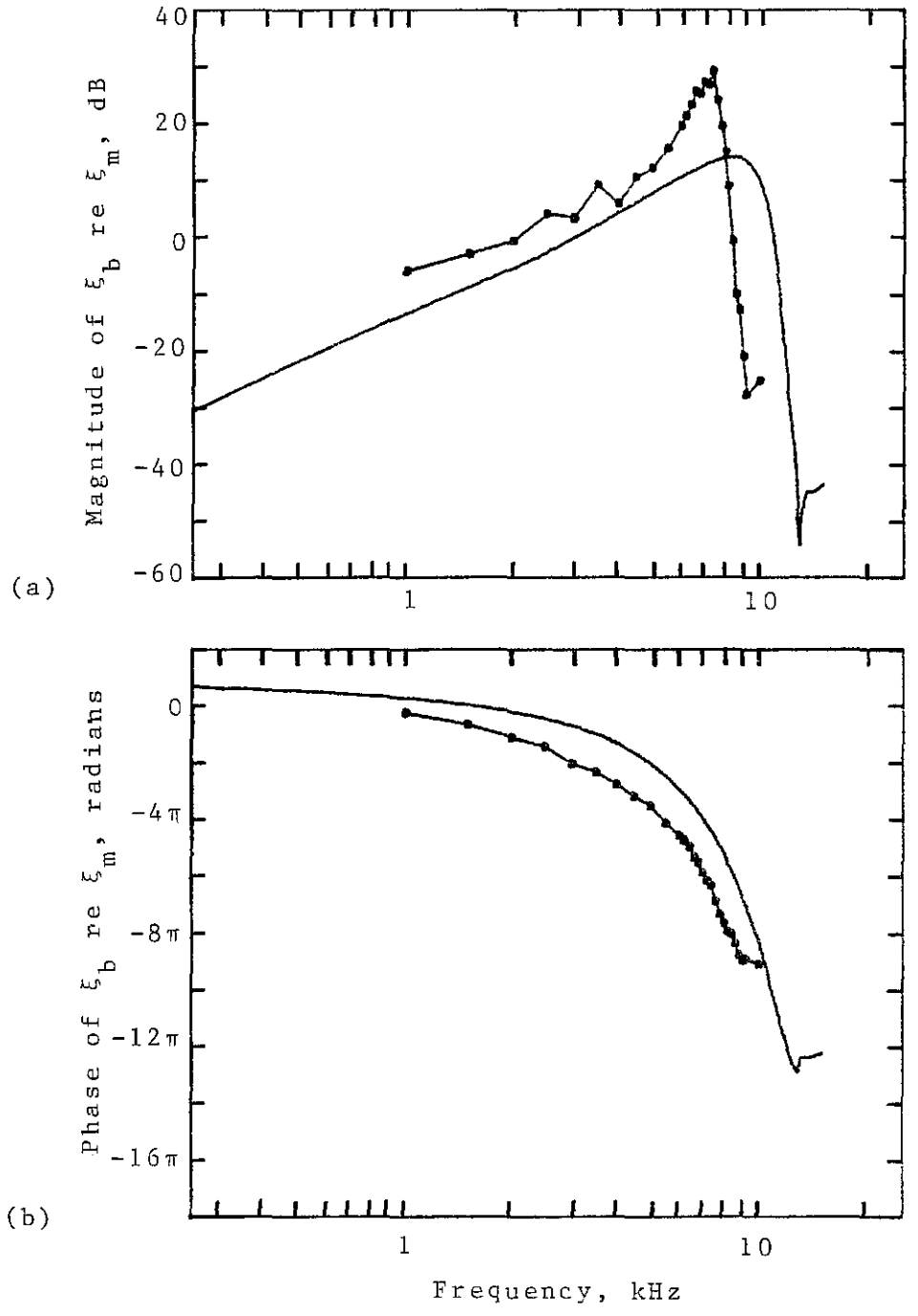

Figure 9.8. Comparison between model results with PSA and Rhode's data for basilar membrane displacement. The curves show basilar membrane displacement at (x/L)=0.25 re malleus displacement from the time-domain model (solid line) and Rhode's Mössbauer measurements (circles) as a function of frequency. (a) Magnitude. (b) Phase. [Rhode's data from animal 69-473 (56) and model data from file IM23-1.]

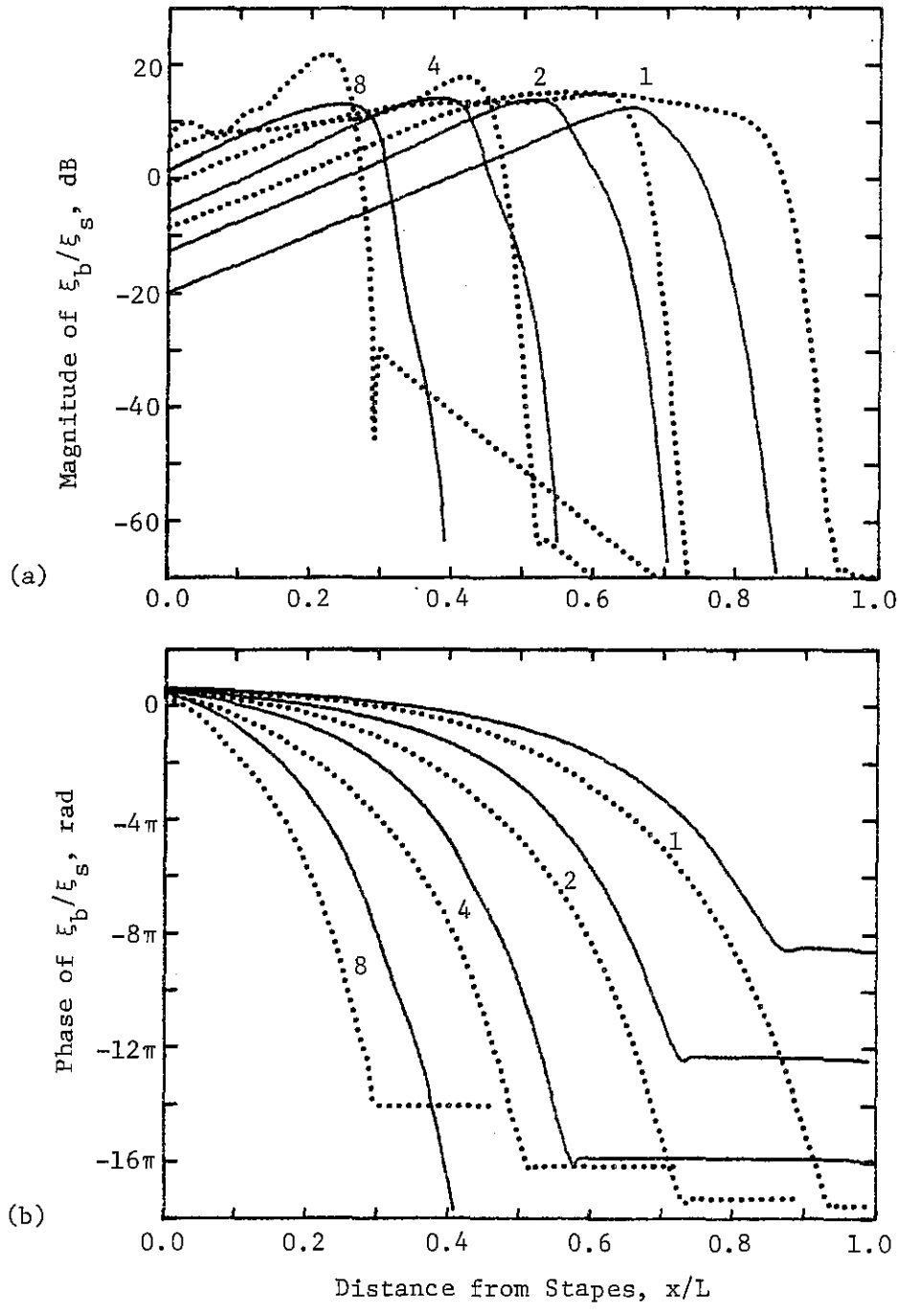

Figure 9.9. Comparison between model results with PSA and model results with PSB. The curves show the ratio of basilar membrane displacement ξ_b to stapes displacement ξ_s from the frequency-domain model at four frequencies for parameter set A (solid line) and parameter set B (dashed line). (a) Magnitude. (b) Phase. The numerals indicate frequency in kHz. (Model data from files A008, A009, A010, A011, B001, B002, B003, and B004.)

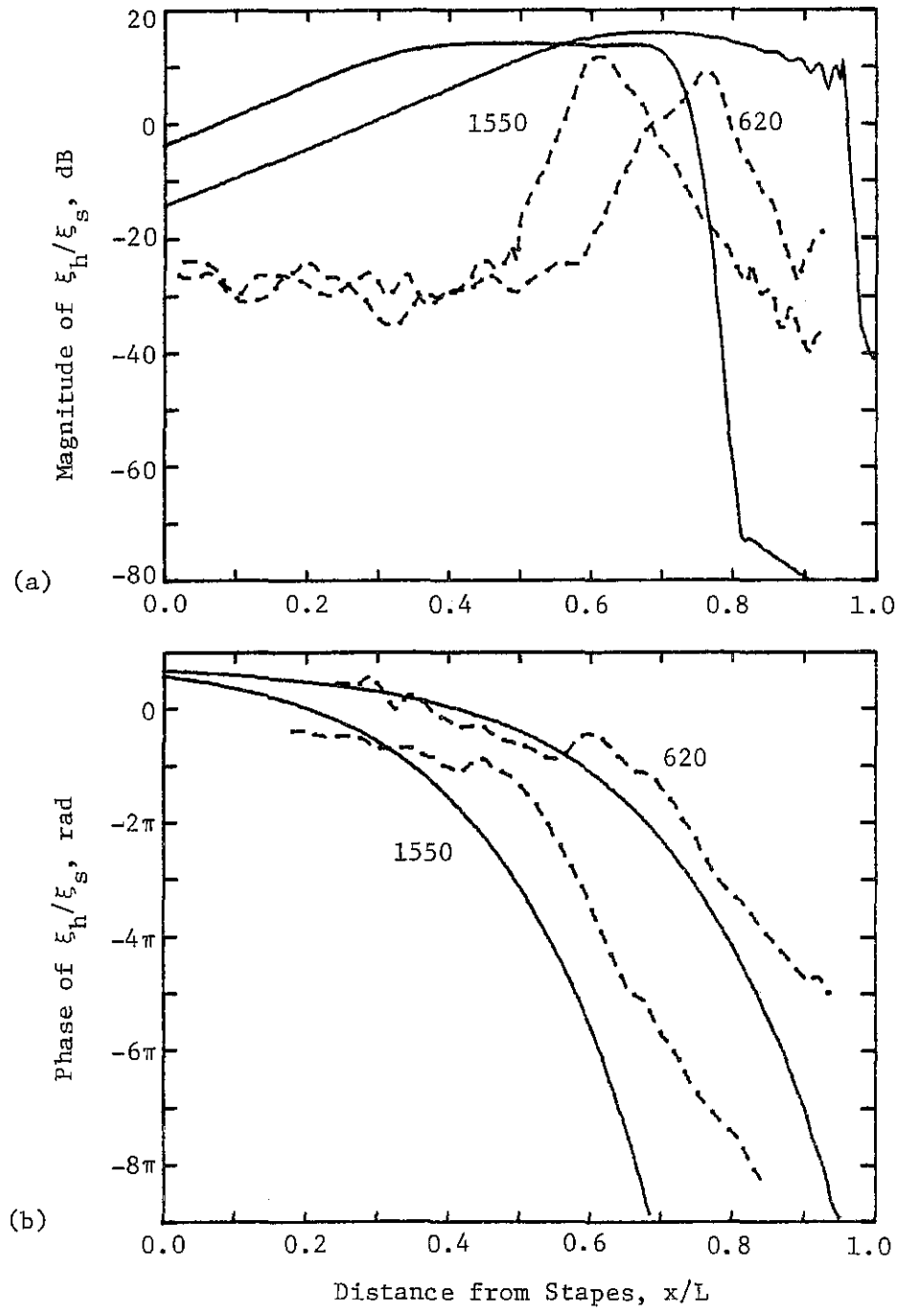

Figure 9.10. Comparison between model results with PSB and neural response data. The solid lines show the ratio of basilar membrane displacement ξ_b to stapes displacement ξ_s from the frequency-domain model at two frequencies. The dashed lines show the neural spatial-mapping data of Kim et al. (4) with Schuknecht's (45) frequency-to-place transformation. (a) Magnitude. (b) Phase. The numerals indicate frequency in Hz. (Model data from files B006 and B007.)

10. BIBLIOGRAPHY

1. von Békésy, G. (1960). Experiments in Hearing, (McGraw-Hill, New York).

2. Zwislocki, J. J. (1980). "Five decades of research on cochlear mechanics," Journal of the Acoustical Society of America, Vol. 67(5), pp. 1679-1685.

3. Rhode, W. S. (1971). "Observations of the Vibration of the Basilar Membrane in Squirrel Monkeys using the Mössbauer Technique," Journal of the Acoustical Society of America, Vol. 49(4), pp. 1218-1231.

4. Kim, D. O., Siegel, J. H., and Molnar, C. E. (1978). "Cochlear nonlinear phenomena in two-tone responses," in Models of the Auditory System and Related Signal Processing Techniques, edited by M. Hoke and E. de Boer, Scandanavian Audiology, Supplement 9, pp. 63-81.

5. Kim, D. O. (1980). "Cochlear Mechanics: Implications of Electrophysiological and Acoustical Observations," Hearing Research, Vol. 2, pp. 297-317.

6. Kim, D. O., Molnar, C. E., Matthews, J. W., and Neely, S. T. (1980). "Nonlinearity, physiological vulnerability, and frequency selectivity of cochlear responses, Journal of the Acoustical Society of America, Vol. 67, Suppl. 1, p. S47 (abstract).

7. Cannon, R. H. (1967). Dynamics of Physical Systems, (McGraw-Hill, New York).

8. Evans, E. F.and Wilson, J. P. (1973). "Frequency selectivity of the cochlea," in Basic Mechanisms in Hearing, edited by A. Møller, (Academic Press, New York), pp. 519-551.

9. Evans, E. F. and Wilson, J. P. (1975). "Cochlear Tuning Properties: Concurrent Basilar Membrane and Single Nerve Fiber Measurements," Science, Vol. 190, pp. 1218-1221.

10. Zwislocki, J. J. and Kletsky, E. J. (1979). "Tectorial Membrane: A Possible Effect on Frequency Analysis in the Cochlea," Science, Vol. 204, No. 11, pp. 639-641.

11. Zwislocki, J. J. (1980). "Two possible mechanisms for the second filter," in Psychophysical, Physiological and Behavioral Studies in Hearing, edited by G. van den Brink and F. A. Bilsen, (Delft University Press, Delft, The Netherlands), pp. 16-23.

12. Allen, J. B. (1980). "A cochlear micromechanical model of transduction," in Psychophysical, Physiological and Behavioral Studies in Hearing, edited by G. van den Brink and F. A. Bilsen, (Delft University Press, Delft, The Netherlands), pp. 85-95.

13. Allen, J. B. (1981). "Cochlear modeling - 1980," IEEE International Conference on Acoustics, Speech, and Signal Processing, Atlanta, Georgia.

14. Allen, J. B. and Sondhi M. M. (1979). "Cochlear macromechanics: Time domain solutions" Journal of the Acoustical Society of America, Vol. 66(1), pp. 123-132.

15. Viergever, M. A. (1980). "Mechanics of the inner ear - a mathematical approach," (Delft University Press, Delft, The Netherlands).

16. Gold, T. (1948). "Hearing II. The physical basis of action in the cochlea," Proceedings of the Royal Society of London B, Vol. 135, pp. 492-498.

17. Kemp, D. T. (1978). "Stimulated acoustic emissions from within the human auditory system," Journal of the Acoustical Society of America, Vol. 64(5), pp. 1386-1391.

18. Kemp, D. T. and Chum, R. (1980). "Properties of the generator of stimulated acoustic emissions," Hearing Research, Vol. 2, pp. 213-232.

19. Kim, D. O., Neely, S. T., Molnar, C. E., and Matthews, J. W. (1980). "An active cochlear model with negative damping in the cochlear partition: comparison with Rhode's ante- and post-mortem observations," in Psychological, Physiological and Behavioral Studies in Hearing, edited by G. van den Brink and F. A. Bilsen, (Delft University Press, Delft, The Netherlands), pp. 7-15.

20. Le Page, E. L. and Johnstone, B. M. (1980). "Nonlinear mechanical behavior of the basilar membrane in the basal turn of the guinea pig cochlea," Hearing Research, Vol. 2, pp. 183-190.

21. Matthews, J. W. (1980). "Mechanical Modeling of Non-linear Phenomena Observed in the Peripheral Auditory System," doctoral dissertation, Washington University, St. Louis, Missouri. (Available from Xerox University Microfilm, Ann Arbor, Michigan.)

22. Helmholtz, H. L. F. (1883). On the Sensation of Tone, english translation by A. J. Ellis (1885), reprinted (1954), (Dover, New York).

23. Romanes, G. J. (1966). Cunningham's Manual of Practical Anatomy, Vol. 3, Head and Neck and Brain, (Oxford, London).

24. Flanagan, J. L. (1972). Speech Analysis, Synthesis, and Perception, (Springer-Verlag, New York).

25. Davis, H. (1957). Chapter 4, in Handbook of Noise Control, (McGraw-Hill, New York).

26. Wever, E., G. (1949). Theory of Hearing, (Wiley, New York).

27. Allen, J. B. (1977). "Cochlear micromechanics - a method for transforming mechanical to neural tuning within the cochlea," Journal of the Acoustical Society of America, Vol. 62(4), pp. 930-939.

28. Rasmussen, G. L. (1943). Outlines of Neuroanatomy, (Brown, New York).

29. Flock, A. (1977) "Physiological Properties of Sensory Hairs," in Psychophysics and Physiology of Hearing, edited by E. F. Evans and J. P. Wilson, (Academic, London), pp. 15-25.

30. Johnstone, B. M., Taylor, K. W., and Boyle, A. J. (1970). "Mechanics of the guinea pig cochlea," Journal of the Acoustical Society of America, Vol. 47, pp. 504-509.

31. Johnstone, B. M. and Boyle, A. J. F. (1967). "Basilar membrane vibration examined with the Mössbauer technique," Science, Vol. 158, pp. 389-390.

32. Helfenstein, W. M. (1974). "Beitrag zur Messung der Akustich Bedingten Bewegun und Identifikation des Meschanischen Teils des Innenohrs der Katz," doctoral dissertation, Eidenoessen Technischen Hochscule, Zurich, West Germany.

33. Rhode, W. S. (1973). "An investigation of post-mortem cochlear mechanics using the Mössbauer effect," in Basic Mechanisms in Hearing, edited by A. Møller, (Academic Press, New York), pp. 49-67.

34. Wilson, J. P. and Johnstone, J. R. (1972). "Capacitive probe measures of basilar membrane vibration," in Hearing Theory 1972 (IPO, Eindhoven, The Netherlands), pp. 172-181.

35. Wilson, J. P. and Johnstone, J. R. (1975). "Basilar membrane and middle ear vibration in guinea pig measured by capacitive probe," Journal of the Acoustical Society of America, Vol. 57, pp. 705-723.

36. Kohllöffel, L. U. E. (1972). "A study of basilar membrane vibrations I. Fuzziness detection: A new method for the analysis of microvibrations with laser light," Acustica, Vol. 27, pp. 49-65.

37. Kohllöffel, L. U. E. (1972). "A study of basilar membrane vibrations II. The vibratory amplitude and phase pattern along the basilar membrane (post-mortem)," Acustica, Vol. 27, pp. 66-81.

38. Kohllöffel, L. U. E. (1972). "A study of basilar membrane vibrations III. "The basilar membrane frequency curve in a living guinea pig," Acustica, Vol. 27, pp. 82-89.

39. Russel, I. J. and Sellick, P. M. (1978). "Intracellular studies of hair cells in the mammalian cochlea," Journal of Physiology, Vol. 284, pp. 261-290.

40. Dallos, P. (1975). "Cochlear potentials," in The Nervous System, Vol. 3, Human Communication and Its Disorders, edited by D. B. Tower, (Raven Press, New York), pp. 69-80.

41. Nedzelnitsky, V. (1980). "Sound pressures in the basal turn of the cat cochlea," Journal of the Acoustical Society of America, Vol. 68(6), pp. 1676-1689.

42. Kiang, N. Y. S. and Moxon, E. C. (1974). "Tails of tuning curves of auditory nerve fibers," Journal of the Acoustical Society of America, Vol. 55, pp. 620-630.

43. Pfeiffer, R. R. and Molnar, C. E. (1970). "Cochlear nerve fiber discharge patterns: relation to the cochlear microphonic," Science, Vol. 167, pp. 1614-1616.

44. Littlefield, W. M. (1973). "Investigation of the linear range of the peripheral auditory system," doctoral dissertation, Washington University, St. Louis, Missouri. (Available from Xerox University Microfilm, Ann Arbor, Michigan.)

45. Schuknecht, H. F. (1960). "Neuroanatomical correlates of auditory sensitivity and pitch discrimination in the cat," in Neural Mechanisms of the Auditory and Vestibular Systems, edited by G. L. Rasmussen and W. Windle, (C. C. Thomas, Springfield, Illinois), pp. 76-90.

46. Kemp, D. T. (1979). "Evidence of mechanical nonlinearity and frequency selective wave amplification in the cochlea," Archives of Otorhinolaryngology, Vol. 224, pp. 37-45.

47. Wit, H. P. and Langevoort, J. C., and Ritsma, R. J. (1981). "Frequency spectra of cochlear acoustic emissions ('Kemp echoes'), " Journal of the Acoustic Society of America, (in press).

48. Zurek, P. M. (1981). "Spontaneous narrowband acoustic signals emitted by human ears," Journal of the Acoustical Society of America, Vol. 69(2), pp. 514-523.

49. Zurek, P. M. (1980). "Objective tonal tinnitus induced by noise exposure in chinchillas," Journal of the Acoustical Society of America, Vol. 68, Suppl. 1, p. S44 (abstract).

50. Zwicker, E. (1974). "A 'second filter' established within the scala media," in Facts and Models in Hearing, edited by E. Zwicker and E. Terhardt, (Springer-Verlag, New York), pp. 95-99.

51. Helle, R. (1974). "Hydromechanical cochlea model with basilar membrane and tectorial membrane," in Facts and Models in Hearing, edited by E. Zwicker and E. Terhardt, (Springer-Verlag, New York), pp. 77-85.

52. Hubbard, A. E. and Geisler, C. D. (1972). "A hybrid-computer model of the cochlear partition," Journal of the Acoustical Society of America, Vol. 51(6), pp. 1895-1903.

53. Zwislocki, J. J. (1950). "Theory of acoustical action in the cochlea," Journal of the Acoustical Society of America, Vol. 22, pp. 778-784.

54. Peterson, L. C. and Bogert, B. P. (1950). "A Dynamical Theory of the Cochlea," Journal of the Acoustical Society of America, Vol. 22(3), pp. 369-381.

55. Fletcher, H. (1953). "On the dynamics of the cochlea," Journal of the Acoustical Society of America, Vol. 23, pp. 637-645.

56. Zweig, G., Lipes, R., and Pierce, J. R. (1976). "The cochlear compromise," Journal of the Acoustical Society of America, Vol. 59, pp. 975-982.

57. Ranke, O. F. (1950). "Theory of Operation of the Cochlea: A Contribution to the Hydrodynamics of the Cochlea," Journal of the Acoustical Society of America, Vol. 22(6), pp. 772-777.

58. Lesser, M. B. and Berkley, D. A. (1972). "Fluid mechanics of the cochlea, Part I," Journal of Fluid Mechanics, Vol. 51(3), pp. 497-512.

59. Allen, J. B. (1977). "Two-dimensional cochlear fluid model: New results," Journal of the Acoustical Society of America, Vol. 61(1), pp. 110-119

60. Lien, M. D. (1973). "A Mathematical Model of the Mechanics of the Cochlea," doctoral dissertation, Washington University, St. Louis, Missouri.

61. Sondhi, M. M. (1978). "Method for computing motion in a two-dimensional cochlear model," Journal of the Acoustical Society of America, Vol. 63(5), pp. 1468-1477.

62. Neely, S. T. (1978). "Mathematical Models of the Mechanics of the Cochlea," Engineer's thesis, California Institute of Technology, Pasadena, California.

63. Neely, S. T. (1981). "Finite difference solution of a two-dimensional mathematical model of the cochlea," Journal of the Acoustical Society of America, Vol. 69(5), pp. 1386-1393.

64. Steele, C. R. and Taber, L. A. (1979). "Comparison of WKB and finite difference calculations for a two-dimensional cochlear model," Journal of the Acoustical Society of America, Vol. 65, pp. 1001-1006.

65. Steele, C. R. and Taber, L. A. (1979). "Comparison of WKB calculations and experimental results for 3-D cochlear models," Journal of the Acoustical Society of America, Vol. 65(4), pp. 1007-1018.

66. Steele, C. R. and Taber, L. A. (1981). "Three-dimensional model calculations for guinea pig cochlea," Journal of the Acoustical Society of America, Vol. 69(4), pp. 1107-1111.

67. Steele, C. R. (1980). "Lecture Notes on Cochlear Mechanics," NSF-CBMS Regional Conference on Mathematical Models of the Hearing Process, Rensselaer Polytechnic Institute, Troy, New York. (To be published in SIAM Review.)

68. de Boer, E. (1981). "Short waves in three-dimensional models: solutions for a 'block' model," Hearing Research, Vol. 4, pp. 53-77.

69. Kim, D. O., Molnar, C. E., and Pfeiffer, R. R. (1973). "A system of nonliner differential equations modeling basilar membrane motion," Journal of the Acoustical Society of America, Vol. 54(6), pp. 1517-1529.

70. Hall, J. L. (1974). "Two-tone distortion products in a nonlinear model of the basilar membrane," Journal of the Acoustical Society of America, Vol. 56, pp. 1818-1828.

71. Tonndorf, J. (1960). "Shearing motion in scala media of cochlear models," Journal of the Acoustical Society of America, Vol. 32, pp. 238-244.

72. Duifuis, H. (1976). "An alternative approach to the second filter," in Facts and Models in Hearing, edited by E. Zwicker and E. Terhardt, (Springer-Verlag, New York), pp. 100-104.

73. Steele, C. R. (1974). "Behavior of the basilar membrane with pure tone excitation," Journal of the Acoustical Society of America, Vol. 55(1), pp. 148-162.

74. Rhode, W. S. and Geisler, C. D. (1967). "Model of the displacement between opposing points on the tectorial membrane and reticular lamina," Journal of the Acoustical Society of America, Vol. 42(1), pp. 185-190.

75. Iurato, S. (1962). "Functional implications of the nature and submicroscopic structure of the tectorial and basilar membranes," Journal of the Acoustical Society of America, Vol. 34, pp. 1386-1395.

76. Völdrich, L. (1978). "Mechanical properties of the basilar membrane," Acta Otolaryngologica, Vol. 86, pp. 331-335.

77. Inselberg A. and Chadwick, R. S. (1976). "Mathematical model of the cochlea, I: Formulation and solution," SIAM Journal of Applied Mathematics Vol. 30, pp. 149-163.

78. Chadwick, R. S., Inselberg, A., and Johnson, K. (1976). "Mathematical model of the cochlea. II: Results and conclusions," SIAM Journal of Applied Mathematics, Vol. 30, pp. 164-179.

79. Allen, J. B. (1980). "Cochlear micromechanics - A physical model of transduction," Journal of the Acoustical Society of America, Vol. 68(6), pp. 1660-1670.

80. Zwislocki, J. J. and Kletsky, E. J. (1981). "Cochlear tuning may reflect tectorial membrane resonance," Journal of the Acoustical Society of America, Vol. 69, Suppl. 1, p. S52 (abstract).

81. Kletsky, E. J. and Zwislocki, J. J. (1981). "A network model of cochlear dynamics," Journal of the Acoustical Society of America, Vol. 69, Suppl. 1, p. S52 (abstract).

82. Siebert, W. A. (1974). "Ranke revisited - a simple short-wave cochlear model," Journal of the Acoustical Society of America, Vol. 56(2), pp. 594-600.

83. Viergever, M. A. and Kalker, J. J. (1975). "A two-dimensional model for the cochlea: I. The exact approach," Journal of Engineering Mathematics, Vol. 9(4), pp. 353-365.

84. Viergever, M. A. (1977). " A two-dimensional model for the cochlea: II. The heuristic approach and numerical results," Journal of Engineering Mathematics, Vol. 11(1), pp. 11-28.

85. Geisler, C. D. (1976). "Mathematical Models of the Mechanics of the Cochlea," in Handbook of Sensory Physiology, Vol V/3, Auditory System - Clinical and Special Topics, edited by W. D. Keidel and W. D. Neff (Springer-Verlag, New York).

86. Weinberger, H. F. (1965). Partial Differential Equations, (Xerox College Publishing, Lexington, Massachusetts).

87. Meirovitch, L. (1967). Analytical Methods in Vibrations, (MacMillan, New York).

88. Kuo, F. F. (1962). Network Analysis and Synthesis, (Wiley, New York).

89. Isaacson E. and Keller, H. B. (1966). Analysis of Numerical Methods (Wiley, New York).

90. Guinan, J. J. and Peake, W. T. (1967). "Middle-Ear Characteristics of Anesthetized Cats," Journal of the Acoustical Society of America, Vol. 41, pp. 1237-1261.

91. Greenwood, D. P. (1960). "Critical bandwidth and the frequency coordinates of the basilar membrane," Journal of the Acoustical Society of America, Vol. 33, pp. 1344-1356.

92. de Boer, E. (1979). "Short-wave world revisited: Resonance in a two-dimensional cochlear model," Hearing Research, Vol. 1, pp. 253-281.

93. Durney, C. H. and Johnson, C. C. (1969). Introduction to Modern Electromagnetics (McGraw-Hill, New York).

94. Kim, D. O. and Molnar, C. E. (1979). "A population study of cochlear nerve fibers: comparison of the spatial distribution of average rate and phase-locking measures of responses to single tones," Journal of Neurophysiology, Vol. 42, pp. 16-30.

95. Lim, D. J. (1980). "Cochlear anatomy related to cochlear micromechanics. A review," Journal of the Acoustical Society of America, Vol. 67(5), pp. 1686-1695.

96. Bohne, B. A. and Carr, C. D. (1979). "Location of structurally similar areas in chinchilla cochleas of different lengths," Journal of the Acoustical Society of America, Vol. 66(2), pp. 411-414.

97. Rhode, W. S. (1978). "Some observations on cochlear mechanics," Journal of the Acoustical Society of America, Vol. 64(1), pp. 158-176.

98. Kim, D. O., Molnar, C. E., and Matthews, J. W. (1980). "Cochlear mechanics: Nonlinear behavior in two-tone responses as reflected in cochlear-nerve-fiber responses and in ear-canal sound pressure," Journal of the Acoustical Society of America, Vol. 67(5), pp. 1704-1721.

99. Flock, A. (1971). "Sensory Transduction in Hair Cells," in Handbook of Sensory Physiology, Vol. I, Principles of Receptor Physiology, edited by W. R. Lowenstein, (Springer-Verlag, New York), pp. 396-441.

100. Hudspeth, A. J. and Corey, D. P. (1977). "Sensitivity, polarity, and conductance change in the response of vertebrate hair cells to controlled mechanical stimuli," Proceedings of the National Academy of Science USA, Vol. 74, No. 6, pp. 2407-2411.

101. Spoendlin, H. (1974). "Neuroanatomy of the cochlea," in Facts and Models in Hearing, edited by E. Zwicker and E. Terhardt, (Springer-Verlag, New York), pp. 18-32.

102. Billone, M. C. (1972). "Mechanical Stimulation of Cochlear Hair Cells," doctoral dissertation, Northwestern University, Evanston, Illinois. (Available from Xerox University Microfilm, Ann Arbor, Michigan.)

103. Siegel, J. H. (personal communication). Washington University, St. Louis, Missouri.

104. Tilney, L. G., DeRosier, D. J., and Mulroy, M. J. (1980). "The Organization of Actin Filaments in the Stereocilia of Cochlear Hair Cells," Journal of Cell Biology, Vol. 86, pp. 244-259.

105. Slepecky, N., Hamernik, R.,P., and Henderson, D. (1980). "A re-examination of a hair cell organelle in the cuticular plate region and its possible relation to active processes in the cochlea," Hearing Research, Vol. 2, pp. 413-421.

106. Holwill, M. E. J. (1974). "Hydrodynamic aspects of ciliary and flagellar movement," in Cilia and Flagella, edited by M. A. Sleigh, (Academic, London), pp. 143-175.

107. Corey, D. P. and Hudspeth, A. J. (1979). "Ionic basis of the receptor potential in a vertebrate hair cell," Nature, Vol. 281, pp. 675-677.

108. Robertson, D. and Johnstone, J. R. (1979). "Aberrant tonotopic organization in the inner ear damaged by kanamycin," Journal of the Acoustical Society of America, Vol. 66(2), pp. 466-469.

109. Evans, E. F. (1974). "Auditory frequency selectivity and the cochlear nerve," in Facts and Model in Hearing, edited by E. Zwicker and E. Terhardt, (Springer-Verlag, New York), pp. 118-119.

110. Wiederhold, M. L. (1969). "Variations in the Effects of Electrical Stimulation of the Crossed Olivocochlear Bundle on Cat Single Auditory-Nerve-Fiber," Journal of the Acoustical Society of America, Vol. 48(4), pp. 966-977.

111. Hiramoto, Y. (1974). "Mechanics of ciliary movement," in Cilia and Flagella, edited by M. A. Sleigh, (Academic, London), pp. 177-196.

112. Beranek, L. L. (1954). Acoustics (McGraw-Hill, New York).

113. Eugen Beyer Elektrotechnische Fabrik GmbH & Co., Postf. 1320, 71 Heilbron, West Germany.

114. Schlemmer, T. (1979). Doctoral dissertation, Technical University of Munich, Munich, West Germany.

115. Lynch, T. J., Nedzelnitsky, V., and Peake, W. T. (1981). "Input impedance of the cochlea in cat," Journal of the Acoustic Society of America, (submitted).

11. VITA

Biographical items on the author of the dissertation, Stephen T. Neely:

1) Born on September 18,1953 in Iloilo City, Philippines.

2) Attended Ottawa University in Ottawa, Kansas from September 1970 to June 1974. Received the degree of Bachelor of Arts (summa cum laude) in Physics and Communication.

3) Attended the California Institute of Technology in Pasadena, California from September 1974 to December 1977. Received the degree of Master of Science in June 1975 and the degree of Electrical Engineer in June 1978. Thesis title: "Mathematical Models of the Mechanics of the Cochlea." Thesis advisor: Professor J. R. Pierce.

4) Management assistant in Applications division of NASA headquarters, Washington, D. C., during summer of 1974. Predoctoral fellow in Acoustics Research department of Bell Laboratories, Murray Hill, New Jersey, during summer of 1976.

5) Married in March 1975 to Donna E. Gonzaga. Daughter, Catherine Anne, born in November 1977 and son, Christopher Edward, born in November 1979.

6) Employed as senior staff in the Tactical Systems Division of ORI, Inc., Silver Spring, Maryland, from December 1977 to January 1979.

7) Attended Washington University from January 1979 to the present date, supported by an NIH grant: "Analytical and computational techniques in physiology."

8) Membership in professional and honor societies: Institute of Electrical and Electronic Engineers (IEEE), Acoustical Society of America, Sigma Pi Sigma (honorary physics society).

Publications and papers presented:

1) Neely, S. T. and Allen J. B. (1979). "Invertibility of a room impulse response," Journal of the Acoustical Society of America, Vol. 66(1), pp. 165-169.

2) Neely, S. T. (1980) "Backward solution of a two-dimensional cochlear model," Journal of the Acoustical Society of America, Vol. 67, Suppl. 1, p. S75 (abstract).

3) Kim, D. O., Molnar, C. E., Matthews, J. W., and Neely, S. T. (1980). "Nonlinearity, physiological vulnerability, and frequency selectivity of cochlear responses," Journal of the Acoustical Society of America, Vol. 67, Suppl. 1, p. S47 (abstract).

4) Kim, D. O., Neely, S. T., Molnar, C. E., and Matthews, J. W. (1980). "An active cochlear model with negative damping in the cochlear partition," in Psychological, Physiological and Behavioral Studies in Hearing, edited by G. van den Brink and F. A. Bilsen, (Delft University Press, Delft, Netherlands), pp. 7-14.

5) Neely, S. T. and Kim, D. O. (1980). "Modeling cochlear echoes," NSF-CBMS Regional Conference on Mathematical Modeling of the Hearing Process, Rensselaer Polytechnic Institute, Troy, New York, (unpublished).

6) Matthews, J. W., Kim, D. O., Molnar, C. E., and Neely, S. T. (1981). "Modeling reverse middle-ear transmission: aural acoustic distortion products, 'echoes', and spontaneous emmissions," Journal of the Acoustical Society of America, Vol. 69, Suppl. 1, p. S43 (abstract).

7) Neely, S. T. (1981). "Finite difference solution of a two-dimensional mathematical model of the cochlea," Journal of the Acoustical Society of America, Vol. 69(5), pp. 1386-1393.

August 1981